Wavelet analysis of microvascular function of women with and without migraine

Applying mathematical techniques to address a medical challenge

Christina Zheng

TU Delft

Wavelet analysis of the microvascular function of women with and without migraine

Applying mathematical techniques to address a medical challenge

by

Christina Zheng

to obtain the degree of Bachelor of Science
at the Delft University of Technology.

Student number:	5470854	
Project duration:	February 25, 2025 – June 20, 2025	
Thesis committee:	Dr. C. Vuik,	TU Delft, supervisor
	Drs. L. Al-Hassany,	Erasmus MC
	Dr. A. Maassen van der Brink,	Erasmus MC
	Dr. M. Keijzer,	TU Delft

An electronic version of this thesis is available at `http://repository.tudelft.nl/`.

TU Delft

Abstract

Migraine is a prevalent, complex neurovascular disorder that mainly affects women. The exact pathophysiology of migraine is unclear, but research indicates that activation of the trigeminal nerve in the trigeminovascular system causes release of calcitonin gene-related peptide (CGRP), which triggers migraine attacks. Additionally, nitric oxide (NO) contributes to the pathophysiology of migraine headaches. Research suggests that migraine patients have an increased risk of cardiovascular disease. Over the past decades, non-invasive techniques, like Laser Doppler imaging (LDI) and Laser speckle contrast imaging (LSCI) have been developed for imaging tissue perfusion, which are valuable tools for investigating the underlying causes for this increased risk and facilitates the study of blood perfusion. The Erasmus Medical Center (Erasmus MC) used these techniques to perform measurements of the microvascular blood flow in the forearm as a measure of the microvasculature of women with and without migraine. This study, also known as the VASCULAR-study, focused on three regions of interest (ROIs), where NO was inhibited using iontophoresis with L-NMMA and neuropeptides were blocked using EMLA cream. The last ROI served as the control region. The measurements also consisted of three different phases: baseline, peak and plateau phase. Studies have shown that distinct biological mechanisms in the body can be linked to different frequency intervals and therefore, Fourier analysis (FA) and wavelet analysis (WA) were used to transform the VASCULAR-study data into the frequency domain. Two preliminary studies used FA to perform the transformation. This study primarily focused on WA. The research question is as follows: *Does wavelet analysis (WA) of the VASCULAR-study data yield more insights than Fourier analysis (FA) into blood flow measurements in women, particularly in examining the role of nitric oxide (NO) and calcitonin gene-related peptide (CGRP) in the microvasculature among women with and without migraine?* To address the research question, WA was conducted using the complex Morlet wavelet. Relative energy density was used as a quantitative metric to compare the group of women with migraine with the group of women without migraine. Relative energy density was also calculated for the results using FA. Statistical significance was assessed using p-values, where p-values below 0.05 were considered significant. The Mann-Whitney U-Test and the Wilcoxon Signed Rank Test were used to calculate the p-values. Significant differences between women without migraine and women with migraine were primarily found in respiratory and endothelial activity for both WA and FA. Women with migraine showed higher respiratory activity in regions where NO was inhibited, for both WA and FA. Although WA and FA revealed many similar results in the VASCULAR-study dataset, there were also some differences. These differences were mainly observed in endothelial activity, in the ROI where NO was inhibited. FA revealed significantly higher values in activity for women without migraine in both NO-independent and NO-dependent endothelial activity. Furthermore, using the time-frequency localization capability of the WA, it showed significantly higher activity in women with migraine between the peak and plateau phase.

Contents

1

Introduction

Migraine is a prevalent, complex neurovascular disorder affecting over one billion people worldwide. Approximately 14% of the global population experience this condition every year. Consequently, it makes migraine the second leading contribution to the global burden of neurological diseases. Therefore, researchers have performed comprehensive research to gain more insights on this neurological disorder [1]. Over the last two decades, our knowledge of the underlying pathophysiology of migraine has improved remarkably [2]. However, the exact pathophysiology of migraine is still unsolved and seems to be a complex combination of genetic predisposition, hormonal influences and neurovascular interactions. [3].

Research also shows that migraine is more prevalent in women compared to men; migraine is three times more common in women than in men. This difference is caused by fluctuations in estrogen and progesterone, which becomes more apparent during puberty, menstruation and pregnancy [4]. Migraine poses a risk factor for cardiovascular diseases. Atherosclerosis is a traditional risk factor of cardiovascular diseases [5]. However, research shows that atherosclerosis is less prevalent among migraine patients [6]. Consequently, the higher risk for cardiovascular diseases observed in migraine patients can not be fully explained by traditional risk factors such as atherosclerosis. This is a paradoxical relationship between migraine and cardiovascular diseases [7]. Since there is no evidence supporting the link between migraine and atherosclerosis in the macrovasculature [8], dysfunction of microvascular function is suggested to be an underlying factor for the risk of cardiovascular diseases [9][10].

Multiple non-invasive techniques have been developed for imaging tissue perfusion, like Laser Doppler imaging (LDI) and Laser speckle contrast imaging (LSCI) [11], which are valuable tools for investigating the underlying causes for this risk of cardiovascular diseases. Over the past decades, wavelet analysis (WA) emerged as an effective tool to characterize blood perfusion in human skin [12][13][14][15][16]. Using LDI and LSCI, speckle patterns are generated and analyzed with WA. The ability of wavelets to provide time as well as frequency information at the same time makes it the ideal tool for analyzing non-stationary and oscillating mechanisms, like blood flow. Using these techniques, researchers from the Erasmus Medical Center (Erasmus MC) conducted measurements of the microvascular blood flow in the forearm of women with and without migraine, also known as the VASCULAR-study. The measurements are recorded in the time domain. Studies have shown that different frequency intervals correspond to distinct biological mechanisms [17]. Transforming data to the frequency domain using Fourier transforms (FT) and wavelet transforms (WT) reveals different information from those obtained in the time domain.

Prior frequency analyses of the VASCULAR-study data have been conducted in two preliminary studies [18][19]. Both studies used Fourier analysis (FA) to transition the data from a temporal to a frequency domain in order to investigate the differences between women with and without migraine. Both investigations successfully transformed the data into the frequency domain. However, no significant differences between women with migraine and women without migraine were observed. WA is introduced aiming to provide additional insight into the difference between the two groups. This yields in the following research question: *Does WA of the VASCULAR-study data yield more insights than FA into blood flow measurements in women, particularly in examining the role of nitric oxide (NO) and calcitonin gene-related peptide (CGRP) in the microvasculature among women with and without migraine?*

As the research question indicates, WA will be used to characterize the frequency components of the VASCULAR-study data. While FT produces a one-dimensional amplitude spectrum representing the different frequencies and their corresponding amplitude, WA provides a two-dimensional time-frequency representation, since it includes time and frequency information. Instead of using amplitude spectra, spectograms are used to visualize the results. Consequently, the frequency bands can be tracked over time, offering huge advantages for analyzing non-stationary signals.

To extract physiologically information from the time-frequency analysis, frequency bands corresponding to different biological mechanisms (e.g., respiratory activity, neurogenic activity and endothelium activity) influencing blood flow are defined. Predefining the frequency bands makes it possible to compare the microvasculature of women with and without migraine.

In order to address the research question, Chapter 2 first introduces all key definitions and concepts. After establishing all necessary theoretical framework, Chapter 3 includes all used methods. First, the chapter presents a description of the experimental design of the VASCULAR-study. Subsequently, the frequency analysis is introduced. The associated results and findings will be presented in Chapter 4. In Chapter 5 and Chapter 6, the discussion and conclusion will be represented respectively.

2

Background

Prior to addressing the research question, the fundamental concepts relevant for this study are first discussed. First, an overview of the medical background of migraine is presented. Accordingly, in Section 2.2, the techniques available for laser speckle contrast are discussed. In the last section (Section 2.3) of this chapter, all concepts about frequency analysis are explained, including FA and WA.

2.1. Migraine

Although the underlying pathophysiology of migraine remains unclear, numerous studies have associated the condition with microvascular dysfunction [9][20][21][22], involving both the endothelial function and the smooth muscle cell function. The endothelium refers to the cells that form the inner lining of blood vessels and the lymphatic system. It plays a huge role in the control of blood flow, by producing and releasing factors that either relax or contract blood vessels, such as NO [23]. Dysfunction of the endothelial causes imbalance in the width of the blood vessels, deficiency of NO bioavailability and inflammatory responses, which lead to the development of cardiovascular diseases [24]. Smooth muscle cells are present all over the body and their major role is to control the diameter and wall movement of internal organs, such as blood vessels. Impairment of smooth muscle cells contributes to the development of cardiovascular diseases, including atherosclerosis, hypertension and myocardial infarction [25]. Since both endothelial and smooth muscle cell functions play key roles in cardiovascular disease, it is essential to first clarify the roles of CGRP and NO, especially in the biology of migraine [9].

2.1.1. Calcitonin gene-related peptide

Until recently, patients of migraine were treated with preventive medications for headaches from other disciplines in medicine. A new promising prospect emerged when an increase in CGRP during a migraine attack was discovered. Researchers found that blocking the CGRP is a promising therapeutic opportunity for the treatment of migraine [26]. CGRP is a neuropeptide which is the body's most potent vasodilator and a transmitter that can be found in both the peripheral and central nervous systems [27]. Neuropeptides are a class of signaling molecules released by neurons in the brain to communicate with each other and with other cells [28]. Vasodilators are substances that dilate blood vessels, which lead to greater blood flow [29]. CGRP is crucial for expanding blood vessels and managing blood pressure [27]. The activation of the trigeminal nerve in the trigeminovascular system causes CGRP release [30]. The trigeminovascular system serves as a bridge between the trigeminal neurons and the blood vessels [31]. During a migraine attack, the release of neuropeptides like CGRP triggers vasodilation, which leads to neurogenic inflammation [32]. Neurogenic inflammation refers to an inflammation that causes redness, heat and pain, which is directly triggered by neurons, unlike immune-mediated inflammation [33].

2.1.2. Nitric oxide

NO is a signaling molecule that is involved in numerous neurophysiological processes and is a potent vasodilator. Migraine headaches are commonly connected with NO [34]. Evidence indicates a relationship between NO and CGRP: NO directly stimulates CGRP release and CGRP can cause vasolidation via NO mechanisms. This is a positive feedback loop, since studies show that NO increases CGRP release, but CGRP also

increases NO production. This loop conserves migraine attacks [35].

2.2. Laser speckle contrast techniques

In this section, different imaging techniques are introduced, including LSCI and LDI. In the last subsection, a comparison between these two techniques is provided.

2.2.1. Laser speckle contrast imaging

LSCI operates on basis of multiple light scattering. When an opaque material, for example the skin, is illuminated with a coherent light source, the backscattered light will create an interference pattern. These interference patterns are also called speckles and consists of bright and dark areas. Analyzing how the speckle pattern changes over time for different pixel values gives insights into the motion within the medium. The quantification of the change over time of the speckle pattern is by speckle contrast. The speckle contrast is the ratio of the standard deviation of the intensity of a pixel to the mean intensity of a pixel. Fast moving particles have a low speckle contrast, since the standard deviation of the intensity of such a pixel is lower compared to slow moving particles. There are different ways to define the speckle contrast. LSCI calculates the contrast in a time sequence. The spatial equivalent of LSCI is Laser speckle contrast analysis (LASCA) [11] [36].

2.2.2. Laser Doppler imaging

Within Laser Doppler Imaging (LDI), two distinct measurement approaches are utilized: Laser Doppler flowmetry (LDF) and Laser Doppler perfusion imaging (LDPI).
LDF makes use of the same techniques as LSCI. However, instead of using one coherent light source, it uses two light sources. One of the two is the light-emitting probe (laser) and the other one is the receiving probe (detector) [37]. Additionally, LDF utilizes the Doppler effect, which "refers to the phenomenon whereby an apparent change in frequency is perceived when relative motion exists between the wave source and the receiver" [38]. In more simple terms, if the red blood cells move toward the detector, the frequency will increase. The reverse will happen if the red blood cells move away from the detector. The change in frequency is only relative to the receiver; the perceived frequency changes, but the emitted frequency does not. Analyzing the shifts in frequencies give more insights in the blood perfusion [38].
The difference between LDF and LDPI lies in the fact that LDPI is a non-contact technique, while LDF uses probes to contact the issue. In addition, LDPI assesses much larger areas compared to LDF. However, the scanning procedure of LDPI is relatively slow compared to LDF, which results in a low temporal resolution [39].

2.2.3. LSCI versus LDI

LSCI is more sensitive to movement and assesses smaller surfaces compared to LDI. On the other hand, LSCI has a higher spatial and temporal resolution [39]. LDI uses a separate light source and detector, which allows this technique to measure perfusion at greater depths compared to LSCI. LSCI illuminates and detects the same area; it looks straight down from a spot [40].

2.3. Frequency analysis

This section is dedicated to the fundamentals of frequency analysis. The first subsection explains the sampling frequency. After that, the FA, discrete Fourier transform (DFT), continuous wavelet transform (CWT) and the discrete wavelet transform (DWT) are introduced. The last subsection gives an overview of the frequency bands corresponding to the biological mechanisms in the body.

2.3.1. Sampling frequency

The sampling frequency (f_s) is a critical parameter in the frequency analysis of both LSCI and LDPI measurements. The sampling frequency plays an important role due to the *Nyquist-Shannon Sampling Theorem*. It states that the maximal resolvable frequency (f_{max}) in the discrete setting must satisfy:

$$f_{max} \leq \frac{f_s}{2}. \tag{2.1}$$

Violation of the theorem leads to a concept called aliasing [37]. Aliasing is a false, distorted feature in signals

that occurs when higher frequencies are observed as lower frequencies [41]. This will become particularly important when FT and WT are introduced.

2.3.2. Fourier analysis

FA is widely used for simplifying data for data analysis. At the foundation of FA lies Fourier's theorem: any (reasonably well-behaved) function can be completely written in terms of the sum of sines and cosines of various amplitudes and frequencies. There are two types of Fourier expansions: Fourier series and FTs. Fourier series is applicable for periodic functions and the Fourier series allow this periodic function to be written into a sum of trigonometric functions:

$$f(x) = a_0 + \sum_{n=1}^{\infty} (a_n cos(\frac{n\pi x}{L}) + b_n sin(\frac{n\pi x}{L})). \tag{2.2}$$

However, most real-world physical phenomena are non-periodic, as this would imply an infinite amount of energy. Therefore, the extension of the Fourier series is introduced: the FTs. The FTs decomposes a general function, not necessarily periodic, as an integral of trigonometric functions. It transforms the function from the time domain into the frequency domain using [42]:

$$F(\omega) = \int_{-\infty}^{+\infty} f(t) e^{-2\pi i \omega t} \, dt. \tag{2.3}$$

2.3.3. Discrete Fourier transform

The DFT is defined as follows:

$$F[k] = \sum_{n=0}^{N-1} f[n] e^{-\frac{2\pi i n k}{N}}, k = 0, ..., N-1, n = 0, ...N-1. \tag{2.4}$$

N denotes the sample size and $f[n]$ is the truncated N-point discrete signal with period N [43].

As mentioned in Section 2.3.1, the Nyquist–Shannon Theorem states that the highest frequency that can be reconstructed is half the sampling frequency. Also interesting to note is the following identity:

$$F[N-k] = \sum_{n=0}^{N-1} f[n] e^{-\frac{2\pi i n (N-k)}{N}} = \sum_{n=0}^{N-1} f[n] e^{-\frac{2\pi i n N}{N}} e^{\frac{2\pi i n k}{N}} = \sum_{n=0}^{N-1} f[n] e^{\frac{2\pi i n k}{N}} = F[-k]. \tag{2.5}$$

This indicates that the negative frequencies are simply the mirrored versions of the positive frequencies. Therefore, it is only necessary to look at either the positive or negative frequencies, since they provide the same information. A fast way to compute the DFT is by using the Fast Fourier Transforms (FFT). This is not a new transformation, but a fast algorithm to compute the DFT. Using this algorithm reduces the computation from $O(N^2)$ to $O(N \log N)$ [44].

2.3.4. Continuous Wavelet transform

Traditional FA is limited to interpreting the signal exclusively in terms of the time or frequency domain. However, biological systems often generate non-stationary signals, requiring dynamic methods for accurate analysis. Heisenberg's uncertainty principle states that it is fundamentally impossible to have both perfect time and frequency resolution simultaneously [45]. WA addresses this constraint by finding a compromise between time and frequency resolution. By accepting minor sacrifices in the resolution in both domains, WT preserves temporal information, while also effectively characterizing frequency information, making it ideal for analyzing non-stationary signals [46].

A technique analogous to WA is the short time Fourier transform (STFT). The STFT is also able to retrieve both frequency and time information from a signal. The idea is to use a finite fixed length window function $g(t)$ and move it along the signal. For every step, FT is performed locally in that segment. Box-shaped windows introduce unwanted high-frequency content in the FT. Instead, the original signal $x(t)$ is multiplied by a smooth window (e.g., Gaussian), centered at time s. This process is called apodization. The STFT is as following:

$$F_{STFT}(s, \omega) = \int_{-\infty}^{+\infty} x(t) g(t-s) e^{-2\pi i \omega t} \, dt. \tag{2.6}$$

The performance of the STFT analysis is influenced by the selection of the window function $g(t)$. This choice inherently involves a trade-off between time resolution and frequency resolution. Shorter windows ensure more accurate temporal localization, but localize poorly in frequency. Longer windows on the other hand yield more precise frequency resolution at the expense of temporal precision. WT builds upon the fundamental concepts of the STFT. It also uses window functions, but instead of using fixed-length windows, WT introduces parameters that enable variable window sizing, allowing flexible time-frequency resolution [46][47][48].

Due to the fixed window function $g(t)$ for the STFT, all resolution cell sizes are equally sized (see Figure 2.1a). Low frequencies (equivalent to long wavelengths) tend to go on for a long time. Consequently, high temporal resolution becomes less important, while high frequency resolution is essential. Alternatively, higher frequencies (equivalent to short wavelengths) are transient and localized in time. Therefore, it is desirable to have a high time resolution, while not knowing the exact frequency value. This behavior is depicted in Figure 2.1b [49].

(a) (b)

Figure 2.1: The tiles represent the concentration of the resolution in the time-frequency plane. (a) Represents the distribution of the resolution for the STFT. (b) Represents the distribution of the resolution for the CWT. Reprinted from [47].

The CWT $W_x(a,b)$ of a time signal $x(t)$ is defined as follows [50]:

$$W_x(a,b) = |a|^{-\frac{1}{2}} \int_{-\infty}^{+\infty} x(t)\, \psi^* \left(\frac{t-b}{a} \right) dt. \tag{2.7}$$

The preceding equation can also be approximated and used for discrete time series [51]. The CWT is the inner product of the signal $x(t)$ and the complex conjugate of the translated and scaled versions of a function $\psi(t)$, also called the *mother wavelet*. The CWT decomposes the signal onto a set of basis functions, which are defined as the scaled and translated versions of the mother wavelet. Unlike the FT, which only uses sine and cosine functions as the basis functions, WT offers many choices. The mother wavelet has to satisfy the two conditions [47] [52]:

1. Admissibility condition:

$$\int_{-\infty}^{+\infty} \psi(t)\, dt = 0.$$

   This implies that the function does not contain a zero frequency component, which is equal to the average value of the function.

2. Finite energy:

$$\int_{-\infty}^{+\infty} |\psi(t)|^2\, dt < \infty.$$

   A wavelet means a small wave. This condition is exactly what makes the function localized in time.

Parameter b is denoted as the *translation parameter* and a is the *scale parameter*. For large values of a, the wavelet is stretched and corresponds to low-frequency components. On the other hand, for small values of a, the wavelet is made narrower, which captures high-frequency components. The center frequency (f_c) is a property of the mother wavelet and does not change. It describes the general behavior of the mother wavelet

by approximating the mother wavelet with a sine wave. The associated frequency is the center frequency [53]. The center frequency of the mother wavelet and the parameter a determines the frequency (f) the wavelet analyzes:

$$f = \frac{f_c}{a}. \tag{2.8}$$

This frequency changes for all different scaled wavelets. The translation parameter b slides the wavelet along the time axis to analyze different segments, similar to the STFT. The factor $|a|^{-\frac{1}{2}}$ is a normalization term and ensures that all scaled functions contribute equally to the transform and all have the same energy. Without this normalization factor, large-scale wavelets would always dominate, since those waves are more stretched out over time compared to low-scale wavelets. [47] [50].

Examples of mother wavelets for the CWT: complex Morlet (complex valued), Mexican Hat and Gaussian wavelets [54]. Among these, the complex Morlet wavelet is the most commonly used in signal analysis. The complex Morlet wavelet is a Gaussian function, combined with a complex sinusoid and is defined as follows (for $\omega_0 > 5$) [51]:

$$\psi(t) = \frac{1}{\pi^{\frac{1}{4}}} e^{-i\omega_0 t} e^{\frac{-1}{2}t^2}, \tag{2.9}$$

where ω_0 denotes the angular frequency. By choosing $\omega_0 = 2\pi$, the frequency and the scale are inversely proportional: $f = \frac{1}{a}$. The formula for the center frequency is [55]:

$$f_c = \frac{\omega_0}{2\pi} f_s. \tag{2.10}$$

The complex Morlet wavelet is one of the most used wavelets, particularly in the biological nature. The formula for time and frequency localization (defined as Δt and Δf respectively) of the complex Morlet wavelet is defined as follows (where f_c is the center frequency and f_b is the bandwidth (see Subsection 3.2.1)):

$$\Delta t = \frac{f_c\sqrt{f_b}}{2},\ \Delta f = \frac{1}{2\pi f_c\sqrt{f_b}}. \tag{2.11}$$

Note that the product $\Delta t \cdot \Delta f = \frac{1}{4\pi}$ only holds for wavelets close to the shape of a Gaussian. This bound serves as a lower bound for the time and frequency resolution. For wavelets not similar to the shape of a Gaussian, the product $\Delta t \cdot \Delta f$ is strictly larger than $\frac{1}{4\pi}$. This phenomenon is also known as the Heisenberg uncertainty principle [17][56]. The complex Morlet wavelet allows for the best time-frequency localization according to the Heisenberg uncertainty principle [14].

The results using CWT are often visualized using a scalogram. Examples of scalograms can be found in Subsection 3.2.1. A scalogram is the squared magnitude of the WT and gives the intensity of the wavelet coefficients in relation to time. Physiologically speaking, it can also be interpreted as the energy density and is given by [17][50]:

$$|W_x(a,b)|^2 = \left||a|^{-\frac{1}{2}} \int_{-\infty}^{+\infty} x(t)\, \psi^*\left(\frac{t-b}{a}\right) dt\right|^2. \tag{2.12}$$

2.3.5. Discrete Wavelet transform

The main difference between the CWT and the DWT is the choice for the scale and translation parameters a and b. In the discrete case, the values are limited and in the form: $a = a_0^j$, $b = kb_0a_0^j$, $k, j \in \mathbb{Z}$ (dyadic scale is often used, where $a = 2$) [46]. The DWT is obtained by discretizing the scale and translation parameters of the continuous wavelet transform [54]. Examples of mother wavelets are: Haar, Daubechies, Coiflets and Symflets [54]. The basis functions of the DWT are of the form:

$$\psi(\frac{n - kb_0a_0^m}{a_0^m}). \tag{2.13}$$

The terms *continuous* and *discrete* in WT can be misleading. They do not describe the signal that is continuous or discrete, but rather refer to how the parameters are being handled in the WT. To use the DWT on

discrete-time signals x[n], the integral in Equation 2.7 is discretized [50] (the CWT can also be discretized and applied to discrete signals in a similar way):

$$DDW_x(m,n) = \frac{1}{\sqrt{a_0^m}} \sum_k x[k]\psi(\frac{n - kb_0a_0^m}{a_0^m}). \tag{2.14}$$

DWT is often implemented with a fast Discrete Wavelet Transform algorithm proposed by Mallat [57], using a two-channel filter bank with different levels. A filter bank is a set of filters that can be divided into two subtypes: analysis bank and synthesis bank. The analysis bank decomposes the signal; it separates the signal into different frequency bands. The synthesis bank reverses the process of the analysis bank; it recombines the separated frequency bands to reconstruct the original signal. In digital signal processing, a conventional way to work is by normalizing the frequencies so that they are all in the range of 0 to π (such that 0 represents the lowest frequency in the signal and π represents the highest).

The analysis part consists of two steps:

1. **Filtering.**
   The analysis bank of DWT often has two filters, also known as the low-pass filter (LPF) and high-pass filter (HPF). Both filters contain half of the frequency interval (so in the normalized case, LPF contains frequencies in the range of $[0, \frac{\pi}{2}]$ and HPF contains frequencies in the range of $[\frac{\pi}{2}, \pi]$). The LPF is defined such that it gives an approximation of the signal. The filter smoothens the signal such that low-frequency components are preserved, while high-frequency components are suppressed. The HPF on the other hand, smoothens the low-frequency components, while keeping the high-frequency components. The HPF operates as a difference operator. In conclusion, the LPF retrieves the approximations and the HPF retrieves the details of a signal. After completion of the filtering part, downsampling will be applied.

2. **Downsampling.**
   After filtering, both the LPF and HPF maintain the original signal length, doubling the total amount of data. Downsampling resolves this redundancy, while preserving all the information. Since every filtered subband contains half of the frequency interval, according to the Nyguist-Shannon sampling Theorem (Subsection 2.3.1), the signal in such a filtering can be fully represented using half the sampling rate. Thus, the amount of data can be reduced in both filtering processes by retaining only the even-numbered components from the LPF and HPF outputs [47][58].

These two steps can be repeated for an arbitrarily amount, each step creating another level. Each level splits the low-frequency subband into two new subbands and the LPF and HPF are applied recursively. Level 1 separates the normalized frequency interval $[0, \pi]$ into $[0, \frac{\pi}{2}]$ (while applying the LPF) and $[\frac{\pi}{2}, \pi]$ (while applying the HPF). Level 2 separates the interval $[0, \frac{\pi}{2}]$ into $[0, \frac{\pi}{4}]$ and $[\frac{\pi}{4}, \frac{\pi}{2}]$, while applying the HPF on the subband $[\frac{\pi}{4}, \frac{\pi}{2}]$, resulting in more detailed results. A graphical representation of the described process can be found in Figure 2.2.

The ith level coefficients can be calculated as follows:

$$x_{i,H} = \sum_{k=0}^{K-1} x_{i-1,H}[2n-k]H[k], \tag{2.15}$$

$$x_{i,L} = \sum_{k=0}^{K-1} x_{i-1,L}[2n-k]L[k]. \tag{2.16}$$

where $H[k]$ and $L[k]$ denote the HPF and LPF respectively. K is the length of the filters. $x_{i,H}$ is the high-frequency coefficient at level i and $x_{i,L}$ is the low-frequency coefficient at level i. These coefficients are obtained by convolving the filters with the coefficients $x_{i-1,H}[2n-k]$ from level $i-1$. Using $2n$ instead of n ensures that only the even-numbered components are kept. [54]

When using DWT with filter banks, representing the wavelet coefficients as depicted in Figure 2.3 is more conventional. Following the methodology for the DWT described earlier, the original signal, $x(t)$, is decomposed. This results in Figure 2.3, where c_{lll} represents the frequency range $[0, \frac{\pi}{8}]$, c_{llh} represents $[\frac{\pi}{8}, \frac{\pi}{4}]$, c_{lh} represents $[\frac{\pi}{4}, \frac{\pi}{2}]$ and c_h represents $[\frac{\pi}{2}, \pi]$. Figure 2.2 provides additional clarity [47].

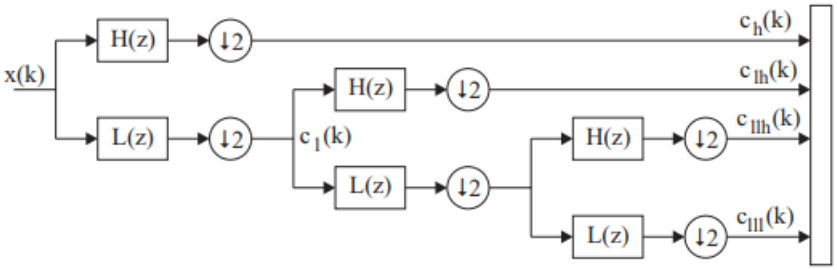

Figure 2.2: Three level filter bank. $x(k)$ is the signal, $H(z)$ represents the HPF and $L(z)$ represents the LPF. $\downarrow 2$ represents the process of downsampling with factor two. $c_i(k)$ are the coefficients at every level. Reprinted from [47].

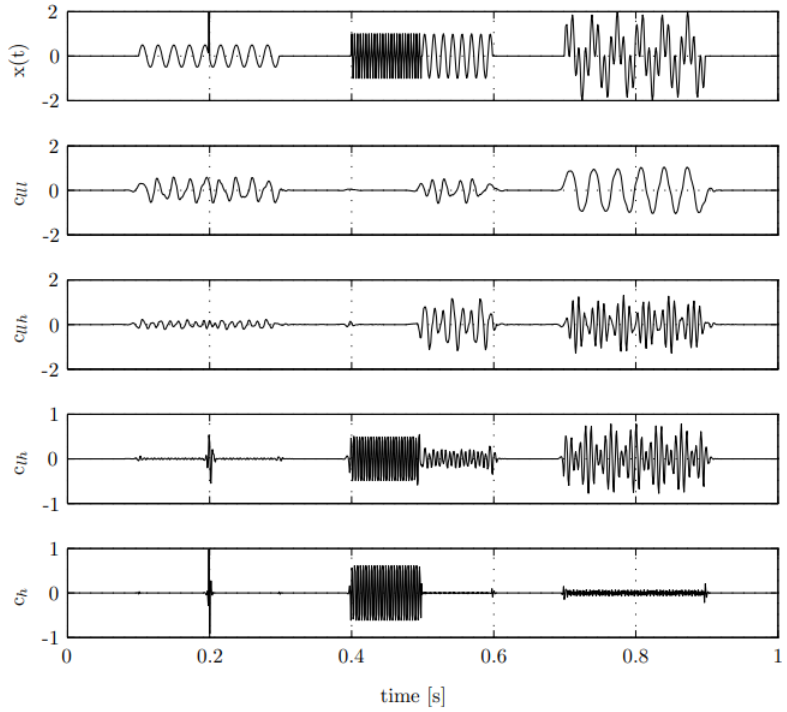

Figure 2.3: Subband representation of the DWT, using a three level filter bank (Figure 2.2 and a Daubechies 4 wavelet. The x-axis represents the time and the y-axis represents the wavelet coefficient. Reprinted from [47].

2.3.6. Frequency bands of biological mechanisms

In the previous subsections, various methods were described to perform a data transformation from the time to frequency domain. Here, these frequencies are interpreted in a physiological context with respect to blood perfusion by linking biological processes to specific frequency bands [13][15][16][17][59]:

1. **Frequency band from 0.4 to 2.0 Hz**: This is the frequency interval of the heartbeat. Under physiological steady state conditions, the heartbeat frequency of a human is approximately 1 Hz; the heart beats once per one second.

2. **Frequency band from 0.15 to 0.4 Hz**: This is the frequency interval of the respiratory function.

3. **Frequency band from 0.06 to 0.15 Hz**: This is the frequency interval attributed with the smooth muscle cells. The peak is around 0.1 Hz.

4. **Frequency band from 0.02 to 0.06 Hz**: This frequency interval is associated with neurogenic activity. Neurogenic activity is important in the regulation of blood pressure, by regulating the radius of the blood vessels. The peak is around 0.04 Hz.

5. **Frequency band from 0.0095 to 0.02 Hz**: This is the frequency interval of the endothelial activity and it is NO-dependent in this frequency domain.

6. **Frequency band from 0.005 to 0.0095 Hz**: This is the frequency interval of the endothelial activity, but now NO-independent.

As discussed in Section 2.1, endothelial activity modulates blood flow through release of substances like NO. To investigate vascular regulation with respect to NO, the frequency domain of 0.0095-0.02 Hz can be examined, as this interval looks at the NO-dependent endothelial activity.

Unlike NO, CGRP does not yet have a clearly defined frequency band. However, since NO can lead to an increase in CGRP release (see Section 2.1), the frequency domain 0.095-0.02 Hz may also indirectly reflect influences on the blood flow mediated by CGRP. Furthermore, Section 2.1 also discussed about the effect of neuropeptides on the smooth muscle cell function. This suggests that the frequency interval of 0.06-0.15 Hz may also reflect effects of CGRP. Lastly, the frequency band 0.02-0.06 Hz corresponding to neurogenic activity could also be relevant, as studies show that CGRP is the most potent vasodilaroty neuropeptide in the migrane pathophysiology [60].

3

Methods

3.1. The VASCULAR-study

The main objective of the VASCULAR-study, conducted by Erasmus MC, was to assess and compare the microvascular function of women with and without migraine. The research population consisted of healthy women, aged 40-60 years. Participants had no prior medical history of vascular or cardiovascular diseases. Measurements were performed on the forearm using LSCI and LDPI (see Section 2.2). The measurements can be divided into three phases. The first five minutes are called the *baseline phase*. Subsequently, the forearm was heated to 40°C, initiating the *peak phase*. Local heating of the skin increases the dermal blood flow, leading to an increase in the blood perfusion in this peak phase. After approximately 30 minutes, the blood perfusion stabilizes. This also marks the beginning of the *plateau phase*, where the blood perfusion remains stable. An example of the data including the different phases is shown in Figure 3.1.

Three areas of the forearm, also called the Region of Interest (ROI), were isolated for the application of different experimental techniques.

1. In ROI 1, NG-monomehtyl-L-arginine (L-NMMA), a NO inhibitor [61], was administered to the skin via iontophoresis. Iontophoresis a non-invasive method used to facilitate the transdermal delivery via low-intensity electric current [62]. Iontophoresis ensures that the L-NMMA is properly delivered in the parts of the skin where the blood perfusion is measured, blocking the production of NO.

2. In ROI 2, eutectic mixture of local anesthetics (EMLA) cream was applied on the skin. EMLA cream acts as a local anesthetic, thereby preventing release of neuropeptides.

3. In ROI 3, nothing was applied to the skin. This region served as a control region.

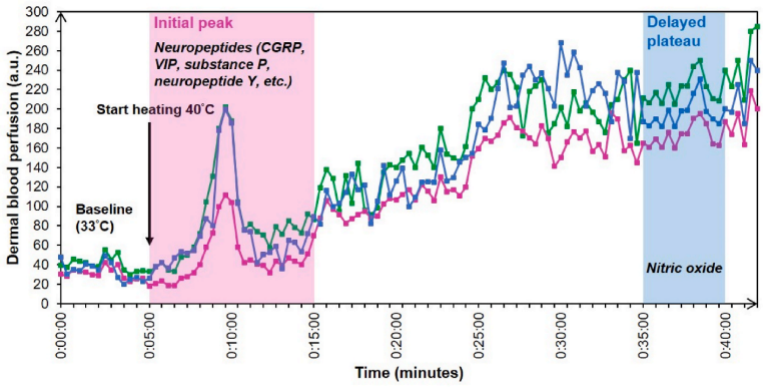

Figure 3.1: Example of data of VASCULAR-study. The first five minutes indicate the baseline. The pink region illustrates the peak phase. The blue region represents the plateau phase. ROI1 is shown in blue, ROI2 in red and ROI3 in green. Reprinted from [9].

3.2. Frequency analysis

This section explains how the frequency analysis was performed. Subsection 3.2.1 describes the implementation details of the WT. Subsection 3.2.2 provides an explanation of how WT was used to extract quantitative information. Finally, Subsection 3.2.3 outlines how this quantitative information was compared using statistical analysis.

3.2.1. Implementation details of the WT

All computations were done using Python. To perform the WT, the PyWavelets library was used. The function *pywt.cwt* takes three arguments:

1. **data**
   The input signal to use.

2. **scales**
   The scales to use. In theory, the CWT uses infinitely many scales and translation parameters. In practice, this is not realizable due to memory and time restrictions. The difference between CWT and DWT is how the scales are discretized. The CWT discretizes the scale much more refined compared to the DWT. The translation parameters are taken care of by the function itself. Wavelet scales and frequencies are not the same. The function *pywt.scale2frequency* was used to convert the scales to the physical frequencies.

3. **wavelet**
   Mother wavelet to use. Examples: Mexican hat wavelet (mexh), Gaussian wavelets (gaus), Morlet wavelets (morl) and complex Morlet wavelets (cmorf_b-f_c, where f_b is the bandwidth and f_c is the center frequency). In Figure 3.2, different values for f_c and f_b are plotted as examples. It demonstrates the importance of choosing appropriate values. The choice for f_b and f_c are highly dependent on the signal itself. An increase in the center frequency parameter f_c results in more oscillations in the Gaussian window of the wavelet. Figure 3.2a illustrates that increasing the value of f_c leads to an increase in the number of oscillations. The bandwidth parameter f_b is also known as the time-decay parameter and controls the decay in the time domain. A smaller value of f_b causes the wavelet to decay more rapidly in time. On the other hand, increasing the value of f_b results in slower decay of the wavelet in the time domain [63]. Consequently, a smaller value for f_b results in better time resolution, while a larger value for f_b results in better frequency resolution. All described behavior can be observed in Figure 3.2 (by comparing the columns for the center frequency values f_c and the rows for the bandwidth parameter f_b).

The function returns two results:

1. **coefs**
   This is a 2D array. The rows correspond to specific scales and the columns correspond to the time step. Then *coefs*$[i, j]$ corresponds to the scale on the ith position of the given argument *scales* at time step j.

2. **frequencies**
   An array with the scales converted to the physical frequencies.

For the choice of mother wavelet, the complex Morlet wavelet was selected to use in this study. In numerous studies [12][13][14][16][59][65] measuring blood flow via LDF and LSCI, the complex Morlet wavelet is the commonly used mother wavelet. The complex Morlet wavelet in Python is given by:

$$\psi(t) = \frac{1}{\sqrt{\pi f_b}} e^{-\frac{t^2}{f_b}} e^{i2\pi f_c t}. \tag{3.1}$$

For the Morlet wavelet to be admissible, the wavelet must satisfy $2\pi f_c \geq 5$. In other words, f_c should be greater than approximately 1 Hz [66]. Since higher values analyze higher frequency components, $f_c = 1$ was chosen, as the frequencies of interest are relatively low. The choice of f_b directly influences the balance between the time and frequency resolution. This is visualized in Figure 3.3. For $f_b = 0.3$, Figure 3.3a shows high temporal resolution, but the frequencies appear spread out. On the other hand, for $f_b = 5.0$, Figure 3.3b is blurred around the time axis. The commonly used function for the complex Morlet wavelet is defined by Equation 2.9.

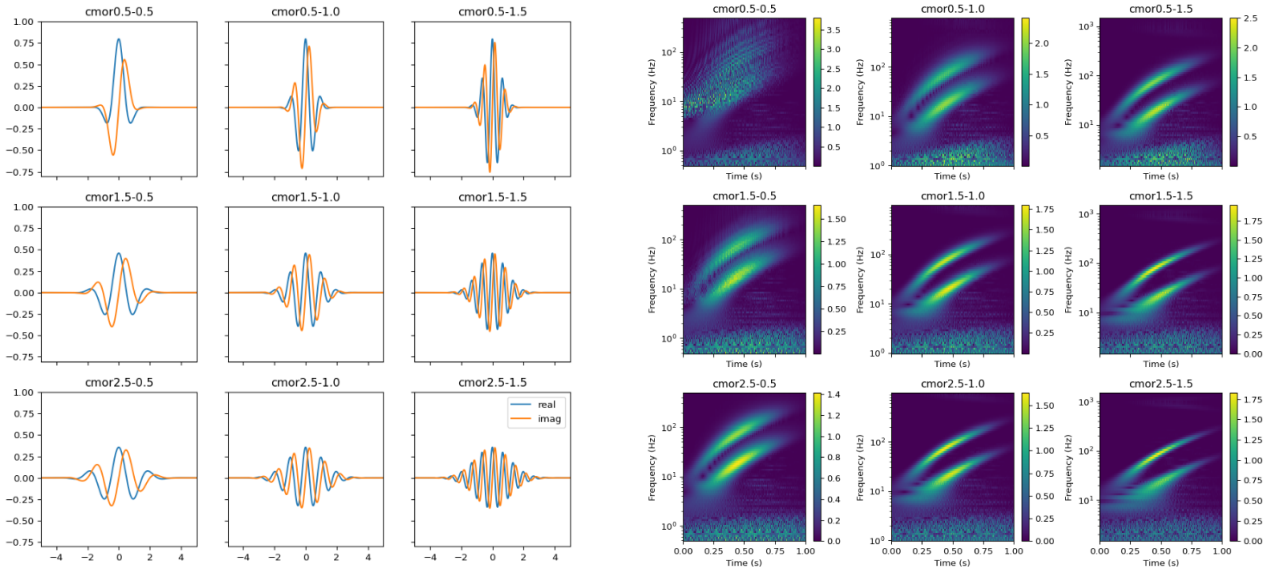

(a) (b)

Figure 3.2: Example of different values for f_b and f_c (cmorf_b-f_c). (a) Represents the complex Morlet wavelets with different values for f_b and f_c. (b) Represents the scalograms of complex Morlet wavelets applied to the same signal. Reprinted from [64].

To align the coefficients in the exponential term, $f_b = 2$ was chosen. Note that this changes the normalization factor. However, this choice was made since the coefficients in the exponential term were considered more critical than maintaining the original normalization term. Equation 3.1 becomes:

$$\psi(t) = \frac{1}{\sqrt{2\pi}} e^{-\frac{t^2}{2}} e^{i2\pi t}. \tag{3.2}$$

Combining Equation 2.8 and 2.10 with $\omega_0 = 2\pi$, $f_s = 1$ and using the Nguist-Shannon Sampling Theorem results in:

$$f_{max} = \frac{\frac{2\pi}{2\pi} f_s}{a} = \frac{1}{a} \leq 0.5 \Rightarrow a = \frac{1}{f_{max}} \geq 2. \tag{3.3}$$

Low frequencies require long wavelets for reliable detection. The maximum usable scale depends on the total length of the signal. Conventionally, it is limited to one-sixth of the entire signal. In this study, the signal is approximately 45 minutes, or equivalently, 2.700 seconds. The longest usable wavelet corresponds to 450 seconds. This translates to to 0.0022 Hz in the frequency domain. The lowest frequency of interest is set 0.005 Hz. Thus, there is no limitation on the maximum value of the scale [67].

WA was performed on the dataset from the VASCULAR-study to assess the potential differences between women with and without migraine. The frequency band between 0.005 Hz and 0.5 Hz was studied. The frequency bands associated with different biological mechanisms, defined in Subsection 2.3.6, was spanned from 0.05 Hz to 2 Hz. However, since the sampling frequency is 1 Hz, the Nyguist-Shannon Sampling Theorem justified the use of the range 0.005 Hz and 0.5 Hz. The associated scales of interest were $s_{min} = 2$ and $s_{max} = 200$. The high values for the scales correspond to low frequencies and the low values for the scale correspond to high frequencies. The scales were discretized exponentially [68]:

$$a_i = a_0 \cdot 2^{\frac{i}{v}},\ i = 1,2,3,\ldots\ and\ v > 1\ (common\ values\ are\ v = 10,12,14,16,32). \tag{3.4}$$

This prevented oversampling of high-frequencies or undersampling of low frequencies. In Equation 3.4, v refers to the number of voices per octave. An octave is a doubling of the scale (e.g. start at 0.5 Hz to 1.0 Hz, then the next octave is from 1.0 Hz to 2.0 Hz). The voices v determine the intermediate steps between the octaves. In this study, v was set to 10 [68][69].

For infinite-length signals, edge effects do not occur when applying the CWT or DWT. However, for finite-length signals, distortions can appear near the edges. The boundary that separates the artifact coefficients

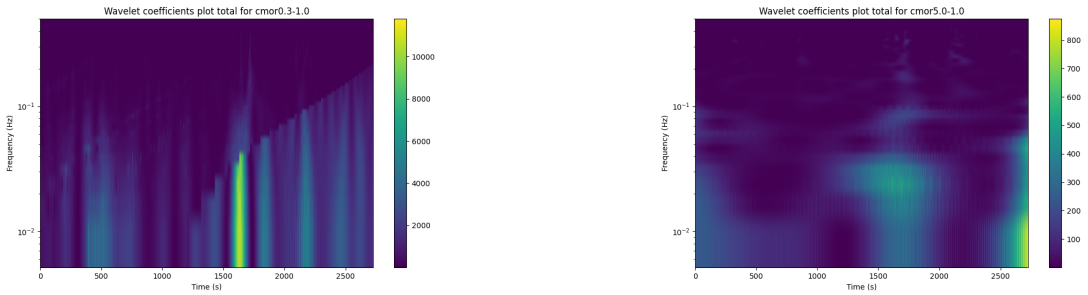

(a) (b)

Figure 3.3: Scalograms of the complex Morlet wavelet for different values. (a) Scalogram for cmor0.3-1.0. (b) Scalogram for cmor5.0-1.0.

from the accurately computed coefficients is known as the cone of influence (COI). The artifacts at the edges appear when convolving the signal and the wavelet function at the beginning and end of the signal. The artifact coefficients depend on the wavelet scales. Larger scales result in more artifacts; therefore, the boundary is a cone shape [70].

To delineate the COI, an approximation based on the $\frac{1}{e^2}$ rule was used. The threshold $\frac{1}{e^2} \approx 0.135$ corresponds to the point where the wavelet energy has decreased to around 13.5% of the maximum value, which is the energy at the center. Regions where the wavelet energy is below this threshold are considered unreliable and cause edge effects. The e-folding time is the time that it takes for the wavelet energy to decrease to $\frac{1}{e^2}$. For Morlet wavelets, this is equal to $\sqrt{2}a$, where a denotes the scale parameter [71][72]. An example can be found in Figure 3.4. Note that because of the edge effect, the accurate coefficients were no longer visible in Figure 3.4a. After removing the COI in Figure 3.4b, the accurately computed coefficients were more visible.

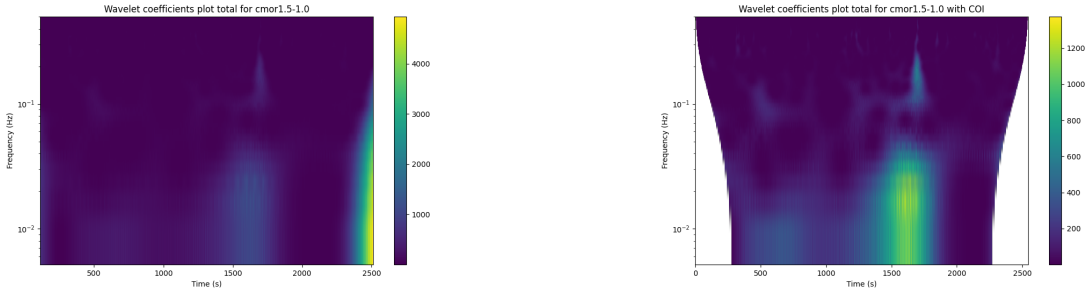

(a) (b)

Figure 3.4: Scalograms of the complex Morlet wavelet with COI and without COI. (a) Scalogram for cmor1.5-1.0 with COI and without applying $\frac{1}{e^2}$ rule. (b) Scalogram for cmor1.5-1.0 without COI and with applying $\frac{1}{e^2}$ rule.

This technique is most effective when the total measured signal is longer than the portion of the signal that is being analyzed. However, that was not the case in the VASCULAR-study data. Removing the COI would result in significant data loss. Therefore, an alternative approach was necessary. To avoid cutting parts of the results, the signal was extended at the start and the end. While several extension techniques were available, this research achieved it using reflection [73]. This was done by reversing the signal and concatenate this to the start and end of the signal. Figure 3.5 shows an example after applying reflecting.

3.2.2. From WT to quantitative information

In order to make a comparison between the different ROIs (defined in Section 3.1) and between blood flow measurements of distinct participants, quantitative measures were needed. The scalogram was introduced in Subsection 2.3.4 as a visualization of the energy density. An alternative visualization approach involved plotting the coefficients in three-dimensional space. Although Figure 3.5 offered valuable insights, it was not enough to extract quantitative information to compare the two groups. Therefore, the following parameters

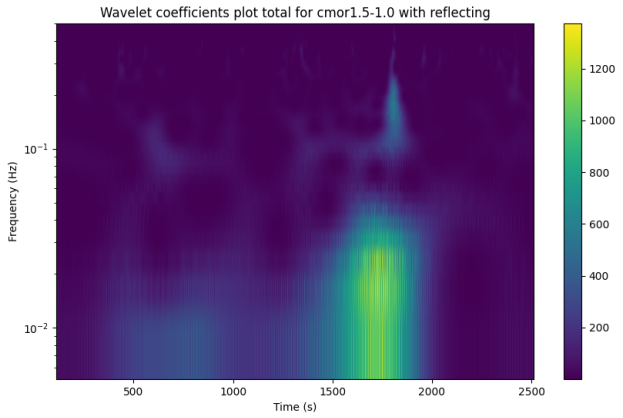

Figure 3.5: Scalogram using the complex Morlet wavelet with center frequency equal to 1.0 and bandwidth equal to 1.5 after applying reflection.

were calculated to perform quantitative analysis on the data: absolute and relative energy density of the total spectrum; relative energy density of each interval corresponding to different biological mechanisms (Subsection 2.3.6). The energy density is the energy per unit length, area or volume [74].

The frequency intervals were analyzed separately and divided as follows (note that the frequency interval related to cardiac activity was not used):

- $f_{11} = 0.4$, $f_{12} = 2.0$ for cardiac activity,
- $f_{21} = 0.15$, $f_{22} = 0.4$ for respiratory activity,
- $f_{31} = 0.06$, $f_{32} = 0.15$ for smooth muscle cells activity,
- $f_{41} = 0.02$, $f_{42} = 0.06$ for neurogenic activity,
- $f_{51} = 0.0095$, $f_{52} = 0.02$ for endothelium activity (NO-dependent),
- $f_{61} = 0.005$, $f_{62} = 0.0095$ for endothelium activity (NO-independent).

The physical quantity behind the scalogram is the energy density. The average energy density (over time) on a given frequency interval $\mathscr{E}_i(f_{i1,i2})$ is given by:

$$\mathscr{E}_i(f_{i1}, f_{i2}) = \frac{1}{t}\int_0^t \int_{\frac{1}{f_{i2}}}^{\frac{1}{f_{i1}}} \frac{1}{a^2}|W_x(a,b)|^2 \, da\, dt. \tag{3.5}$$

Since the wavelet coefficients are discrete data points, the integral was approximated using the trapezoidal rule (implemented using the $np.trapz$ function in Python).

The relative average energy density is defined as follows:

$$e_i(f_{i1}, f_{i2}) = \frac{\mathscr{E}_i(f_{i1,i2})}{\mathscr{E}_{total}}, \tag{3.6}$$

where $\mathscr{E}_{total}$ is the energy of the signal contained in the total frequency interval, between 0.005 and 0.5 Hz.

An useful tool for comparing and visualizing the calculated energy densities are box plots. A box plot shows the median, which is a horizontal line that indicates the center of the data: 50% of all data lie below and 50% lie above. A box is drawn from the first quartile (Q1) to the third quartile (Q3). A quartile marks 25% of the data. One vertical line goes from the minimum value to Q1 and the other vertical line goes from Q3 to the maximum value. These vertical lines are often called whiskers. However, if the minimum or maximum value exceeds 1.5 times the interquartile range (IQR), which is the range from the third quartile to the first quartile (Q3-Q1), the whiskers stop at the last value within that range. Data values that exceed the IQR are called outliers and are frequently shown as individual dots.

3.2.3. Statistical analysis

A tool was still needed to compare the different values from different measurements of the group of women with migraine and the group of women without migraine. This was done using p-values. The p-value represents the probability of observing results that would have occurred by chance, assuming the null hypothesis is true [75]. A p-value less than 0.05 was considered statistically significant. In this study, two different statistical tests were used to obtain the p-values: the Mann-Whitney U-Test and the Wilcoxon Signed Rank Test.

The Mann-Whitney U-Test is a non-parametric test that compares two independent groups. The test is the non-parametric counterpart of the t-test. The null hypothesis from this test is that the two groups come from the same population, the alternative hypothesis is that the two groups are not from the same population. The test does not assume a normal distribution of the data. Rather than comparing the difference in mean values, the Mann-Whitney U-Test compares the rank sum. All data from both groups are combined and ranked. Then for each group, the ranks are summed. These rank sums are subsequently used to calculate a U statistic, which is used to determine the p-value. This test was used to determine whether there were significant differences between the group of women with migraine and the group of women without migraine [76].

To determine the significance of results within the same group— whether among participants with migraine or those without—the Wilcoxon Signed Rank Test was used. The Wilcoxon Signed Rank Test is a non-parametric equivalent of the paired t-test and also does not assume normality of the distribution of the data. The difference with the Mann-Whitney U-Test is that the Wilcoxon Signed Rank Test compared dependent groups. It calculates the difference between the paired values and ranks them accordingly. Then, the rank sums are computed for the positive and negative differences. The test statistic W is calculated and used to determine the p-value [77].

3.3. Method overview

In the following chapter, the results of the study are presented. In this section, a systematic overview of how the results were interpreted and compared will be given. This study comprised a wide range of different combinations to study, resulting from the comparison of two groups across three phases (baseline, peak and plateau) and three ROIs (ROI1, ROI2 and ROI3).

In this study, the respiratory activity, smooth muscle cells activity, neurogenic activity and endothelium activity (both NO-dependent and NO-independent) were studied in women with and without migraine. This was done by calculating the relative energy density for each group individually. Using the p-value, the differences between the two groups were examined. A p-value smaller than 0.05 was considered statistically significant. This method was applied to examine the following:

1. Analysis of differences of absolute energy density between women with migraine and without migraine across the entire measurement region using WT.
2. Analysis of differences between women with migraine and without migraine across the entire measurement region using the WT and DFT.
3. Analysis of differences between women with migraine and without migraine using WT, looking at the baseline, peak and plateau phase individually and DFT.
4. Analysis of differences in the DFT and WT method.

4

Results

In this chapter, the results will be presented and interpreted, integrating all the information gathered throughout the study, by building on the foundation of all fundamental concepts introduced in Chapter 2 and the methods described in Chapter 3. In Section 4.1, examples of scalograms and three-dimensional plots using the VASCULAR-study data are shown. Section 4.2 shows and compares the absolute energy density of the women without migraine and the women with migraine. Section 4.3 and 4.4 show the results using WT. Section 4.5 and 4.6 show the results using DFT.

4.1. Examples of resulting plots

In the previous chapters, visualization tools were introduced as useful tools for displaying wavelet coefficients. This section is dedicated to introduce these visualization tools for illustrative purposes. However, for quantitative analysis, these illustrative tools are not used in this research.

4.1.1. Scalogram

Scalograms were introduced in Subsection 2.3.4 and show the squared wavelet coefficients. The physiological interpretation is the energy density, which will be used as a quantitative measurement for the wavelet coefficients. Examples can be found in Figure 4.1, Figure 4.2 and Figure 4.3. The colors indicate the intensities. Not all scalograms had similar shapes and color intensities. The scalograms in Figure 4.1, Figure 4.2 and Figure 4.3 show a notable increase in color intensity around 1500 seconds. This time point fell outside the defined baseline, peak and plateau phase and was right between the peak and plateau phases. Capturing this pattern required analysis of the entire measurement period (from the start of the baseline phase to the end of the plateau phase). An explanation of this behavior at approximately 1500 seconds is currently not known, since this period in the measurements does not correspond to a well-defined phase like the baseline, peak or plateau phase and thus requires further investigation. This topic is further discussed in Section 4.2.

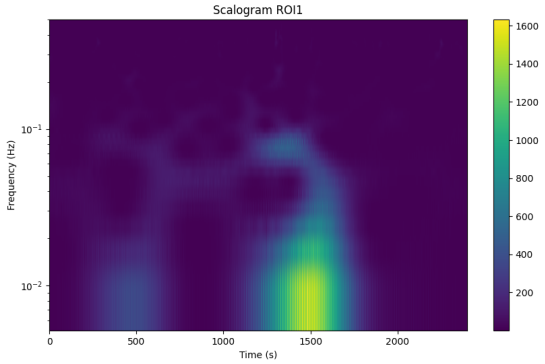

Figure 4.1: Example of scalogram of the WT coefficients for ROI1 and women without migraine. The axes represent frequency (Hz) in log scale, time (s) and the color indicates the intensity (magnitude) of the coefficient, in arbitrary units (AU).

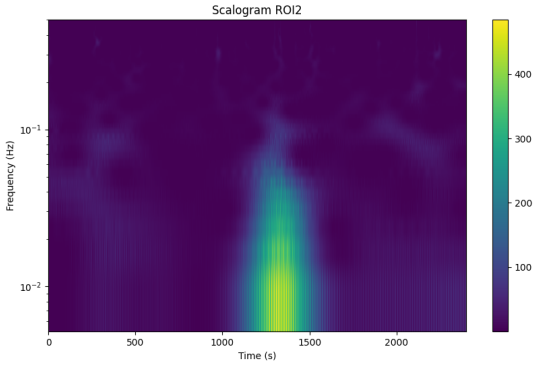

Figure 4.2: Example of scalogram of the WT coefficients for ROI2 and women without migraine. The axes represent frequency (Hz) in log scale, time (s) and the color indicates the intensity (magnitude) of the coefficient, in arbitrary units (AU).

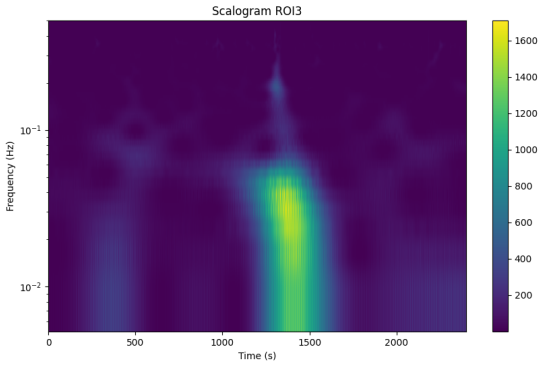

Figure 4.3: Example of scalogram of the WT coefficients for ROI3 and women without migraine. The axes represent frequency (Hz) in log scale, time (s) and the color indicates the intensity (magnitude) of the coefficient, in arbitrary units (AU).

4.1.2. Absolute values of wavelet coefficients

The scalogram displays the squared wavelet. Therefore, the visibility of high-magnitude values was more enhanced compared to the lower values. Alternatively, it is possible to plot the absolute values of the wavelet coefficients of the same data used for the scalograms in Figure 4.1, Figure 4.2 and Figure 4.3. These can be found in Figure 4.4, Figure 4.5 and Figure 4.6.

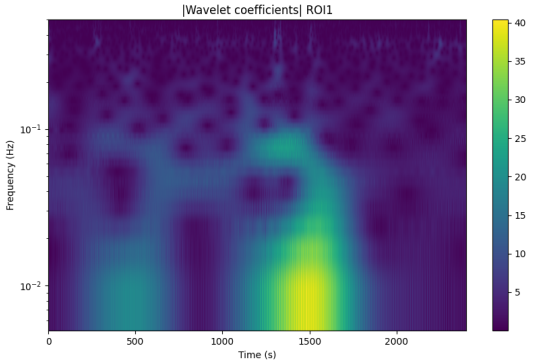

Figure 4.4: Example plot of absolute values of the WT coefficients for ROI1 and women without migraine. The axes represent frequency (Hz) in log scale, time (s) and the color indicates the intensity (magnitude) of the coefficient, in arbitrary units (AU).

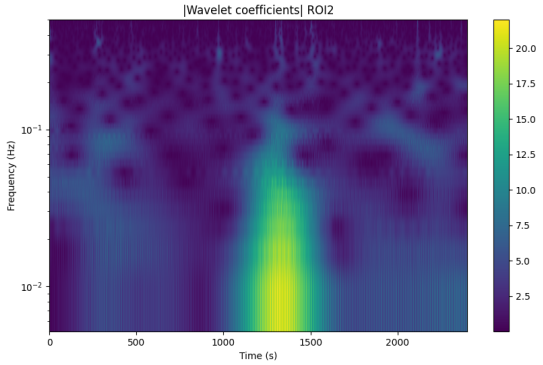

Figure 4.5: Example plot of absolute values of the WT coefficients for ROI2 and women without migraine. The axes represent frequency (Hz) in log scale, time (s) and the color indicates the intensity (magnitude) of the coefficient, in arbitrary units (AU).

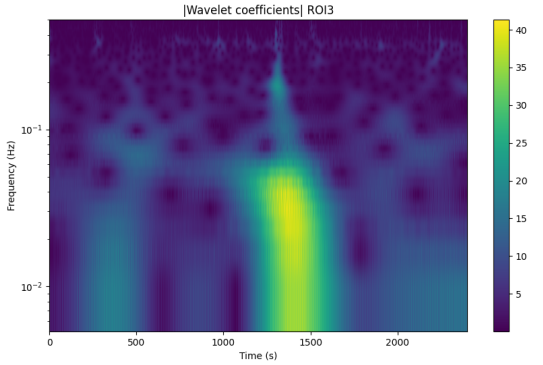

Figure 4.6: Example plot of absolute values of the WT coefficients for ROI3 and women without migraine. The axes represent frequency (Hz) in log scale, time (s) and the color indicates the intensity (magnitude) of the coefficient, in arbitrary units (AU).

4.1.3. Three-dimensional plot

In Subsection 3.2.2, an example three-dimensional plot has already been shown. Figure 4.7, Figure 4.8 and Figure 4.9 illustrate the three-dimensional plots, generated using the same data that was used to create the scalograms. The figures show the absolute value of the wavelet coefficients.

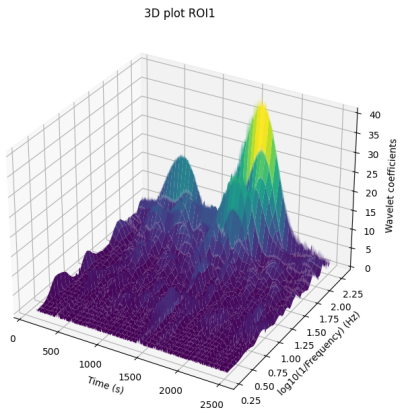

Figure 4.7: Example of three-dimensional plot of the absolute values of the WT coefficients for ROI1 and women without migraine. The axes represent frequency (Hz) in log scale, time (s) and WT coefficients, in arbitrary units (AU).

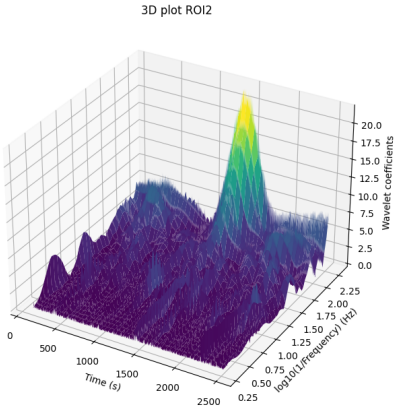

Figure 4.8: Example of three-dimensional plot of the absolute values of the WT coefficients for ROI2 and women without migraine. The axes represent frequency (Hz) in log scale, time (s) and WT coefficients, in arbitrary units (AU).

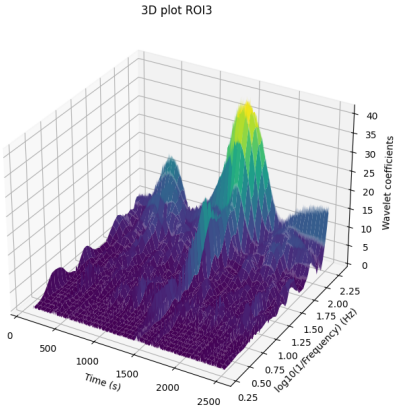

Figure 4.9: Example of three-dimensional plot of the absolute values of the WT coefficients for ROI3 and women without migraine. The axes represent frequency (Hz) in log scale, time (s) and WT coefficients, in arbitrary units (AU).

4.2. Average energy density

To determine the average energy density for each group, the individual energy densities were summed and divided by the number of women in that group. Figure 4.10 presents the resulting average energy density plots for women without migraine and women with migraine in the different ROIs. Notably, an significant increase in color intensity was observed around 1500 seconds for women with migraine. This phenomenon was previously noticed in Subsection 4.1.1 for a woman without migraine, where the underlying cause was found to be unclear. Figure 4.10 shows that, on average, the color intensity around 1500 was much higher for women with migraine compared to women without migraine. Figures 4.11, 4.12 and 4.13 illustrate the differences in energy density between the two groups in the different ROIs. These plots further support the observation that women with migraine exhibited increased color intensity around 1500 seconds.

Using Equation 3.5, the average energy density (over time) was calculated for the different ROIs for each women in both groups. The p-values comparing the two groups across the ROIs indicated no significant differences ($p = 0.22$, $p = 0.26$ and $p = 0.11$ respectively).

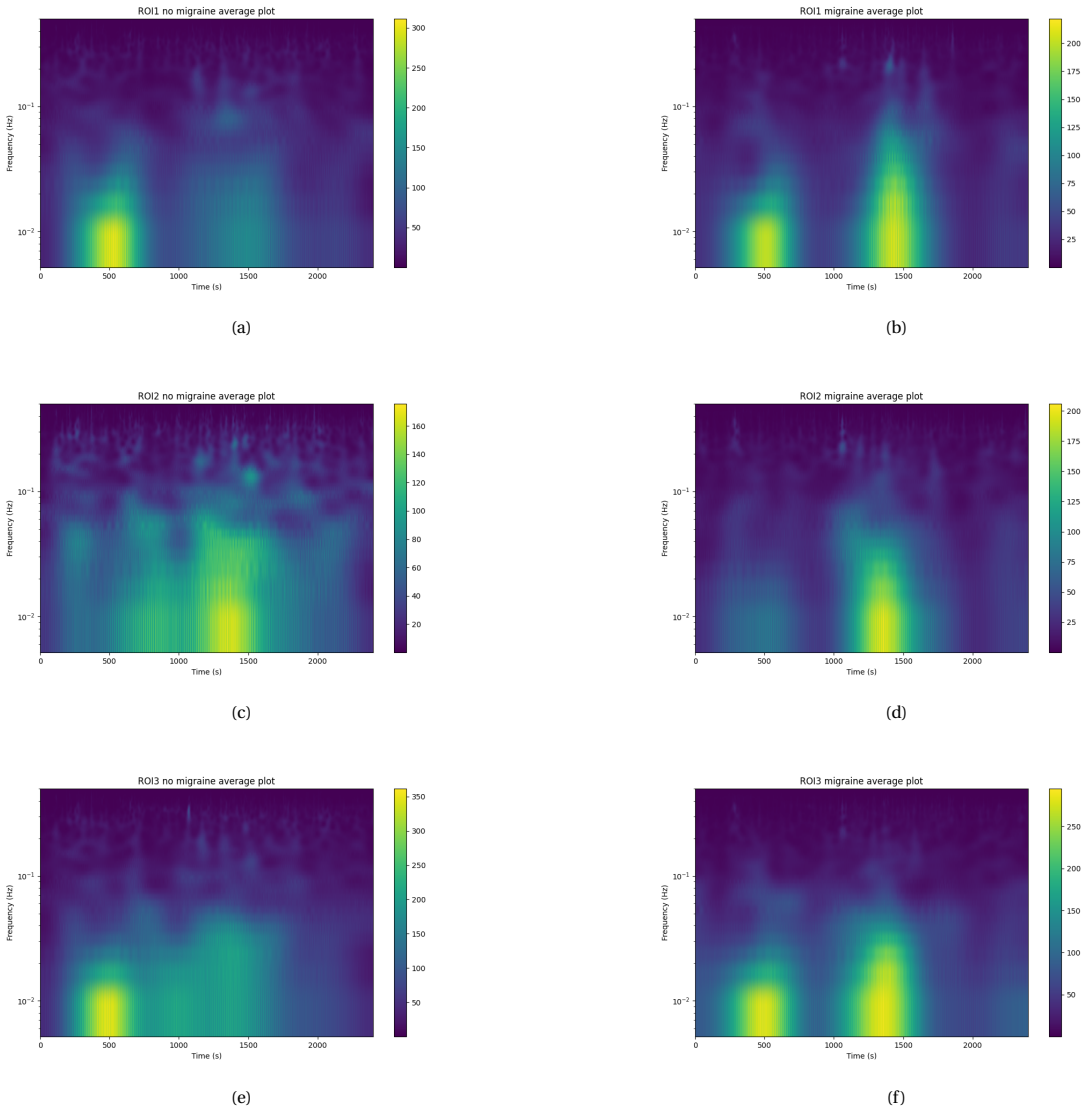

(a) (b) (c) (d) (e) (f)

Figure 4.10: Plots of average values for energy density for (a) women without migraine in ROI1 (b) women with migraine in ROI1 (c) women without migraine in ROI2 (d) women with migraine in ROI2 (e) women without migraine in ROI3 (f) women without migraine in ROI3.

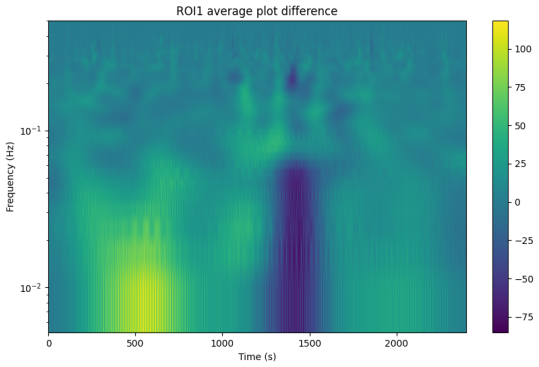

Figure 4.11: Plot of difference between the average values of women without migraine and women with migraine in ROI1 (no migraine - migraine). Negative values indicate larger values for women with migraine.

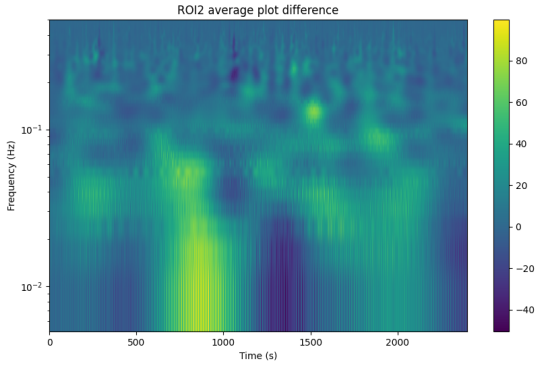

Figure 4.12: Plot of difference between the average values of women without migraine and women with migraine in ROI2 (no migraine - migraine). Negative values indicate larger values for women with migraine.

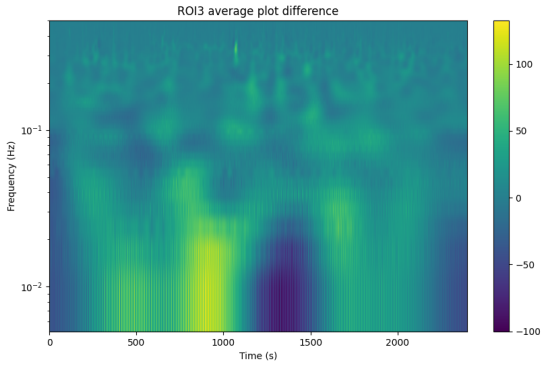

Figure 4.13: Plot of difference between the average values of women without migraine and women with migraine in ROI3 (no migraine - migraine). Negative values indicate larger values for women with migraine.

4.3. Entire measurement region evaluation using WT

In this section, before looking at the different phases (baseline, peak and plateau), the entire measurement region was evaluated for ROI1, ROI2 and ROI3 individually. A statistical analysis, as outlined in Subsection 3.2.3, was conducted to determine the significance of the results. P-values below 0.05 were considered significant. Only tables with statistically significant results are shown. The remaining tables can be found in Appendix A.1. For the evaluation of the entire measurement region using WT, there were only significant results for the respiratory activity.

4.3.1. Respiratory activity

Table 4.1 shows a significant difference in ROI1 ($p = 0.02$). The boxplot in Figure 4.14 shows higher values for the group of women with migraine. When comparing the values for ROI1 and ROI3 (control region) within the group of women without migraine and the group of women with migraine separately, no significant differences were found ($p = 0.86$ and $p = 0.22$ respectively). This suggested that the significantly higher values in women with migraine were not due to a process occurring specifically in ROI1. Table 4.1 supports this claim: the p-value for ROI3 may not be significant ($p = 0.09$).

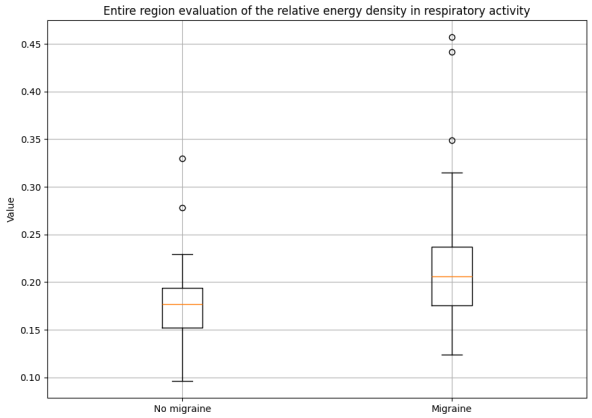

Figure 4.14: Boxplot of relative energy density of women without (left) and with migraine (right) for ROI1, across the entire measurement region.

Relative energy density respiratory activity			
Blank	No migraine	Migraine	Significance ($p < 0.05$)
ROI1	0.18 (0.10-0.33)	0.21 (0.12-0.46)	Yes ($p = 0.02493$)
ROI2	0.19 (0.12-0.32)	0.19 (0.12-0.37)	No ($p = 0.52586$)
ROI3	0.17 (0.11-0.31)	0.20 (0.14-0.44)	No ($p = 0.09478$)

Table 4.1: Table of p-values for the relative energy density, evaluated across the entire measurement region of the respiratory activity of women with and without migraine, for all different ROIs. Mean values and ranges are given in each case.

4.4. Evaluation of phase characteristics using WT

In this section, the results obtained using the WT and the method described in Section 3.3 are presented. An evaluation of the whole measurement region using WT (see Section 4.3) only showed significant results in respiratory activity. A statistical analysis, as outlined in Subsection 3.2.3, was conducted to determine the significance of the results. P-values below 0.05 were considered significant. This was done for all different frequency domains, each corresponding to a distinct biological mechanism. Only tables with statistically significant results are shown. The remaining tables can be found in Appendix A.2. For the evaluation of phase characteristics using WT, there were only significant results for respiratory activity and endothelial activity (NO-dependent).

4.4.1. Respiratory activity

Table 4.2 shows a significant difference ($p = 0.01$) in respiratory activity between the group of women without migraine and women with migraine in the peak phase of ROI1. Figure 4.15 displays the boxplot of the relative energy density of women without migraine and women with migraine. It shows that the values of women with migraine are higher compared to women without migraine. Together, these findings indicated that women with migraine had a significantly higher relative energy density in the peak phase of ROI1. The observed difference was not due to a general increase across all three regions, but especially for the peak phase in ROI1. The p-values for women without migraine and women with migraine individually of ROI1 and ROI3 were $p = 0.94$ and $p = 0.01$ respectively, which indicated that for women with migraine there was a significant difference between ROI1 and the control region. The values for women with migraine were higher in ROI1 compared to ROI3. This result suggests that there was a difference in respiratory activity between women with and without migraine in the peak phase of ROI1. Studies [78][79] suggest that there is an association between migraine and respiratory disorders, such as asthma and bronchitis. However, since the relative energy density appeared to be higher in women with migraine compared to women without migraine, and the difference was only significant during the peak phase of ROI1, the biological interpretation of this result remained uncertain. The interpretation of these results should be taken with caution. The reliability is uncertain, since no women with migraine with respiratory problems were included in this research.

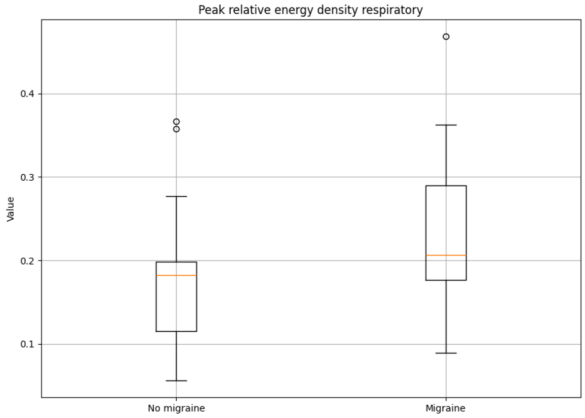

Figure 4.15: Boxplot of relative energy density of women without (left) and with migraine (right), in the peak phase of ROI1.

Relative energy density respiratory activity			
Blank	No migraine	Migraine	Significance ($p < 0.05$)
ROI1 Baseline	0.20 (0.10-0.39)	0.22 (0.06-0.71)	No ($p = 0.07840$)
ROI1 Peak	0.18 (0.06-0.37)	0.21 (0.09-0.49)	Yes ($p = 0.01333$)
ROI1 Plateau	0.20 (0.13-0.34)	0.22 (0.10-0.49)	No ($p = 0.66155$)
ROI2 Baseline	0.22 (0.11-0.43)	0.24 (0.09-0.57)	No ($p = 0.34819$)
ROI2 Peak	0.20 (0.06-0.40)	0.21 (0.11-0.45)	No ($p = 0.35745$)
ROI2 Plateau	0.20 (0.11-0.40)	0.17 (0.06-0.36)	No ($p = 0.29588$)
ROI3 Baseline	0.21 (0.11-0.40)	0.22 (0.03-0.61)	No ($p = 0.37643$)
ROI3 Peak	0.17 (0.08-0.34)	0.18 (0.10-0.53)	No ($p = 0.30421$)
ROI3 Plateau	0.19 (0.14-0.39)	0.19 (0.09-0.39)	No ($p = 0.93591$)

Table 4.2: Table of p-values for the relative energy density of the respiratory activity of women with and without migraine, for all different combinations of ROIs and phases. Mean values and ranges are given in each case.

4.4.2. Endothelial activity (NO-dependent)

Table 4.3 shows a significant difference in the endothelial activity (NO-dependent) in the peak phase of ROI3 of women with migraine ($p = 0.008$). The boxplot in Figure 4.16 shows higher values of the relative energy density for women with migraine. This suggests increased NO activity in women with migraine. This significant difference was only detected in the peak phase of ROI3 and not in the entire measurement region.

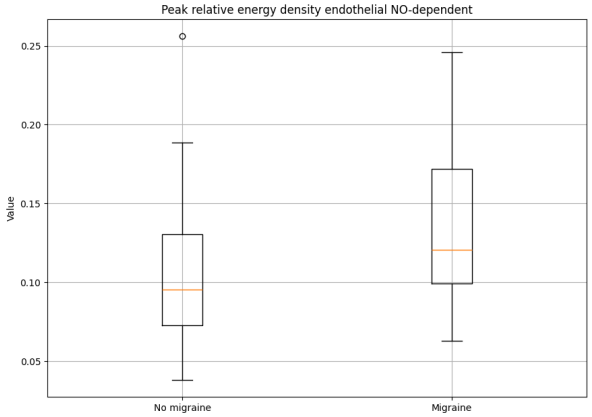

Figure 4.16: Boxplot of relative energy density of women without (left) and with migraine (right), in the peak phase of ROI3.

Relative energy density endothelial activity (NO-dependent)			
Blank	No migraine	Migraine	Significance ($p < 0.05$)
ROI1 Baseline	0.17 (0.04-0.34)	0.08 (0.04-0.20)	No ($p = 0.07840$)
ROI1 Peak	0.19 (0.06-0.34)	0.11 (0.06-0.22)	No ($p = 0.20777$)
ROI1 Plateau	0.21 (0.09-0.34)	0.07 (0.03-0.16)	No ($p = 0.50281$)
ROI2 Baseline	0.09 (0.03-0.25)	0.07 (0.04-0.18)	No ($p = 0.05941$)
ROI2 Peak	0.09 (0.03-0.22)	0.10 (0.03-0.20)	No ($p = 0.30421$)
ROI2 Plateau	0.08 (0.02-0.21)	0.07 (0.03-0.18)	No ($p = 0.92171$)
ROI3 Baseline	0.10 (0.04-0.20)	0.08 (0.04-0.21)	No ($p = 0.37643$)
ROI3 Peak	0.10 (0.04-0.26)	0.12 (0.06-0.25)	Yes ($p = 0.00797$)
ROI3 Plateau	0.09 (0.03-0.21)	0.09 (0.03-0.27)	No ($p = 0.86521$)

Table 4.3: Table of p-values for the relative energy density of the endothelial activity (NO-dependent) of women with and without migraine, for all different combinations of ROIs and phases. Mean values and ranges are given in each case.

4.5. Entire measurement region evaluation using DFT

In this section, the results obtained using the DFT are presented to assess whether there are clear differences compared to the WT method and to determine if one approach has a practical advantage over the other for this specific dataset. Before looking at the different phases (baseline, peak and plateau) using DFT, the entire measurement region was evaluated for ROI1, ROI2 and ROI3 individually. A statistical analysis, as outlined in Subsection 3.2.3, was conducted to determine the significance of the results. P-values below 0.05 were considered significant. Only tables with statistically significant results are shown. The remaining tables can be found in the Appendix A.3. For the evaluation of the entire measurement region using DFT, there were significant results for respiratory activity and endothelial activity for both NO-dependent and NO-independent cases.

4.5.1. Respiratory activity

Table 4.4 shows significant results for ROI1. This was in accordance with Table 4.1, where the WT was used. However, when comparing the values of ROI1 and ROI3 (control region) for the women without migraine and the women with migraine separately, the p-values were $p = 0.02$ and $p < 0.00005$. The values for both groups were significantly higher in ROI1 than ROI3. There was no significant difference between the values in ROI3 ($p = 0.46$) and the values for women with migraine were higher. This suggests a higher increase in values for women with migraine in respiratory activity. The interpretation of these results should be with caution, since the reliability is uncertain. Moreover, the biological interpretation is unknown.

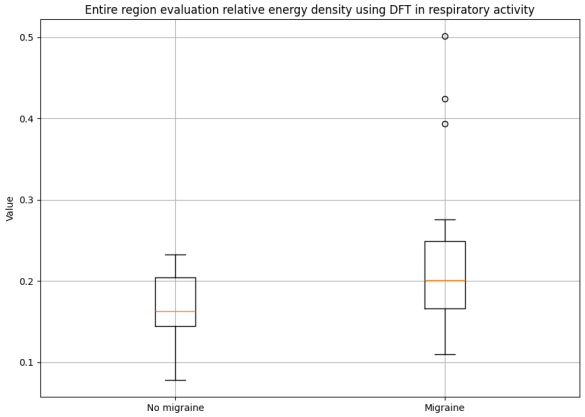

Figure 4.17: Boxplot of relative energy density of women without (left) and with migraine (right) for ROI1, across the entire measurement region using the DFT.

Relative energy density respiratory activity			
Blank	No migraine	Migraine	Significance ($p < 0.05$)
ROI1	0.16 (0.08-0.23)	0.20 (0.11-0.50)	Yes ($p = 0.00797$)
ROI2	0.18 (0.09-0.33)	0.20 (0.12-0.41)	No ($p = 0.20777$)
ROI3	0.15 (0.09-0.22)	0.15 (0.09-0.46)	No ($p = 0.45836$)

Table 4.4: Table of p-values for the relative energy density, evaluated across the entire measurement region of the respiratory activity of women with and without migraine, for all different ROIs, using DFT. Mean values and ranges are given in each case.

4.5.2. Endothelial activity (NO-dependent)

Table 4.5 shows significant differences in ROI1 ($p = 0.002$). The boxplot in Figure 4.18 shows higher values for the group of women without migraine. No significant differences between the values in ROI1 and ROI3 were detected for women without migraine ($p = 0.46$). For women with migraine, the values in ROI1 were significantly lower compared to the control region ($p = 0.0006$). Since NO was inhibited in ROI1, lower values in ROI1 compared to ROI3 were expected. This was only the case in the group of women with migraine. However, it seemed unlikely that NO inhibition was only effective in women with migraine and not in those without migraine. An explanation could be that women with migraine have higher levels of NO compared to women without migraine. Consequently, there could be more NO-related activity simply because there is more NO present in women with migraine. The relative energy density only reflects the activity, but not the amount of NO. If this interpretation holds, it would align with the well-known paradox linking migraine and cardiovascular disease. Migraine patients have a higher chance of cardiovascular disease, but not due to traditional risk factors [7], such as atherosclerosis, since more NO-related activity is detected in women with migraine, which relates to less atherosclerosis [6].

When using WT, no significant differences were found in the endothelial activity that depends on NO (see Section 4.3).

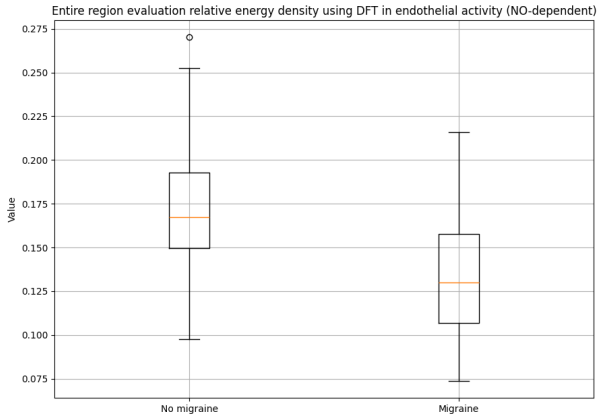

Figure 4.18: Boxplot of relative energy density of women without (left) and with migraine (right) for ROI1, across the entire measurement region.

Relative energy density endothelial activity (NO-dependent)			
Blank	No migraine	Migraine	Significance ($p < 0.05$)
ROI1	0.17 (0.10-0.27)	0.13 (0.07-0.22)	Yes ($p = 0.00152$)
ROI2	0.16 (0.08-0.25)	0.14 (0.05-0.19)	No ($p = 0.19516$)
ROI3	0.18 (0.10-0.23)	0.17 (0.09-0.26)	No ($p = 0.42653$)

Table 4.5: Table of p-values for the relative energy density, evaluated across the entire measurement region of the endothelial activity (NO-dependent) of women with and without migraine, for all different ROIs, using DFT. Mean values and ranges are given in each case.

4.5.3. Endothelial activity (NO-independent)

Table 4.6 shows a significant difference in ROI1. The boxplot in Figure 4.19 shows higher values for women without migraine. The ROI1 values of women without migraine compared to ROI3 in the control region were lower ($p = 0.003$). This was also the case for women with migraine ($p < 0.00005$). The values in ROI3 were not significantly different ($p = 0.73$). These observations suggest that the decrease in energy was larger in women with migraine compared to women without migraine, as a significant difference was observed in ROI1, but not in ROI3. The biological interpretation of this result is unknown.

When using WT, no significant differences were found in endothelial activity independent of NO (see Section 4.3).

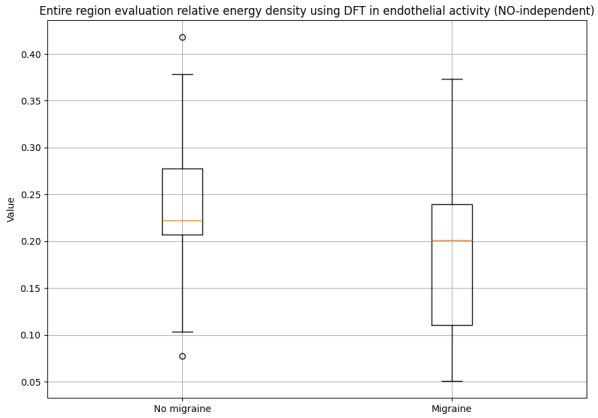

Figure 4.19: Boxplot of relative energy density of women without (left) and with migraine (right) for ROI1, across the entire measurement region.

Relative energy density endothelial activity (NO-independent)			
Blank	No migraine	Migraine	Significance ($p < 0.05$)
ROI1	0.22 (0.08-0.42)	0.20 (0.05-0.37)	Yes ($p = 0.03422$)
ROI2	0.20 (0.05-0.40)	0.19 (0.07-0.33)	No ($p = 0.25652$)
ROI3	0.29 (0.16-0.42)	0.28 (0.06-0.42)	No ($p = 0.72751$)

Table 4.6: Table of p-values for the relative energy density, evaluated across the entire measurement region of the endothelial activity (NO-independent) of women with and without migraine, for all different ROIs, using DFT. Mean values and ranges are given in each case.

4.6. Evaluation of phase characteristics using DFT

Similarly to Section 4.4, a statistical analysis as outlined in Subsection 3.2.3, was conducted to determine the significance of the results. This will be done for all different frequency domains, each corresponding to a distinct biological mechanism. A p-value smaller than 0.05 was considered significant. Only tables with statistically significant results are shown. The remaining tables can be found in the Appendix A.4. For the evaluation of phase characteristics using DFT, there were only significant results for respiratory activity and endothelial activity (NO-dependent).

4.6.1. Respiratory activity

Table 4.7 presents the relative energy densities and p-values of women without migraine and women with migraine, using the DFT. Similarly to the WT (Table 4.2), the only significant difference was found in the peak phase for ROI1. The p-values were also calculated for the differences of values in the peak phase in ROI1 and ROI3 of women without and with migraine. These were $p = 0.03$ and $p = 0.01$ respectively. The values in the peak phase of ROI1 were significantly higher compared to the values in ROI3 for both groups.

The interpretation of these results should be with caution, since the reliability is uncertain. Moreover, the biological interpretation is unknown.

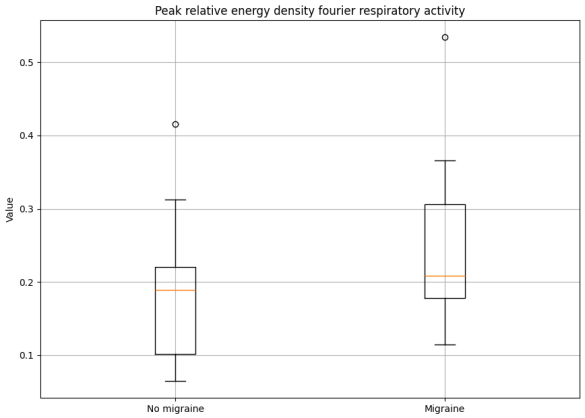

Figure 4.20: Boxplot of relative energy density of women without (left) and with migraine (right), in the peak phase of ROI1.

Relative energy density respiratory activity			
Blank	No migraine	Migraine	Significance ($p < 0.05$)
ROI1 Baseline	0.24 (0.12-0.43)	0.27 (0.09-0.77)	No ($p = 0.13107$)
ROI1 Peak	0.19 (0.07-0.42)	0.21 (0.11-0.53)	Yes ($p = 0.01547$)
ROI1 Plateau	0.23 (0.15-0.47)	0.25 (0.12-0.58)	No ($p = 0.62315$)
ROI2 Baseline	0.25 (0.14-0.47)	0.27 (0.11-0.65)	No ($p = 0.15545$)
ROI2 Peak	0.22 (0.03-0.40)	0.25 (0.11-0.54)	No ($p = 0.31270$)
ROI2 Plateau	0.21 (0.13-0.48)	0.20 (0.06-0.46)	No ($p = 0.27968$)
ROI3 Baseline	0.23 (0.14-0.44)	0.25 (0.05-0.69)	No ($p = 0.46926$)
ROI3 Peak	0.15 (0.03-0.24)	0.17 (0.06-0.58)	No ($p = 0.10586$)
ROI3 Plateau	0.21 (0.15-0.46)	0.21 (0.12-0.44)	No ($p = 0.61057$)

Table 4.7: Table of p-values for the relative energy density of the respiratory activity of women with and without migraine, for all different combinations of ROIs and phases, using DFT. Mean values and ranges are given in each case.

4.6.2. Endothelial activity (NO-dependent)

Table 4.8 presents the relative energy densities and p-values of women with and without migraine. Two significant differences between the two groups were found in the baseline phase for ROI1 and the baseline phase for ROI2. The corresponding boxplots can be found in Figure 4.21. When using the WT, Table 4.3 did not show these two differences as statistically significant. However, when using the WT, Table 4.3 shows that the corresponding p-values were relatively small ($p = 0.08$ and $p = 0.06$ respectively) and that the values for women without migraine were lower compared to women with migraine. Another distinction was that the significant difference in the peak phase for ROI3 observed with the WT is no longer present when using the DFT.

When comparing ROI1 and the control region in the baseline phase for women without migraine and with migraine, the p-values were $p = 0.28$ and $p = 0.05$ respectively. This means that, in the baseline phase, the values of ROI1 and ROI3 for women without migraine were similar. Women with migraine showed smaller values in ROI1 compared to ROI3. A similar pattern was present when comparing ROI2 with the control region. The p-values for women without migraine and women with migraine were respectively $p = 0.86$ and $p = 0.009$. This exact behavior was also observed in Subsection 4.5.2 and therefore, the same reasoning applies here.

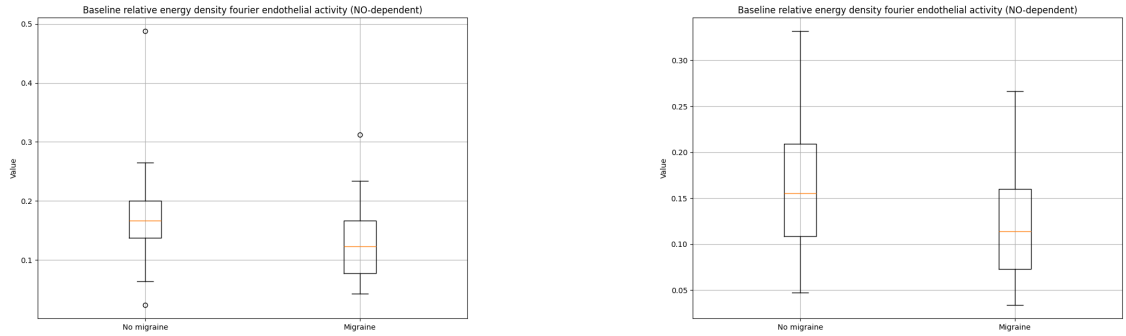

(a) (b)

Figure 4.21: Boxplot of relative energy density of women without (left) and with migraine (right), in the baseline phase (a) of ROI1. (b) of ROI2.

Relative energy density endothelial activity (NO-dependent)			
Blank	No migraine	Migraine	Significance ($p < 0.05$)
ROI1 Baseline	0.17 (0.02-0.49)	0.12 (0.04-0.31)	Yes ($p = 0.02380$)
ROI1 Peak	0.12 (0.04-0.27)	0.14 (0.06-0.23)	No ($p = 0.68765$)
ROI1 Plateau	0.12 (0.02-0.32)	0.11 (0.02-0.24)	No ($p = 0.26409$)
ROI2 Baseline	0.16 (0.05-0.33)	0.11 (0.03-0.27)	Yes ($p = 0.02860$)
ROI2 Peak	0.11 (0.03-0.28)	0.11 (0.02-0.20)	No ($p = 0.96437$)
ROI2 Plateau	0.12 (0.01-0.35)	0.10 (0.05-0.28)	No ($p = 0.68765$)
ROI3 Baseline	0.16 (0.03-0.31)	0.14 (0.04-0.35)	No ($p = 0.46926$)
ROI3 Peak	0.15 (0.05-0.34)	0.16 (0.07-0.27)	No ($p = 0.57353$)
ROI3 Plateau	0.11 (0.03-0.29)	0.11 (0.05-0.28)	No ($p = 0.86521$)

Table 4.8: Table of p-values for the relative energy density of the endothelium activity (NO-dependent) of women with and without migraine, for all different combinations of ROIs and phases, using DFT. Mean values and ranges are given in each case.

5

Discussion

This study investigated whether wavelet analysis (WA) of the VASCULAR-study data yield more insights than Fourier analysis (FA) into bloodflow measurements in women, particularly in examining the role of nitric oxide (NO) and calcitonin gene-related peptide (CGRP) in the microvasculature among women with and without migraine. This was achieved by performing WA using the complex Morlet wavelet as the mother wavelet. Relative energy density served as a quantitative measure. Differences between women with migraine and women without migraine were assessed through statistical analyses using p-values. Both WA and FA were applied to examine differences across the entire measurement region and within specific phases (baseline, peak and plateau).

5.1. Main findings

When investigating the entire measurement region using WA, significant differences in relative energy density were only found in the respiratory activity of ROI1. However, statistical comparison of ROI1 and the control region ROI3 within the two groups individually did not show any significant differences, suggesting similar values in ROI1 and ROI3 for both groups.

Looking at the phases individually, significant differences were found in the respiratory activity during the peak phase of ROI1. The values for ROI1 of women without migraine were similar to the values of the control region ROI3. The values for ROI1 of women with migraine were significantly higher compared to the control region. However, since the relative energy density appeared to be higher in women with migraine and this difference is only observed in the peak phase of ROI1, the biological clarification remains unclear and the result should be interpreted with caution.

Furthermore, significant differences were found in the endothelial activity dependent on NO during the peak phase of ROI3. The values of women with migraine appeared higher in the peak phase of ROI3. This difference was not significant in the entire measurement region and therefore, the biological interpretation remains unclear.

When using FA, the same significant difference was found in the respiratory activity of ROI1. The values of women with migraine appeared to be higher. This same pattern was observed when using WA.

Additionally, significant differences were found in both NO-dependent and NO-independent endothelial activity. For NO-dependent endothelial activity, a significant decrease in relative energy density was observed for women with migraine. This same pattern was not discovered in the group of women without migraine. A decrease in NO activity is as expected, since NO is inhibited in ROI1. However, a decrease in relative energy density was only observed in ROI1 for women with migraine, while no such decrease occurred in women without migraine. A possible explanation could be that women with migraine have higher levels of NO and thus more NO-related activity. This would also be consistent with the paradoxical relationship between migraine and cardiovascular disease; the traditional risk factor of cardiovascular disease is atherosclerosis, but more NO-related activity relates to less atherosclerosis, which is also observed in women with migraine [6][7]. The exact explanation of the detected difference in activity remains unknown and requires further research.

For the NO-independent endothelial activity, values in ROI1 for both groups were significantly smaller compared to ROI3.

Looking at the phases individually, the same significant difference was found in the respiratory activity of ROI1 in the peak phase. The values in the peak phase for both groups were significantly higher in ROI1 compared to the peak phase of ROI3.

Moreover, significant differences were found in the endothelial activity associated with NO in the baseline phase in both ROI1 and ROI2. In both regions, women with migraine had significantly smaller value, whereas no notable differences were found in women without migraine. The same pattern was visible when considering the entire measurement region, instead of the phases separately. The biological interpretation of these results remains unclear.

A major advantage of WA over FA is its ability to enable time and frequency localization, both at the same time. One notable observation using WA was that, around 1500 seconds, a pronounced difference in activity was noticed between women with migraine and women without migraine. This difference emerged between the peak and plateau phase. The underlying cause of this difference remains unclear. This was the only notable observation identified when analyzing the data in both the frequency and time domain using the WA. To calculate relative energy density as a quantitative measure, the wavelet coefficients were averaged over time. This facilitated comparison between the two groups of women. However, in this way, the time information was lost by the averaging process. Given that WA trades frequency resolution for time-frequency localization at the same time, FA may be more suitable in this study for this specific dataset as it offers more precise frequency resolution. Moreover, using relative energy density as quantitative measure eliminates the time-localization advantage of WA.

5.2. Limitations and strengths

Several limitations are present in this study. One of them is related to the WA, since it involves multiple choices during implementation. One of them is the choice for the mother wavelet. In addition, many mother wavelets also provide additional parameters from which to choose. While this flexibility allows the mother wavelet to be adapted to the specific characteristics of the data, it also is a disadvantage, since there is no standardized measure found to assess how well the mother wavelet fits the data. In this study, the parameters were chosen based on the commonly used values in the literature.

Moreover, the division of the frequency intervals into distinct biological mechanisms varies across the literature [13][15][16][17][59]. In this study, one specific classification was chosen. However, there exist other studies that have defined these intervals differently.

Additionally, the sample frequency used in this study was relatively low. Consequently, no significant differences were observed in the frequency intervals associated with the neurogenic activity ($0.02-0.06$ Hz) and smooth muscle cells activity ($0.06-0.15$ Hz) did not show any results. Although some results were detected for respiratory activity ($0.15-0.4$ Hz), the reliability of these results is uncertain. Significant results were found in the two lowest frequency intervals, which are associated with endothelial activity.

One of the strengths of this study is the combined use of WA and FA. Each method has its own advantage. FA provides good frequency localization, while WA offers both frequency and time localization, while sacrificing part of the frequency resolution. By using both methods, the study ensures reliable frequency resolution, by comparing the results using WA and the results using FA, and also time localization, since WA also provides information in the time domain.

5.3. Future work

The primary recommendation for future research is to adjust the sampling frequency to a higher value. The sample frequency plays a critical role in frequency-based analyses. In this study, a sampling frequency of 1 Hz was used. However, many studies utilize much higher frequencies of for example 40 Hz. Increasing the sample frequency would also enable analysis of the cardiac activity, as it would satisfy the requirements of the Nyguist-Shannon Sampling Theorem. In PIMSoft, the software used by researchers of ERASMUS MC to acquire LSCI data, the sampling frequency is determined by two parameters: the *frame rate* and the *record with averaging*. The frame rate denotes the number of images captured per second. The record with averaging is the number of images averaged to compute a single speckle contrast value. The resulting *effective frame rate*, which corresponds to the sampling frequency, is given by the ratio:

$$f_s = \frac{frame\ rate}{record\ with\ averaging}. \tag{5.1}$$

A higher sampling frequency is obtained by increasing the frame rate or decreasing the record with averaging.

This study employed continuous wavelet transform (CWT) using the complex Morlet wavelet as the mother wavelet, which is commonly used in blood perfusion analysis. While this choice is reasonable, it may still be interesting and valuable to explore other mother wavelet options to assess whether the results differ significantly. Moreover, this study focused on using CWT, but future studies could also use the discrete wavelet transform (DWT) for the same reason.

It could also be interesting to repeat this research by focusing on the group of women with migraine with aura and women without migraine.

As mentioned earlier, a significant difference was observed around 1500 seconds between women with migraine and without migraine. Further investigation into the underlying cause of this difference would be interesting.

Erasmus MC is currently conducting new measurements on the forehead instead of the forearm. Comparing these results with those obtained from the forearm could be of interest and may reveal different results.

6

Conclusion

Both wavelet analysis (WA) and Fourier analysis (FA) revealed significant differences in respiratory activity within ROI1, with higher values in relative energy density observed in women with migraine. When looking at phase-specific analysis in respiratory activity, this difference was reflected in the peak phase of ROI1 for both WA and FA. In addition, both methods identified significant differences in endothelial activity associated with NO, when evaluating the phases individually. WA detected significant differences in the peak phase of ROI3, with higher values for women with migraine. FA revealed the significant differences at the baseline of ROI1 and ROI2, where values for women without migraine appeared to be higher. WA also yielded notably low p-values for the baseline phase of ROI1 and ROI2, suggesting possible patterns that were suggestive but not statistically significant. The biological explanation behind these observed patterns is not yet understood and further research is required to investigate them. WA did show statistical significance in the peak phase of ROI3, while, FA did not. Moreover, FA identified significant differences in both NO-dependent and NO-independent endothelial activity in ROI1. These differences were not observed with WA. Although many similar patterns were observed for the WA and FA for the VASCULAR-study dataset, there were also subtle differences. These subtle differences are likely due to the higher frequency resolution of FA, whereas WA sacrifices frequency resolution to achieve time and frequency localization at the same time. Using this advantage of WA, a significant increase in activity was observed in women with migraine between the peak and plateau phase.

Bibliography

[1] L. Dong, W. Dong, Y. Jin, and et al., "The global burden of migraine: A 30-year trend review and future projections by age, sex, country, and region," *Pain and Therapy*, vol. 14, pp. 297–315, 2025.

[2] F. Puledda, R. Messina, and P. J. Goadsby, "An update on migraine: current understanding and future directions," *Journal of Neurology*, vol. 264, no. 9, pp. 2031–2039, 2017.

[3] F. Puledda, E. M. Silva, K. Suwanlaong, and P. J. Goadsby, "Migraine: from pathophysiology to treatment," *Journal of Neurology*, vol. 270, no. 7, pp. 3654–3666, 2023.

[4] C. Todd, A. M. Lagman-Bartolome, and C. Lay, "Women and migraine: the role of hormones," *Current Neurology and Neuroscience Reports*, vol. 18, no. 7, p. 42, 2018.

[5] J. Frostegård, "Immunity, atherosclerosis and cardiovascular disease," *BMC Medicine*, vol. 11, p. 117, 2013.

[6] H. J. van Os, I. A. Mulder, A. Broersen, A. Algra, I. C. van der Schaaf, L. J. Kappelle, B. K. Velthuis, G. M. Terwindt, W. J. Schonewille, M. C. Visser, M. D. Ferrari, M. A. van Walderveen, and M. J. Wermer, "Migraine and cerebrovascular atherosclerosis in patients with ischemic stroke," *Stroke*, vol. 48, no. 7, pp. 1973–1975, 2017.

[7] L. Al-Hassany, A. MaassenVanDenBrink, and T. Kurth, "Cardiovascular risk scores and migraine status," *JAMA Network Open*, vol. 7, no. 10, p. e2440577, 2024.

[8] C. Gollion, B. Guidolin, F. Lerebours, V. Rousseau, M. Barbieux-Guillot, and V. Larrue, "Migraine and large artery atherosclerosis in young adults with ischemic stroke," *Headache*, vol. 62, no. 2, pp. 191–197, 2022.

[9] L. Al-Hassany, K. M. Linstra, C. Meun, J. van den Berg, E. Boersma, A. J. Danser, B. C. Fauser, J. S. Laven, M. J. Wermer, G. M. Terwindt, and A. Maassen Van Den Brink, "Decreased role of neuropeptides in the microvascular function in migraine patients with polycystic ovary syndrome," *Atherosclerosis*, vol. 384, p. 117172, 2023. Influence of sex and gender on the biology of atherosclerotic cardiovascular disease.

[10] S. Sacco, S. Ricci, D. Degan, and A. Carolei, "Migraine in women: the role of hormones and their impact on vascular diseases," *The Journal of Headache and Pain*, vol. 13, no. 3, pp. 177–189, 2012.

[11] M. Draijer, E. Hondebrink, T. van Leeuwen, and W. Steenbergen, "Review of laser speckle contrast techniques for visualizing tissue perfusion," *Lasers in Medical Science*, vol. 24, no. 4, pp. 639–651, 2009.

[12] A. Bagno and R. Martini, "Wavelet analysis of the laser doppler signal to assess skin perfusion," in *Annual International Conference of the IEEE Engineering in Medicine and Biology Society*, IEEE Engineering in Medicine and Biology Society. Annual International Conference, pp. 7374–7377, IEEE, 2015.

[13] I. Mizeva, V. Dremin, E. Potapova, E. Zherebtsov, I. Kozlov, and A. Dunaev, "Wavelet analysis of the temporal dynamics of the laser speckle contrast in human skin," *IEEE Transactions on Biomedical Engineering*, vol. 67, no. 7, pp. 1882–1889, 2020.

[14] N. Golubova, E. Potapova, E. Seryogina, and V. Dremin, "Time–frequency analysis of laser speckle contrast for transcranial assessment of cerebral blood flow," *Biomedical Signal Processing and Control*, vol. 85, p. 104969, 2023.

[15] M. Bračič and A. Stefanovska, "Wavelet-based analysis of human blood-flow dynamics," *Bulletin of Mathematical Biology*, vol. 60, pp. 919–935, September 1998. Received: 08 October 1997; Accepted: 21 January 1998.

[16] M. Geyer, Y.-K. Jan, D. Brienza, and M. Boninger, "Using wavelet analysis to characterize the thermoregulatory mechanisms of sacral skin blood flow," *Journal of rehabilitation research and development*, vol. 41, pp. 797–806, 11 2004.

[17] A. Stefanovska, M. Bracic, and H. D. Kvernmo, "Wavelet analysis of oscillations in the peripheral blood circulation measured by laser doppler technique," *IEEE Transactions on Biomedical Engineering*, vol. 46, no. 10, pp. 1230–1239, 1999.

[18] N. Agnihotri, "Fourier analysis of the microvascular function of women with and without migraine," 2023. Supervised by C. Vuik; Committee members: Marleen Keijzer, Linda Al-Hassany, and Antoinette Maassen-Van den Brink.

[19] M. van Santen, "Fourier analyse van de bloeddoorstroming in vrouwen met en zonder migraine," 2024. Mentors: Kees Vuik and Linda Al-Hassany; Committee members: Antoinette Maassen-Van den Brink and E.G. Rens.

[20] S. Sacco, P. Ripa, D. Grassi, F. Pistoia, R. Ornello, A. Carolei, and T. Kurth, "Peripheral vascular dysfunction in migraine: a review," *The Journal of Headache and Pain*, vol. 14, no. 1, p. 80, 2013.

[21] F. Tang, M. Trinh, A. Duong, A. Ly, F. Stapleton, Z. Chen, Z. Ge, and I. Razzak, "Discriminating retinal microvascular and neuronal differences related to migraines: Deep learning based crossectional study," 2024.

[22] G. Aslan, L. E. Sade, B. Yetis, H. Bozbas, S. Eroglu, B. Pirat, U. Can, and H. Müderrisoğlu, "Flow in the left anterior descending coronary artery in patients with migraine headache," *The American Journal of Cardiology*, vol. 112, no. 10, pp. 1540–1544, 2013.

[23] M. Félétou, *The Endothelium: Part 1: Multiple Functions of the Endothelial Cells—Focus on Endothelium-Derived Vasoactive Mediators*. Colloquium Series on Integrated Systems Physiology, San Rafael, CA: Morgan & Claypool Life Sciences, 2011.

[24] H.-J. Sun, Z.-Y. Wu, X.-W. Nie, and J.-S. Bian, "Role of endothelial dysfunction in cardiovascular diseases: The link between inflammation and hydrogen sulfide," *Frontiers in Pharmacology*, vol. 10, p. 1568, 2020.

[25] Y. Zhuge, J. Zhang, F. Qian, Z. Wen, C. Niu, K. Xu, H. Ji, X. Rong, M. Chu, and C. Jia, "Role of smooth muscle cells in cardiovascular disease," *International Journal of Biological Sciences*, vol. 16, no. 14, pp. 2741–2751, 2020.

[26] K. Maasumi, R. L. Michael, and A. M. Rapoport, "CGRP and migraine: The role of blocking calcitonin gene-related peptide ligand and receptor in the management of migraine," *Drugs*, vol. 78, no. 9, pp. 913–928, 2018.

[27] Z. Kee, X. Kodji, and S. D. Brain, "The role of calcitonin gene related peptide (CGRP) in neurogenic vasodilation and its cardioprotective effects," *Frontiers in Physiology*, vol. 9, p. 1249, 2018.

[28] J. P. Burbach, "What are neuropeptides?," *Methods in Molecular Biology*, vol. 789, pp. 1–36, 2011.

[29] L. Hariri and J. B. Patel, *Vasodilators*. Treasure Island (FL): StatPearls Publishing, 2025. Updated 2023 Aug 14. In: StatPearls [Internet].

[30] P. L. Durham, "Calcitonin gene-related peptide (CGRP) and migraine," *Headache*, vol. 46, no. Suppl 1, pp. S3–S8, 2006. Supplemental issue.

[31] Y. Sharav and R. Benoliel, "Chapter 9 - migraine and possible facial variants (neurovascular orofacial pain)," in *Orofacial Pain and Headache* (Y. Sharav and R. Benoliel, eds.), pp. 193–224, Edinburgh: Mosby, 2008.

[32] G. L. Peters, "Migraine overview and summary of current and emerging treatment options," *The American Journal of Managed Care*, vol. 25, no. 2 Suppl, pp. S23–S34, 2019.

[33] I. R. Bell and C. M. Baldwin, "Chapter 94 - multiple chemical sensitivity," in *Women and Health (Second Edition)* (M. B. Goldman, R. Troisi, and K. M. Rexrode, eds.), pp. 1379–1394, Academic Press, second edition ed., 2013.

[34] A. A. Pradhan, Z. Bertels, and S. Akerman, "Targeted nitric oxide synthase inhibitors for migraine," *Neurotherapeutics*, vol. 15, no. 2, pp. 391–401, 2018. Journal of the American Society for Experimental NeuroTherapeutics.

[35] N. Karsan, H. Gosalia, and P. J. Goadsby, "Molecular mechanisms of migraine: Nitric oxide synthase and neuropeptides," *International Journal of Molecular Sciences*, vol. 24, no. 15, p. 11993, 2023.

[36] J. Buijs, J. V. Gucht, and J. Sprakel, "Fourier transforms for fast and quantitative laser speckle imaging," *Scientific Reports*, vol. 9, no. 1, p. 13279, 2019.

[37] W. Qi, *Fourier and wavelet analysis of skin laser doppler flowmetry signals*. PhD thesis, University of Southampton, 2011.

[38] D. de Ziegler, I. Streuli, P. Santulli, and C. Chapron, "Chapter 35 - pelvic imaging in reproductive endocrinology," in *Yen Jaffe's Reproductive Endocrinology (Seventh Edition)* (J. F. Strauss and R. L. Barbieri, eds.), pp. 851–889.e11, Philadelphia: W.B. Saunders, seventh edition ed., 2014.

[39] G. Guven, A. Dijkstra, T. M. Kuijper, N. Trommel, M. E. van Baar, A. Topeli, C. Ince, and C. H. van der Vlies, "Comparison of laser speckle contrast imaging with laser doppler perfusion imaging for tissue perfusion measurement," *Microcirculation*, vol. 30, no. 1, p. e12795, 2023. New York, N.Y. : 1994.

[40] O. B. Thompson, E. R. Hirst, and M. K. Andrews, "Is there a difference between laser speckle and laser doppler in depth sensitivity?," in *Dynamics and Fluctuations in Biomedical Photonics VIII*, vol. 7898 of *Proceedings of SPIE*, p. 78980E, February 2011.

[41] G. Ellis, "Chapter 5 - the z-domain," in *Control System Design Guide (Fourth Edition)* (G. Ellis, ed.), pp. 73–96, Boston: Butterworth-Heinemann, fourth edition ed., 2012.

[42] A. L. Schoenstadt, "An introduction to fourier analysis: Fourier series, partial differential equations and fourier transforms," 2006.

[43] M. Taboga, "Discrete Fourier transform – frequencies," *StatLect*, 2021.

[44] J. Yiu, "Chapter 19 - digital signal processing on the cortex-m33 processor," in *Definitive Guide to Arm® Cortex®-M23 and Cortex-M33 Processors* (J. Yiu, ed.), pp. 751–798, Newnes, 2021.

[45] W. Heisenberg, "Heisenberg uncertainty principle," *Zeitschrift für Physik*, vol. 43, p. 172, 1927.

[46] B. K. Alsberg, A. M. Woodward, and D. B. Kell, "An introduction to wavelet transforms for chemometricians: A time-frequency approach," *Chemometrics and Intelligent Laboratory Systems*, vol. 37, no. 2, pp. 215–239, 1997.

[47] R. Merry, *Wavelet theory and applications: a literature study*. DCT rapporten, Technische Universiteit Eindhoven, 2005. DCT 2005.053.

[48] O. Rioul and M. Vetterli, "Wavelets and signal processing," *Signal Processing Magazine, IEEE*, vol. 8, pp. 14 – 38, 10 1991.

[49] E. Foufoula-Georgiou and P. Kumar, eds., *Wavelets in Geophysics*, vol. 4 of *Wavelet Analysis and Its Applications*. San Diego, California: Academic Press, 1994. Volume 4 in the Wavelet Analysis and Its Applications series.

[50] A. Mertins and D. Mertins, "Signal analysis: Wavelets, filter banks, time-frequency transforms and applications," 11 2001.

[51] P. Wallisch, M. Lusignan, M. Benayoun, T. I. Baker, A. S. Dickey, and N. G. Hatsopoulos, "Chapter 9 - wavelets," in *Matlab for Neuroscientists* (P. Wallisch, M. Lusignan, M. Benayoun, T. I. Baker, A. S. Dickey, and N. G. Hatsopoulos, eds.), pp. 133–140, London: Academic Press, 2009.

[52] P. Fryzlewicz, "Wavelet methods," *Wiley Interdisciplinary Reviews: Computational Statistics*, vol. 2, no. 6, pp. 654–667, 2010.

[53] E. Gomez-Luna, G. Aponte, and J. Pleite, "Application of wavelet transform to obtain the frequency response of a transformer from transient signals—part ii: Practical assessment and validation," *Power Delivery, IEEE Transactions on*, vol. 29, pp. 2231–2238, 10 2014.

[54] T. Guo, T. Zhang, E. Lim, M. López-Benítez, F. Ma, and L. Yu, "A review of wavelet analysis and its applications: Challenges and opportunities," *IEEE Access*, vol. 10, pp. 58869–58903, 2022.

[55] MathWorks, *dsp.Channelizer Center Frequencies*, 2023.

[56] P. He, P. Li, and H. Sun, "Feature extraction of acoustic signals based on complex morlet wavelet," *Procedia Engineering*, vol. 15, pp. 464–468, 2011. CEIS 2011.

[57] S. Mallat, "A theory for multiresolution signal decomposition: the wavelet representation," *IEEE Transactions on Pattern Analysis and Machine Intelligence*, vol. 11, no. 7, pp. 674–693, 1989.

[58] A. Meyer-Baese and V. Schmid, "Chapter 3 - subband coding and wavelet transform," in *Pattern Recognition and Signal Analysis in Medical Imaging (Second Edition)* (A. Meyer-Baese and V. Schmid, eds.), pp. 71–111, Oxford: Academic Press, second edition ed., 2014.

[59] A. V. Tankanag and N. K. Chemeris, "Adaptive wavelet analysis of oscillations in the human peripheral blood flow," *Biophysics*, vol. 54, no. 3, pp. 375–380, 2009. Received: February 26, 2008; Original Russian Text published in Biofizika, 2009, Vol. 54, No. 3, pp. 537–544.

[60] A.-S. Wattiez, L. P. Sowers, and A. F. Russo, "Calcitonin gene-related peptide (CGRP): role in migraine pathophysiology and therapeutic targeting," *Expert Opinion on Therapeutic Targets*, vol. 24, no. 2, pp. 91–100, 2020.

[61] J. Semba, M. Sakai, R. Miyoshi, and S. Kito, "NG-monomethyl-L-arginine, an inhibitor of nitric oxide synthase, increases extracellular GABA in the striatum of the freely moving rat," *Neuroreport*, vol. 6, no. 10, pp. 1426–1428, 1995.

[62] B. Priya, T. Rashmi, and M. B. and, "Transdermal iontophoresis," *Expert Opinion on Drug Delivery*, vol. 3, no. 1, pp. 127–138, 2006. PMID: 16370945.

[63] The MathWorks, Inc., "cmorwavf — complex morlet wavelet." `https://nl.mathworks.com/help/wavelet/ref/cmorwavf.html`, 2025.

[64] PyWavelets Developers, "Continuous wavelet transform (CWT) — pywavelets documentation," 2023.

[65] I. Mizeva, E. Potapova, I. Kozlov, V. Dremin, A. Dunaev, and G. Krasnikov, "Heterogeneity of cutaneous blood flow respiratory-related oscillations quantified via lsci wavelet decomposition," in *2020 11th Conference of the European Study Group on Cardiovascular Oscillations (ESGCO)*, pp. 1–2, 2020.

[66] M. Farge *et al.*, "Wavelet transforms and their applications to turbulence," *Annual review of fluid mechanics*, vol. 24, no. 1, pp. 395–458, 1992.

[67] A. Bagno and R. Martini, "Wavelet transform analysis of skin perfusion during thermal stimulation," *Clinical Hemorheology and Microcirculation*, vol. 64, no. 2, pp. 167–175, 2016.

[68] MathWorks, "Continuous and discrete wavelet transforms," 2023. MATLAB Wavelet Toolbox Documentation.

[69] T. Bergmann, L. Froese, A. Gomez, A. S. Sainbhi, N. Vakitbilir, A. Islam, K. Stein, I. Marquez, F. Amenta, K. Park, Y. Ibrahim, and F. A. Zeiler, "Evaluation of Morlet Wavelet Analysis for Artifact Detection in Low-Frequency Commercial Near-Infrared Spectroscopy Systems," *Bioengineering*, vol. 11, no. 1, p. 33, 2023. Open access.

[70] X. Chen, R. S. Gupta, and L. Gupta, "Exploiting the cone of influence for improving the performance of wavelet transform-based models for erp/eeg classification," *Brain Sciences*, vol. 13, no. 1, p. 21, 2022.

[71] C. Torrence and G. P. Compo, "A practical guide to wavelet analysis," *Bulletin of the American Meteorological Society*, vol. 79, no. 1, pp. 61–78, 1998.

[72] L. Kralj, M. Hultman, and H. Lenasi, "Wavelet analysis and the cone of influence: Does the cone of influence impact wavelet analysis results?," *Applied Sciences*, vol. 14, no. 24, p. 11736, 2024. This article belongs to the Special Issue "Novel Insights into the Cardiovascular System: From Analytical Approach to Application".

[73] M. X. Cohen, *Analyzing Neural Time Series Data: Theory and Practice*. The MIT Press, 01 2014.

[74] N. Kwabena Adomako, N. Haghdadi, and S. Primig, "Electron and laser-based additive manufacturing of ni-based superalloys: A review of heterogeneities in microstructure and mechanical properties," *Materials Design*, vol. 223, p. 111245, 2022.

[75] J. Shreffler and M. Huecker, "Hypothesis testing, p values, confidence intervals, and significance," in *StatPearls [Internet]* (S. Publishing, ed.), Treasure Island (FL): StatPearls Publishing, 2023.

[76] DATAtab Team, "Mann-whitney u-test." `https://datatab.net/tutorial/mann-whitney-u-test`, 2025.

[77] M. Jesussek, "Wilcoxon signed-rank test." `https://datatab.net/tutorial/wilcoxon-test`, 2025.

[78] J. H. Kim, Y. K. Lee, Y. S. Kwon, and J. H. Sohn, "Clinical implications of the association between respiratory and gastrointestinal disorders in migraine and non-migraine headache patients," *Journal of Clinical Medicine*, vol. 12, no. 10, p. 3434, 2023.

[79] G. Davey, P. Sedgwick, W. Maier, G. Visick, D. P. Strachan, and H. R. Anderson, "Association between migraine and asthma: matched case-control study," *The British Journal of General Practice: The Journal of the Royal College of General Practitioners*, vol. 52, no. 482, pp. 723–727, 2002.

A

Tables and figures

A.1. Tables: Entire measurement region evaluation using WT

Relative energy density smooth muscle cells activity			
Blank	No migraine	Migraine	Significance ($p < 0.05$)
ROI1	0.24 (0.15-0.36)	0.22 (0.12-0.43)	No ($p = 0.97862$)
ROI2	0.24 (0.17-0.31)	0.23 (0.14-0.38)	No ($p = 0.85117$)
ROI3	0.24 (0.14-0.44)	0.20 (0.14-0.44)	No ($p = 0.09478$)

Table A.1: Table of p-values for the relative energy density, evaluated across the entire measurement region of the smooth muscle cells activity of women with and without migraine, for all different ROIs. Mean values and ranges are given in each case.

Relative energy density neurogenic activity			
Blank	No migraine	Migraine	Significance ($p < 0.05$)
ROI1	0.21 (0.12-0.35)	0.23 (0.11-0.31)	No ($p = 0.82326$)
ROI2	0.24 (0.16-0.33)	0.23 (0.14-0.37)	No ($p = 0.79556$)
ROI3	0.20 (0.13-0.37)	0.21 (0.11-0.31)	No ($p = 0.52586$)

Table A.2: Table of p-values for the relative energy density, evaluated across the entire measurement region of the neurogenic activity of women with and without migraine, for all different ROIs. Mean values and ranges are given in each case.

Relative energy density endothelial activity (NO-dependent)			
Blank	No migraine	Migraine	Significance ($p < 0.05$)
ROI1	0.13 (0.07-0.23)	0.10 (0.06-0.20)	No ($p = 0.06973$)
ROI2	0.11 (0.06-0.17)	0.11 (0.05-0.18)	No ($p = 0.75451$)
ROI3	0.12 (0.05-0.19)	0.11 (0.06-0.17)	No ($p = 0.89339$)

Table A.3: Table of p-values for the relative energy density, evaluated across the entire measurement region of the endothelial activity (NO-dependent) of women with and without migraine, for all different ROIs. Mean values and ranges are given in each case.

Relative energy density endothelial activity (NO-independent)			
Blank	No migraine	Migraine	Significance ($p < 0.05$)
ROI1	0.14 (0.05-0.29)	0.10 (0.04-0.30)	No ($p = 0.19516$)
ROI2	0.09 (0.05-0.30)	0.08 (0.04-0.31)	No ($p = 0.37643$)
ROI3	0.13 (0.05-0.32)	0.14 (0.04-0.28)	No ($p = 0.66155$)

Table A.4: Table of p-values for the relative energy density, evaluated across the entire measurement region of the endothelial activity (NO-independent) of women with and without migraine, for all different ROIs. Mean values and ranges are given in each case.

A.2. Tables: Evaluation of phase characteristics using WT

Relative energy density smooth muscle cells activity			
Blank	No migraine	Migraine	Significance ($p < 0.05$)
ROI1 Baseline	0.22 (0.12-0.42)	0.26 (0.08-0.37)	No ($p = 0.37643$)
ROI1 Peak	0.19 (0.08-0.35)	0.20 (0.04-0.28)	No ($p = 0.54944$)
ROI1 Plateau	0.31 (0.14-0.48)	0.30 (0.15-0.52)	No ($p = 0.64864$)
ROI2 Baseline	0.24 (0.16-0.36)	0.24 (0.11-0.37)	No ($p = 0.86521$)
ROI2 Peak	0.22 (0.10-0.39)	0.22 (0.08-0.32)	No ($p = 0.43699$)
ROI2 Plateau	0.27 (0.15-0.49)	0.24 (0.14-0.52)	No ($p = 0.67455$)
ROI3 Baseline	0.24 (0.16-0.31)	0.24 (0.08-0.34)	No ($p = 0.74097$)
ROI3 Peak	0.21 (0.11-0.45)	0.20 (0.06-0.27)	No ($p = 0.17731$)
ROI3 Plateau	0.29 (0.20-0.46)	0.28 (0.16-0.47)	No ($p = 0.74097$)

Table A.5: Table of p-values for the relative energy density of the smooth muscle cells activity of women with and without migraine, for all different combinations of ROIs and phases. Mean values and ranges are given in each case.

Relative energy density neurogenic activity			
Blank	No migraine	Migraine	Significance ($p < 0.05$)
ROI1 Baseline	0.21 (0.07-0.39)	0.19 (0.03-0.38)	No ($p = 0.35745$)
ROI1 Peak	0.21 (0.12-0.38)	0.22 (0.07-0.35)	No ($p = 0.97862$)
ROI1 Plateau	0.21 (0.08-0.36)	0.21 (0.11-0.39)	No ($p = 0.76812$)
ROI2 Baseline	0.23 (0.09-0.33)	0.23 (0.04-0.34)	No ($p = 0.90754$)
ROI2 Peak	0.24 (0.09-0.34)	0.23 (0.09-0.43)	No ($p = 0.79556$)
ROI2 Plateau	0.22 (0.12-0.36)	0.27 (0.10-0.44)	No ($p = 0.24184$)
ROI3 Baseline	0.22 (0.09-0.32)	0.17 (0.04-0.34)	No ($p = 0.22777$)
ROI3 Peak	0.20 (0.12-0.42)	0.19 (0.06-0.34)	No ($p = 0.45836$)
ROI3 Plateau	0.19 (0.10-0.36)	0.21 (0.09-0.34)	No ($p = 0.74097$)

Table A.6: Table of p-values for the relative energy density of the neurogenic activity of women with and without migraine, for all different combinations of ROIs and phases. Mean values and ranges are given in each case.

Relative energy density endothelial activity (NO-independent)			
Blank	No migraine	Migraine	Significance ($p < 0.05$)
ROI1 Baseline	0.11 (0.03-0.26)	0.09 (0.02-0.27)	No ($p = 0.17731$)
ROI1 Peak	0.18 (0.04-0.41)	0.13 (0.02-0.40)	No ($p = 0.13569$)
ROI1 Plateau	0.08 (0.01-0.21)	0.05 (0.02-0.30)	No ($p = 0.63584$)
ROI2 Baseline	0.11 (0.02-0.22)	0.09 (0.01-0.18)	No ($p = 0.27180$)
ROI2 Peak	0.09 (0.02-0.54)	0.08 (0.02-0.37)	No ($p = 0.82326$)
ROI2 Plateau	0.06 (0.02-0.20)	0.05 (0.004-0.27)	No ($p = 0.59811$)
ROI3 Baseline	0.12 (0.03-0.23)	0.11 (0.03-0.43)	No ($p = 0.79556$)
ROI3 Peak	0.19 (0.03-0.45)	0.14 (0.03-0.44)	No ($p = 0.61057$)
ROI3 Plateau	0.08 (0.02-0.27)	0.09 (0.02-0.26)	No ($p = 0.74097$)

Table A.7: Table of p-values for the relative energy density of the endothelial activity (NO-independent) of women with and without migraine, for all different combinations of ROIs and phases. Mean values and ranges are given in each case.

A.3. Tables: Entire measurement region evaluation using DFT

Relative energy density smooth muscle cells activity			
Blank	No migraine	Migraine	Significance ($p < 0.05$)
ROI1	0.18 (0.12-0.35)	0.20 (0.11-0.33)	No ($p = 0.17731$)
ROI2	0.20 (0.11-0.32)	0.20 (0.14-0.32)	No ($p = 0.59811$)
ROI3	0.16 (0.10-0.35)	0.15 (0.11-0.34)	No ($p = 0.48031$)

Table A.8: Table of p-values for the relative energy density, evaluated across the entire measurement region of the smooth muscle cells activity of women with and without migraine, for all different ROIs, using DFT. Mean values and ranges are given in each case.

Relative energy density neurogenic activity			
Blank	No migraine	Migraine	Significance ($p < 0.05$)
ROI1	0.20 (0.11-0.28)	0.20 (0.10-0.30)	No ($p = 0.76812$)
ROI2	0.20 (0.14-0.29)	0.20 (0.14-0.34)	No ($p = 0.45836$)
ROI3	0.18 (0.14-0.27)	0.18 (0.11-0.24)	No ($p = 0.54944$)

Table A.9: Table of p-values for the relative energy density, evaluated across the entire measurement region of the neurogenic activity of women with and without migraine, for all different ROIs, using DFT. Mean values and ranges are given in each case.

A.4. Tables: Evaluation of phase characteristics using DFT

Relative energy density smooth muscle cells activity			
Blank	No migraine	Migraine	Significance ($p < 0.05$)
ROI1 Baseline	0.24 (0.11-0.45)	0.27 (0.08-0.42)	No ($p = 0.67455$)
ROI1 Peak	0.15 (0.09-0.34)	0.18 (0.04-0.28)	No ($p = 0.92171$)
ROI1 Plateau	0.32 (0.12-0.53)	0.27 (0.15-0.57)	No ($p = 0.66155$)
ROI2 Baseline	0.23 (0.13-0.37)	0.25 (0.10-0.40)	No ($p = 0.71414$)
ROI2 Peak	0.20 (0.05-0.32)	0.21 (0.08-0.30)	No ($p = 0.72751$)
ROI2 Plateau	0.29 (0.14-0.50)	0.26 (0.14-0.56)	No ($p = 0.74097$)
ROI3 Baseline	0.26 (0.14-0.38)	0.27 (0.05-0.38)	No ($p = 0.86521$)
ROI3 Peak	0.15 (0.07-0.33)	0.16 (0.05-0.26)	No ($p = 0.61057$)
ROI3 Plateau	0.31 (0.15-0.46)	0.29 (0.17-0.53)	No ($p = 0.89339$)

Table A.10: Table of p-values for the relative energy density of the smooth muscle cells activity of women with and without migraine, for all different combinations of ROIs and phases, using DFT. Mean values and ranges are given in each case.

Relative energy density neurogenic activity			
Blank	No migraine	Migraine	Significance ($p < 0.05$)
ROI1 Baseline	0.19 (0.07-0.37)	0.20 (0.03-0.39)	No ($p = 0.67455$)
ROI1 Peak	0.19 (0.07-0.34)	0.19 (0.05-0.40)	No ($p = 0.72751$)
ROI1 Plateau	0.20 (0.08-0.34)	0.20 (0.09-0.38)	No ($p = 0.96437$)
ROI2 Baseline	0.18 (0.08-0.31)	0.23 (0.03-0.38)	No ($p = 0.36686$)
ROI2 Peak	0.20 (0.04-0.34)	0.21 (0.08-0.40)	No ($p = 0.62315$)
ROI2 Plateau	0.22 (0.11-0.38)	0.26 (0.12-0.49)	No ($p = 0.43699$)
ROI3 Baseline	0.20 (0.08-0.31)	0.19 (0.04-0.32)	No ($p = 0.97862$)
ROI3 Peak	0.18 (0.06-0.30)	0.18 (0.04-0.35)	No ($p = 0.83719$)
ROI3 Plateau	0.18 (0.09-0.37)	0.20 (0.09-0.33)	No ($p = 0.87928$)

Table A.11: Table of p-values for the relative energy density of the neurogenic activity of women with and without migraine, for all different combinations of ROIs and phases, using DFT. Mean values and ranges are given in each case.

Relative energy density endothelial activity (NO-independent)			
Blank	No migraine	Migraine	Significance ($p < 0.05$)
ROI1 Baseline	0.08 (0.01-0.26)	0.07 (0.001-0.26)	No ($p = 0.15032$)
ROI1 Peak	0.30 (0.07-0.65)	0.19 (0.04-0.51)	No ($p = 0.05475$)
ROI1 Plateau	0.05 (0.001-0.25)	0.04 (0.0009-0.38)	No ($p = 0.99287$)
ROI2 Baseline	0.10 (0.01-0.30)	0.07 (0.006-0.24)	No ($p = 0.11794$)
ROI2 Peak	0.15 (0.02-0.76)	0.12 (0.009-0.50)	No ($p = 0.27180$)
ROI2 Plateau	0.03 (0.0005-0.24)	0.05 (0.001-0.26)	No ($p = 0.11379$)
ROI3 Baseline	0.09 (0.01-0.28)	0.09 (0.0002-0.51)	No ($p = 0.59811$)
ROI3 Peak	0.31 (0.05-0.72)	0.27 (0.05-0.61)	No ($p = 0.43699$)
ROI3 Plateau	0.05 (0.002-0.32)	0.07 (0.003-0.37)	No ($p = 0.64864$)

Table A.12: Table of p-values for the relative energy density of the endothelial activity (NO-independent) of women with and without migraine, for all different combinations of ROIs and phases, using DFT. Mean values and ranges are given in each case.

A.5. Tables: P-values within each group across all phases

Relative energy density respiratory activity using WT		
Blank	Significance (no migraine)	Significance (migraine)
ROI1 Baseline-Peak	No ($p = 0.19738$)	No ($p = 0.15567$)
ROI1 Baseline-Plateau	No ($p = 0.33051$)	No ($p = 0.13733$)
ROI1 Peak-Plateau	No ($p = 0.11396$)	No ($p = 0.42937$)
ROI2 Baseline-Peak	No ($p = 0.68399$)	No ($p = 0.25601$)
ROI2 Baseline-Plateau	No ($p = 0.52706$)	Yes ($p = 0.00153$)
ROI2 Peak-Plateau	No ($p = 0.96645$)	Yes ($p = 0.01788$)
ROI3 Baseline-Peak	Yes ($p = 0.04906$)	Yes ($p = 0.04552$)
ROI3 Baseline-Plateau	No ($p = 0.70476$)	No ($p = 0.07976$)
ROI3 Peak-Plateau	No ($p = 0.11396$)	No ($p = 0.68557$)

Table A.13: Table of p-values for the relative energy density of the respiratory activity of women with and without migraine, analyzed separately within each group across the phases (baseline vs. peak, baseline vs. plateau and peak vs. plateau) in all the ROIs.

Relative energy density smooth muscle cells activity using WT		
Blank	Significance (no migraine)	Significance (migraine)
ROI1 Baseline-Peak	No ($p = 0.06043$)	Yes ($p = 0.00010$)
ROI1 Baseline-Plateau	Yes ($p = 0.00871$)	No ($p = 0.06229$)
ROI1 Peak-Plateau	Yes ($p = 0.00057$)	Yes ($p = 0.0000005$)
ROI2 Baseline-Peak	No ($p = 0.85534$)	No ($p = 0.10086$)
ROI2 Baseline-Plateau	Yes ($p = 0.02486$)	No ($p = 0.16885$)
ROI2 Peak-Plateau	Yes ($p = 0.03399$)	Yes ($p = 0.00198$)
ROI3 Baseline-Peak	No ($p = 0.09510$)	Yes ($p = 0.00380$)
ROI3 Baseline-Plateau	Yes ($p = 0.00281$)	Yes ($p = 0.00988$)
ROI3 Peak-Plateau	Yes ($p = 0.00065$)	Yes ($p = 0.0000003$)

Table A.14: Table of p-values for the relative energy density of the smooth muscle cells activity of women with and without migraine, analyzed separately within each group across the phases (baseline vs. peak, baseline vs. plateau and peak vs. plateau) in all the ROIs.

Relative energy density neurogenic activity using WT		
Blank	Significance (no migraine)	Significance (migraine)
ROI1 Baseline-Peak	No ($p = 0.49080$)	No ($p = 0.19762$)
ROI1 Baseline-Plateau	No ($p = 0.94411$)	No ($p = 0.25601$)
ROI1 Peak-Plateau	No ($p = 0.37475$)	No ($p = 0.83136$)
ROI2 Baseline-Peak	No ($p = 0.43893$)	No ($p = 0.27463$)
ROI2 Baseline-Plateau	No ($p = 0.83337$)	No ($p = 0.06551$)
ROI2 Peak-Plateau	No ($p = 0.94411$)	Yes ($p = 0.03863$)
ROI3 Baseline-Peak	No ($p = 0.98881$)	No ($p = 0.59400$)
ROI3 Baseline-Plateau	No ($p = 0.60331$)	No ($p = 0.22971$)
ROI3 Peak-Plateau	No ($p = 0.24053$)	No ($p = 0.44202$)

Table A.15: Table of p-values for the relative energy density of the neurogenic activity of women with and without migraine, analyzed separately within each group across the phases (baseline vs. peak, baseline vs. plateau and peak vs. plateau) in all the ROIs.

Relative energy density endothelial activity (NO-dependent) using WT		
Blank	Significance (no migraine)	Significance (migraine)
ROI1 Baseline-Peak	No ($p = 0.70476$)	Yes ($p = 0.01058$)
ROI1 Baseline-Plateau	No ($p = 0.17798$)	No ($p = 0.74932$)
ROI1 Peak-Plateau	No ($p = 0.42234$)	Yes ($p = 0.00694$)
ROI2 Baseline-Peak	No ($p = 0.81154$)	Yes ($p = 0.01132$)
ROI2 Baseline-Plateau	No ($p = 0.31651$)	No ($p = 0.55035$)
ROI2 Peak-Plateau	No ($p = 0.52706$)	Yes ($p = 0.04552$)
ROI3 Baseline-Peak	No ($p = 0.96645$)	Yes ($p = 0.02155$)
ROI3 Baseline-Plateau	No ($p = 0.62309$)	No ($p = 0.89834$)
ROI3 Peak-Plateau	No ($p = 0.60331$)	Yes ($p = 0.00074$)

Table A.16: Table of p-values for the relative energy density of the endothelial activity (NO-dependent) of women with and without migraine, analyzed separately within each group across the phases (baseline vs. peak, baseline vs. plateau and peak vs. plateau) in all the ROIs.

Relative energy density endothelial activity (NO-independent) using WT		
Blank	Significance (no migraine)	Significance (migraine)
ROI1 Baseline-Peak	Yes ($p = 0.00533$)	Yes ($p = 0.04083$)
ROI1 Baseline-Plateau	Yes ($p = 0.02293$)	No ($p = 0.18283$)
ROI1 Peak-Plateau	Yes ($p = 0.00224$)	Yes ($p = 0.00801$)
ROI2 Baseline-Peak	No ($p = 0.37475$)	No ($p = 0.94907$)
ROI2 Baseline-Plateau	Yes ($p = 0.01260$)	No ($p = 0.35785$)
ROI2 Peak-Plateau	No ($p = 0.10110$)	No ($p = 0.36923$)
ROI3 Baseline-Peak	Yes ($p = 0.02913$)	Yes ($p = 0.01382$)
ROI3 Baseline-Plateau	Yes ($p = 0.04249$)	No ($p = 0.20533$)
ROI3 Peak-Plateau	Yes ($p = 0.00032$)	Yes ($p = 0.00215$)

Table A.17: Table of p-values for the relative energy density of the endothelial activity (NO-independent) of women with and without migraine, analyzed separately within each group across the phases (baseline vs. peak, baseline vs. plateau and peak vs. plateau) in all the ROIs.

A.6. Tables: P-values within each group across all ROIs using WT

Relative energy density respiratory activity		
Blank	Significance (no migraine)	Significance (migraine)
Baseline ROI1-ROI3	Yes ($p = 0.01152$)	No ($p = 0.09633$)
Baseline ROI2-ROI3	Yes ($p = 0.03665$)	No ($p = 0.068870$)
Peak ROI1-ROI3	No ($p = 0.94411$)	Yes ($p = 0.01211$)
Peak ROI2-ROI3	Yes ($p = 0.00004$)	Yes ($p = 0.00074$)
Plateau ROI1-ROI3	No ($p = 0.89957$)	No ($p = 0.28427$)
Plateau ROI2-ROI3	No ($p = 0.76830$)	No ($p = 0.32500$)

Table A.18: Table of p-values for the relative energy density of the respiratory activity of women with and without migraine, analyzed separately within each group across the ROIs (ROI1 vs. ROI3 and ROI2 vs. ROI3) in every phase. ROI3 is the control region.

Relative energy density smooth muscle cells activity		
Blank	Significance (no migraine)	Significance (migraine)
Baseline ROI1-ROI3	No ($p = 0.94411$)	No ($p = 0.12065$)
Baseline ROI2-ROI3	No ($p = 0.96645$)	No ($p = 0.50830$)
Peak ROI1-ROI3	No ($p = 0.39025$)	No ($p = 0.59400$)
Peak ROI2-ROI3	No ($p = 0.25225$)	Yes ($p = 0.00006$)
Plateau ROI1-ROI3	No ($p = 0.87741$)	No ($p = 0.78186$)
Plateau ROI2-ROI3	No ($p = 0.39025$)	No ($p = 0.38084$)

Table A.19: Table of p-values for the relative energy density of the smooth muscle cells activity of women with and without migraine, analyzed separately within each group across the ROIs (ROI1 vs. ROI3 and ROI2 vs. ROI3) in every phase. ROI3 is the control region.

Relative energy density neurogenic activity		
Blank	Significance (no migraine)	Significance (migraine)
Baseline ROI1-ROI3	No ($p = 0.94411$)	No ($p = 0.41692$)
Baseline ROI2-ROI3	No ($p = 0.78984$)	Yes ($p = 0.00516$)
Peak ROI1-ROI3	No ($p = 0.42234$)	Yes ($p = 0.02583$)
Peak ROI2-ROI3	No ($p = 0.21822$)	Yes ($p = 0.00019$)
Plateau ROI1-ROI3	No ($p = 0.87741$)	No ($p = 0.41692$)
Plateau ROI2-ROI3	No ($p = 0.08392$)	Yes ($p = 0.00030$)

Table A.20: Table of p-values for the relative energy density of the neurogenic activity of women with and without migraine, analyzed separately within each group across the ROIs (ROI1 vs. ROI3 and ROI2 vs. ROI3) in every phase. ROI3 is the control region.

Relative energy density endothelial activity (NO-dependent)		
Blank	Significance (no migraine)	Significance (migraine)
Baseline ROI1-ROI3	No ($p = 0.12084$)	No ($p = 0.34668$)
Baseline ROI2-ROI3	No ($p = 0.34488$)	Yes ($p = 0.00380$)
Peak ROI1-ROI3	No ($p = 0.72574$)	No ($p = 0.14937$)
Peak ROI2-ROI3	No ($p = 0.24053$)	Yes ($p = 0.00005$)
Plateau ROI1-ROI3	No ($p = 0.72574$)	No ($p = 0.57928$)
Plateau ROI2-ROI3	No ($p = 0.22919$)	No ($p = 0.25601$)

Table A.21: Table of p-values for the relative energy density of the endothelial activity (NO-dependent) of women with and without migraine, analyzed separately within each group across the ROIs (ROI1 vs. ROI3 and ROI2 vs. ROI3) in every phase. ROI3 is the control region..

Relative energy density endothelial activity (NO-independent)		
Blank	Significance (no migraine)	Significance (migraine)
Baseline ROI1-ROI3	No ($p = 0.30290$)	Yes ($p = 0.00276$)
Baseline ROI2-ROI3	No ($p = 0.06465$)	Yes ($p = 0.00254$)
Peak ROI1-ROI3	No ($p = 0.81154$)	Yes ($p = 0.01211$)
Peak ROI2-ROI3	Yes ($p = 0.00065$)	Yes ($p = 0.00002$)
Plateau ROI1-ROI3	No ($p = 0.50877$)	No ($p = 0.06229$)
Plateau ROI2-ROI3	No ($p = 0.28967$)	No ($p = 0.05920$)

Table A.22: Table of p-values for the relative energy density of the endothelial activity (NO-independent) of women with and without migraine, analyzed separately within each group across the ROIs (ROI1 vs. ROI3 and ROI2 vs. ROI3) in every phase. ROI3 is the control region.

Tables: P-values within each group across all ROIs using FT

Relative energy density respiratory activity		
Blank	Significance (no migraine)	Significance (migraine)
Baseline ROI1-ROI3	No ($p = 0.31651$)	No ($p = 0.18283$)
Baseline ROI2-ROI3	No ($p = 0.19738$)	No ($p = 0.15567$)
Peak ROI1-ROI3	No ($p = 0.06043$)	Yes ($p = 0.00012$)
Peak ROI2-ROI3	Yes ($p = 0.00002$)	Yes ($p = 0.00002$)
Plateau ROI1-ROI3	No ($p = 1.0$)	No ($p = 0.07976$)
Plateau ROI2-ROI3	No ($p = 0.49080$)	No ($p = 0.63912$)

Table A.23: Table of p-values for the relative energy density of the respiratory activity of women with and without migraine, analyzed separately within each group across the ROIs (ROI1 vs. ROI3 and ROI2 vs. ROI3) in every phase, using DFT. ROI3 is the control region.

Relative energy density smooth muscle cells activity		
Blank	Significance (no migraine)	Significance (migraine)
Baseline ROI1-ROI3	No ($p = 0.54567$)	No ($p = 0.15567$)
Baseline ROI2-ROI3	No ($p = 0.06910$)	No ($p = 0.62393$)
Peak ROI1-ROI3	No ($p = 0.06465$)	Yes ($p = 0.03654$)
Peak ROI2-ROI3	Yes ($p = 0.00718$)	Yes ($p = 0.00003$)
Plateau ROI1-ROI3	No ($p = 0.85534$)	No ($p = 0.66995$)
Plateau ROI2-ROI3	No ($p = 0.30290$)	No ($p = 0.05064$)

Table A.24: Table of p-values for the relative energy density of the smooth muscle cells activity of women with and without migraine, analyzed separately within each group across the ROIs (ROI1 vs. ROI3 and ROI2 vs. ROI3) in every phase, using DFT. ROI3 is the control region.

Relative energy density neurogenic activity		
Blank	Significance (no migraine)	Significance (migraine)
Baseline ROI1-ROI3	No ($p = 0.22919$)	No ($p = 0.22137$)
Baseline ROI2-ROI3	No ($p = 0.89957$)	No ($p = 0.07599$)
Peak ROI1-ROI3	No ($p = 0.16881$)	Yes ($p = 0.04552$)
Peak ROI2-ROI3	Yes ($p = 0.04906$)	Yes ($p = 0.00117$)
Plateau ROI1-ROI3	No ($p = 0.85534$)	No ($p = 0.32500$)
Plateau ROI2-ROI3	No ($p = 0.07873$)	Yes ($p = 0.00037$)

Table A.25: Table of p-values for the relative energy density of the neurogenic activity of women with and without migraine, analyzed separately within each group across the ROIs (ROI1 vs. ROI3 and ROI2 vs. ROI3) in every phase, using DFT. ROI3 is the control region.

Relative energy density endothelial activity (NO-dependent)		
Blank	Significance (no migraine)	Significance (migraine)
Baseline ROI1-ROI3	No ($p = 0.27682$)	Yes ($p = 0.04552$)
Baseline ROI2-ROI3	No ($p = 0.85534$)	Yes ($p = 0.00922$)
Peak ROI1-ROI3	Yes ($p = 0.03148$)	Yes ($p = 0.01058$)
Peak ROI2-ROI3	Yes ($p = 0.00533$)	Yes ($p = 0.00005$)
Plateau ROI1-ROI3	No ($p = 0.94411$)	No ($p = 0.18283$)
Plateau ROI2-ROI3	No ($p = 0.98881$)	No ($p = 0.60888$)

Table A.26: Table of p-values for the relative energy density of the endothelial activity (NO-dependent) of women with and without migraine, analyzed separately within each group across the ROIs (ROI1 vs. ROI3 and ROI2 vs. ROI3) in every phase, using DFT. ROI3 is the control region..

Relative energy density endothelial activity (NO-independent)		
Blank	Significance (no migraine)	Significance (migraine)
Baseline ROI1-ROI3	No ($p = 0.25225$)	Yes ($p = 0.01294$)
Baseline ROI2-ROI3	No ($p = 0.60331$)	No ($p = 0.59400$)
Peak ROI1-ROI3	No ($p = 0.07873$)	Yes ($p = 0.00182$)
Peak ROI2-ROI3	Yes ($p = 0.00015$)	Yes ($p = 0.00006$)
Plateau ROI1-ROI3	No ($p = 0.50877$)	No ($p = 0.16885$)
Plateau ROI2-ROI3	No ($p = 0.17798$)	No ($p = 0.48120$)

Table A.27: Table of p-values for the relative energy density of the endothelial activity (NO-independent) of women with and without migraine, analyzed separately within each group across the ROIs (ROI1 vs. ROI3 and ROI2 vs. ROI3) in every phase, using DFT. ROI3 is the control region.

A.7. Tables: Women with aura using WT

Relative energy density respiratory activity			
Blank	No migraine	Migraine with aura	Significance ($p < 0.05$)
ROI1	0.18 (0.10-0.33)	0.20 (0.12-0.46)	No ($p = 0.06175$)
ROI2	0.19 (0.12-0.32)	0.19 (0.12-0.37)	No ($p = 0.51691$)
ROI3	0.17 (0.11-0.31)	0.21 (0.14-0.44)	No ($p = 0.13705$)

Table A.28: Table of p-values for the relative energy density, evaluated across the entire measurement region of the respiratory activity of women with migraine with aura and women without migraine, for all different ROIs. Mean values and ranges are given in each case.

Relative energy density respiratory activity			
Blank	No migraine	Migraine with aura	Significance ($p < 0.05$)
ROI1 Baseline	0.20 (0.10-0.39)	0.21 (0.06-0.71)	No ($p = 0.17390$)
ROI1 Peak	0.18 (0.06-0.37)	0.21 (0.09-0.47)	Yes ($p = 0.01144$)
ROI1 Plateau	0.20 (0.13-0.34)	0.23 (0.10-0.49)	No ($p = 0.30331$)
ROI2 Baseline	0.22 (0.11-0.43)	0.24 (0.09-0.57)	No ($p = 0.31540$)
ROI2 Peak	0.20 (0.06-0.40)	0.23 (0.14-0.45)	No ($p = 0.28005$)
ROI2 Plateau	0.20 (0.11-0.40)	0.21 (0.06-0.32)	No ($p = 0.90894$)
ROI3 Baseline	0.21 (0.11-0.40)	0.21 (0.03-0.61)	No ($p = 0.50061$)
ROI3 Peak	0.17 (0.08-0.34)	0.19 (0.10-0.53)	No ($p = 0.39452$)
ROI3 Plateau	0.19 (0.14-0.39)	0.22 (0.09-0.39)	No ($p = 0.43822$)

Table A.29: Table of p-values for the relative energy density of the respiratory activity of women with migraine with aura and women without migraine, for all different combinations of ROIs and phases. Mean values and ranges are given in each case.

Relative energy density smooth muscle cells activity			
Blank	No migraine	Migraine with aura	Significance ($p < 0.05$)
ROI1	0.24 (0.15-0.36)	0.22 (0.12-0.43)	No ($p = 1.0$)
ROI2	0.24 (0.17-0.31)	0.22 (0.14-0.38)	No ($p = 0.67494$)
ROI3	0.24 (0.14-0.44)	0.22 (0.16-0.36)	No ($p = 0.56741$)

Table A.30: Table of p-values for the relative energy density, evaluated across the entire measurement region of the smooth muscle cells activity of women with migraine with aura and women without migraine, for all different ROIs. Mean values and ranges are given in each case.

Relative energy density smooth muscle cells activity			
Blank	No migraine	Migraine with aura	Significance ($p < 0.05$)
ROI1 Baseline	0.22 (0.12-0.42)	0.26 (0.08-0.37)	No ($p = 0.40878$)
ROI1 Peak	0.19 (0.08-0.35)	0.20 (0.04-0.28)	No ($p = 0.38056$)
ROI1 Plateau	0.31 (0.14-0.48)	0.30 (0.15-0.52)	No ($p = 0.90894$)
ROI2 Baseline	0.24 (0.16-0.36)	0.25 (0.11-0.37)	No ($p = 0.82896$)
ROI2 Peak	0.22 (0.10-0.39)	0.22 (0.08-0.32)	No ($p = 0.48458$)
ROI2 Plateau	0.27 (0.15-0.49)	0.31 (0.18-0.52)	No ($p = 0.65647$)
ROI3 Baseline	0.24 (0.16-0.31)	0.24 (0.08-0.34)	No ($p = 0.75071$)
ROI3 Peak	0.21 (0.11-0.45)	0.19 (0.06-0.26)	No ($p = 0.19931$)
ROI3 Plateau	0.29 (0.20-0.46)	0.31 (0.16-0.45)	No ($p = 0.53348$)

Table A.31: Table of p-values for the relative energy density of the smooth muscle cells activity of women with migraine with aura and women without migraine, for all different combinations of ROIs and phases. Mean values and ranges are given in each case.

Relative energy density neurogenic activity			
Blank	No migraine	Migraine with aura	Significance ($p < 0.05$)
ROI1	0.21 (0.12-0.35)	0.20 (0.11-0.27)	No ($p = 0.38056$)
ROI2	0.24 (0.16-0.33)	0.22 (0.14-0.34)	No ($p = 0.56741$)
ROI3	0.20 (0.13-0.37)	0.20 (0.11-0.25)	No ($p = 0.17390$)

Table A.32: Table of p-values for the relative energy density, evaluated across the entire measurement region of the neurogenic activity of women with migraine with aura and women without migraine, for all different ROIs. Mean values and ranges are given in each case.

Relative energy density neurogenic activity			
Blank	No migraine	Migraine with aura	Significance ($p < 0.05$)
ROI1 Baseline	0.21 (0.07-0.39)	0.19 (0.03-0.33)	No ($p = 0.36691$)
ROI1 Peak	0.21 (0.12-0.38)	0.18 (0.07-0.30)	No ($p = 0.17390$)
ROI1 Plateau	0.21 (0.08-0.36)	0.19 (0.11-0.31)	No ($p = 0.45338$)
ROI2 Baseline	0.23 (0.09-0.33)	0.18 (0.04-0.34)	No ($p = 0.62016$)
ROI2 Peak	0.24 (0.09-0.34)	0.20 (0.09-0.35)	No ($p = 0.17390$)
ROI2 Plateau	0.22 (0.12-0.36)	0.20 (0.10-0.42)	No ($p = 0.56741$)
ROI3 Baseline	0.22 (0.09-0.32)	0.17 (0.04-0.34)	No ($p = 0.21769$)
ROI3 Peak	0.20 (0.12-0.42)	0.14 (0.06-0.34)	No ($p = 0.07316$)
ROI3 Plateau	0.19 (0.10-0.36)	0.17 (0.09-0.34)	No ($p = 0.36691$)

Table A.33: Table of p-values for the relative energy density of the neurogenic activity of women with migraine with aura and women without migraine, for all different combinations of ROIs and phases. Mean values and ranges are given in each case.

Relative energy density endothelial activity (NO-dependent)			
Blank	No migraine	Migraine with aura	Significance ($p < 0.05$)
ROI1	0.13 (0.07-0.23)	0.11 (0.07-0.20)	No ($p = 0.15836$)
ROI2	0.11 (0.06-0.17)	0.11 (0.07-0.18)	No ($p = 0.75071$)
ROI3	0.12 (0.05-0.19)	0.12 (0.08-0.16)	No ($p = 0.69361$)

Table A.34: Table of p-values for the relative energy density, evaluated across the entire measurement region of the endothelial activity (NO-dependent) of women with migraine with aura and women without migraine, for all different ROIs. Mean values and ranges are given in each case.

Relative energy density endothelial activity (NO-dependent)			
Blank	No migraine	Migraine with aura	Significance ($p < 0.05$)
ROI1 Baseline	0.10 (0.04-0.30)	0.07 (0.04-0.20)	Yes ($p = 0.04602$)
ROI1 Peak	0.10 (0.04-0.23)	0.12 (0.07-0.22)	No ($p = 0.09596$)
ROI1 Plateau	0.08 (0.02-0.22)	0.07 (0.03-0.16)	No ($p = 0.51691$)
ROI2 Baseline	0.09 (0.03-0.25)	0.07 (0.04-0.15)	No ($p = 0.06175$)
ROI2 Peak	0.09 (0.03-0.22)	0.11 (0.05-0.19)	No ($p = 0.25804$)
ROI2 Plateau	0.08 (0.02-0.21)	0.07 (0.03-0.18)	No ($p = 0.94934$)
ROI3 Baseline	0.10 (0.04-0.20)	0.08 (0.04-0.20)	No ($p = 0.23724$)
ROI3 Peak	0.10 (0.04-0.26)	0.14 (0.10-0.25)	Yes ($p = 0.00260$)
ROI3 Plateau	0.09 (0.03-0.21)	0.09 (0.03-0.19)	No ($p = 0.84882$)

Table A.35: Table of p-values for the relative energy density of the endothelial activity (NO-dependent) of women with migraine with aura and women without migraine, for all different combinations of ROIs and phases. Mean values and ranges are given in each case.

Relative energy density endothelial activity (NO-independent)			
Blank	No migraine	Migraine with aura	Significance ($p < 0.05$)
ROI1	0.14 (0.05-0.29)	0.11 (0.05-0.30)	No ($p = 0.65647$)
ROI2	0.09 (0.05-0.30)	0.10 (0.04-0.31)	No ($p = 0.77007$)
ROI3	0.13 (0.05-0.32)	0.14 (0.07-0.28)	No ($p = 0.53348$)

Table A.36: Table of p-values for the relative energy density, evaluated across the entire measurement region of the endothelial activity (NO-independent) of women with migraine with aura and women without migraine, for all different ROIs. Mean values and ranges are given in each case.

Relative energy density endothelial activity (NO-independent)			
Blank	No migraine	Migraine	Significance ($p < 0.05$)
ROI1 Baseline	0.11 (0.03-0.26)	0.09 (0.02-0.27)	No ($p = 0.38056$)
ROI1 Peak	0.18 (0.04-0.41)	0.15 (0.02-0.40)	No ($p = 0.32781$)
ROI1 Plateau	0.08 (0.01-0.21)	0.05 (0.02-0.30)	No ($p = 0.60234$)
ROI2 Baseline	0.11 (0.02-0.22)	0.10 (0.03-0.18)	No ($p = 0.50061$)
ROI2 Peak	0.09 (0.02-0.54)	0.09 (0.02-0.37)	No ($p = 0.78957$)
ROI2 Plateau	0.06 (0.02-0.20)	0.04 (0.004-0.27)	No ($p = 0.26889$)
ROI3 Baseline	0.12 (0.03-0.23)	0.11 (0.03-0.43)	No ($p = 0.63821$)
ROI3 Peak	0.19 (0.03-0.45)	0.14 (0.07-0.44)	No ($p = 0.94934$)
ROI3 Plateau	0.08 (0.02-0.27)	0.09 (0.02-0.26)	No ($p = 0.56741$)

Table A.37: Table of p-values for the relative energy density of the endothelial activity (NO-independent) of women with migraine with aura and women without migraine, for all different combinations of ROIs and phases. Mean values and ranges are given in each case.

A.8. Tables: Women with aura using DFT

Relative energy density respiratory activity			
Blank	No migraine	Migraine with aura	Significance ($p < 0.05$)
ROI1	0.16 (0.08-0.23)	0.19 (0.11-0.50)	No ($p = 0.08623$)
ROI2	0.18 (0.09-0.33)	0.19 (0.12-0.41)	No ($p = 0.35356$)
ROI3	0.15 (0.09-0.22)	0.16 (0.10-0.46)	No ($p = 0.39452$)

Table A.38: Table of p-values for the relative energy density, evaluated across the entire measurement region of the respiratory activity of women with migraine with aura and women without migraine, for all different ROIs, using DFT. Mean values and ranges are given in each case.

Relative energy density respiratory activity			
Blank	No migraine	Migraine with aura	Significance ($p < 0.05$)
ROI1 Baseline	0.24 (0.12-0.43)	0.26 (0.09-0.77)	No ($p = 0.20835$)
ROI1 Peak	0.19 (0.07-0.42)	0.23 (0.11-0.53)	Yes ($p = 0.02977$)
ROI1 Plateau	0.23 (0.15-0.47)	0.25 (0.12-0.58)	No ($p = 0.42335$)
ROI2 Baseline	0.25 (0.14-0.47)	0.29 (0.11-0.65)	No ($p = 0.13705$)
ROI2 Peak	0.22 (0.03-0.39)	0.25 (0.11-0.54)	No ($p = 0.35356$)
ROI2 Plateau	0.21 (0.13-0.48)	0.21 (0.06-0.46)	No ($p = 0.82896$)
ROI3 Baseline	0.23 (0.14-0.44)	0.27 (0.05-0.69)	No ($p = 0.32781$)
ROI3 Peak	0.5 (0.03-0.24)	0.16 (0.06-0.58)	No ($p = 0.28005$)
ROI3 Plateau	0.21 (0.15-0.46)	0.22 (0.12-0.44)	No ($p = 0.80920$)

Table A.39: Table of p-values for the relative energy density of the respiratory activity of women with migraine with aura and women without migraine, for all different combinations of ROIs and phases, using DFT. Mean values and ranges are given in each case.

Relative energy density smooth muscle cells activity			
Blank	No migraine	Migraine with aura	Significance ($p < 0.05$)
ROI1	0.18 (0.12-0.35)	0.21 (0.11-0.33)	No ($p = 0.30331$)
ROI2	0.20 (0.11-0.32)	0.19 (0.14-0.32)	No ($p = 0.98986$)
ROI3	0.16 (0.10-0.35)	0.16 (0.13-0.32)	No ($p = 0.71247$)

Table A.40: Table of p-values for the relative energy density, evaluated across the entire measurement region of the smooth muscle cells activity of women with migraine with aura and women without migraine, for all different ROIs, using DFT. Mean values and ranges are given in each case.

Relative energy density smooth muscle cells activity			
Blank	No migraine	Migraine with aura	Significance ($p < 0.05$)
ROI1 Baseline	0.24 (0.11-0.45)	0.29 (0.08-0.42)	No ($p = 0.51691$)
ROI1 Peak	0.15 (0.09-0.34)	0.17 (0.04-0.28)	No ($p = 0.69361$)
ROI1 Plateau	0.32 (0.12-0.53)	0.29 (0.15-0.57)	No ($p = 0.80920$)
ROI2 Baseline	0.23 (0.13-0.37)	0.27 (0.10-0.40)	No ($p = 0.78957$)
ROI2 Peak	0.20 (0.05-0.32)	0.20 (0.08-0.30)	No ($p = 0.55032$)
ROI2 Plateau	0.29 (0.14-0.50)	0.28 (0.18-0.56)	No ($p = 0.78957$)
ROI3 Baseline	0.26 (0.14-0.38)	0.26 (0.06-0.38)	No ($p = 0.75071$)
ROI3 Peak	0.15 (0.07-0.33)	0.15 (0.05-0.26)	No ($p = 0.36691$)
ROI3 Plateau	0.31 (0.15-0.46)	0.34 (0.17-0.53)	No ($p = 0.58475$)

Table A.41: Table of p-values for the relative energy density of the smooth muscle cells activity of women with migraine with aura and women without migraine, for all different combinations of ROIs and phases, using DFT. Mean values and ranges are given in each case.

Relative energy density neurogenic activity			
Blank	No migraine	Migraine with aura	Significance ($p < 0.05$)
ROI1	0.20 (0.11-0.28)	0.19 (0.10-0.26)	No ($p = 0.42335$)
ROI2	0.20 (0.14-0.29)	0.20 (0.14-0.34)	No ($p = 0.80920$)
ROI3	0.18 (0.14-0.27)	0.17 (0.11-0.22)	No ($p = 0.28005$)

Table A.42: Table of p-values for the relative energy density, evaluated across the entire measurement region of the neurogenic activity of women with migraine with aura and women without migraine, for all different ROIs, using DFT. Mean values and ranges are given in each case.

Relative energy density neurogenic activity			
Blank	No migraine	Migraine with aura	Significance ($p < 0.05$)
ROI1 Baseline	0.19 (0.07-0.38)	0.19 (0.03-0.30)	No ($p = 0.78957$)
ROI1 Peak	0.19 (0.07-0.34)	0.18 (0.05-0.34)	No ($p = 0.46884$)
ROI1 Plateau	0.20 (0.08-0.34)	0.18 (0.03-0.38)	No ($p = 0.19931$)
ROI2 Baseline	0.18 (0.08-0.31)	0.18 (0.03-0.38)	No ($p = 0.94934$)
ROI2 Peak	0.20 (0.04-0.34)	0.16 (0.08-0.38)	No ($p = 0.21769$)
ROI2 Plateau	0.22 (0.11-0.38)	0.19 (0.04-0.31)	No ($p = 0.42335$)
ROI3 Baseline	0.20 (0.08-0.31)	0.15 (0.04-0.35)	No ($p = 0.82896$)
ROI3 Peak	0.18 (0.06-0.30)	0.15 (0.05-0.26)	No ($p = 0.13705$)
ROI3 Plateau	0.18 (0.09-0.37)	0.17 (0.09-0.29)	No ($p = 0.26889$)

Table A.43: Table of p-values for the relative energy density of the neurogenic activity of women with migraine with aura and women without migraine, for all different combinations of ROIs and phases, using DFT. Mean values and ranges are given in each case.

Relative energy density endothelial activity (NO-dependent)			
Blank	No migraine	Migraine with aura	Significance ($p < 0.05$)
ROI1	0.16 (0.08-0.25)	0.14 (0.08-0.19)	Yes ($p = 0.00392$)
ROI2	0.20 (0.14-0.29)	0.20 (0.14-0.34)	No ($p = 0.60234$)
ROI3	0.18 (0.10-0.23)	0.17 (0.12-0.26)	No ($p = 0.46884$)

Table A.44: Table of p-values for the relative energy density, evaluated across the entire measurement region of the endothelial activity (NO-dependent) of women with migraine with aura and women without migraine, for all different ROIs, using DFT. Mean values and ranges are given in each case.

Relative energy density endothelial activity (NO-dependent)			
Blank	No migraine	Migraine with aura	Significance ($p < 0.05$)
ROI1 Baseline	0.17 (0.02-0.49)	0.11 (0.04-0.31)	Yes ($p = 0.04075$)
ROI1 Peak	0.12 (0.04-0.27)	0.13 (0.07-0.22)	No ($p = 0.73151$)
ROI1 Plateau	0.12 (0.02-0.32)	0.11 (0.02-0.24)	No ($p = 0.50061$)
ROI2 Baseline	0.16 (0.05-0.33)	0.11 (0.03-0.27)	Yes ($p = 0.02977$)
ROI2 Peak	0.11 (0.03-0.28)	0.11 (0.06-0.20)	No ($p = 0.88883$)
ROI2 Plateau	0.12 (0.01-0.35)	0.10 (0.05-0.28)	No ($p = 0.80920$)
ROI3 Baseline	0.16 (0.03-0.31)	0.11 (0.05-0.35)	No ($p = 0.30331$)
ROI3 Peak	0.15 (0.05-0.34)	0.15 (0.09-0.24)	No ($p = 0.51691$)
ROI3 Plateau	0.11 (0.03-0.29)	0.12 (0.05-0.22)	No ($p = 0.88883$)

Table A.45: Table of p-values for the relative energy density of the endothelial activity (NO-dependent) of women with migraine with aura and women without migraine, for all different combinations of ROIs and phases, using DFT. Mean values and ranges are given in each case.

Relative energy density endothelial activity (NO-independent)			
Blank	No migraine	Migraine with aura	Significance ($p < 0.05$)
ROI1	0.22 (0.08-0.42)	0.21 (0.06-0.37)	No ($p = 0.19930$)
ROI2	0.20 (0.05-0.39)	0.20 (0.07-0.33)	No ($p = 0.58475$)
ROI3	0.29 (0.16-0.42)	0.29 (0.11-0.42)	No ($p = 0.90894$)

Table A.46: Table of p-values for the relative energy density, evaluated across the entire measurement region of the endothelial activity (NO-independent) of women with migraine with aura and women without migraine, for all different ROIs, using DFT. Mean values and ranges are given in each case.

Relative energy density endothelial activity (NO-independent)			
Blank	No migraine	Migraine with aura	Significance ($p < 0.05$)
ROI1 Baseline	0.08 (0.01-0.26)	0.07 (0.002-0.26)	No ($p = 0.39452$)
ROI1 Peak	0.30 (0.07-0.65)	0.23 (0.04-0.51)	No ($p = 0.32781$)
ROI1 Plateau	0.05 (0.002-0.25)	0.04 (0.003-0.38)	No ($p = 0.84882$)
ROI2 Baseline	0.10 (0.01-0.30)	0.09 (0.008-0.23)	No ($p = 0.42335$)
ROI2 Peak	0.15 (0.02-0.76)	0.12 (0.03-0.50)	No ($p = 0.80920$)
ROI2 Plateau	0.03 (0.005-0.24)	0.06 (0.001-0.26)	No ($p = 0.35356$)
ROI3 Baseline	0.09 (0.01-0.28)	0.09 (0.0002-0.24)	No ($p = 0.75071$)
ROI3 Peak	0.31 (0.05-0.72)	0.33 (0.05-0.61)	No ($p = 0.98986$)
ROI3 Plateau	0.05 (0.002-0.32)	0.06 (0.003-0.37)	No ($p = 0.98986$)

Table A.47: Table of p-values for the relative energy density of the endothelial activity (NO-independent) of women with migraine with aura and women without migraine, for all different combinations of ROIs and phases, using DFT. Mean values and ranges are given in each case.

B

Python code

```
import numpy as np
import matplotlib.pyplot as plt
import pywt
import numpy as np
import pandas as pd
from math import ceil
from scipy.fft import fft, fftfreq

#Maken arrays tijden per fase
# baseline_b=[116, 100, 111, 78, 105, 126, 82, 2750, 100, 170, 1617, 75, 1329, 57, 57,
    147, 96, 1163, 81, 73, 247, 1249, 90, 949, 959, 57, 78, 75, 139, 74, 72, 63, 960,
    116, 41, 1048, 64, 108, 88, 946, 64, 152, 112, 83, 165, 81, 88, 83, 48, 135, 71,
    945, 76]
baseline_b=[116, 40, 111, 78, 105, 126, 82, 2750, 100, 170, 1617, 75, 1329, 57, 57,
    147, 96, 1163, 81, 73, 247, 1249, 90, 949, 959, 57, 78, 75, 139, 74, 72, 63, 960,
    116, 41, 1048, 64, 108, 88, 946, 64, 152, 112, 83, 165, 81, 88, 83, 48, 135, 71,
    945, 76]
baseline_e=[416, 340, 411, 378, 405, 426, 382, 3050, 400, 470, 1917, 375, 1629, 357,
    357, 447, 396, 1463, 381, 373, 547, 1549, 390, 1249, 1259, 357, 378, 375, 439, 374,
     372, 363, 1260, 416, 341, 1348, 364, 408, 388, 1246, 364, 452, 412, 383, 465, 381,
     388, 383, 348, 435, 371, 1245, 376]
piek_b=[416, 340, 411, 378, 405, 426, 382, 3050, 400, 470, 1917, 375, 1629, 357, 357,
    447, 396, 1463, 381, 373, 547, 1549, 390, 1249, 1259, 357, 378, 375, 439, 374, 372,
     363, 1260, 416, 341, 1348, 364, 408, 388, 1246, 364, 452, 412, 383, 465, 381, 388,
     383, 348, 435, 371, 1245, 376]
piek_e=[1016, 940, 1011, 978, 1005, 1026, 982, 3650, 1000, 1070, 2517, 975, 2229, 957,
    957, 1047, 996, 2063, 981, 973, 1147, 2149, 990, 1849, 1859, 957, 978, 975, 1039,
    974, 972, 963, 1860, 1016, 941, 1948, 964, 1008, 988, 1846, 964, 1052, 1012, 983,
    1065, 981, 988, 983, 948, 1035, 971, 1845, 976]
plateau_b=[2216, 2140, 2211, 2178, 2205, 2226, 2182, 4853, 2200, 2270, 3717, 2175,
    3429, 2157, 2157, 2247, 2196, 3263, 2181, 2173, 2347, 3349, 2190, 3049, 3059, 2157,
     2178, 2175, 2239, 2174, 2172, 2163, 3060, 2216, 2141, 3148, 2164, 2208, 2188,
    3046, 2164, 2252, 2212, 2183, 2265, 2181, 2188, 2183, 2148, 2235, 2171, 3045, 2176]
plateau_e=[2516, 2440, 2511, 2478, 2505, 2526, 2482, 5150, 2500, 2570, 4017, 2475,
    3729, 2457, 2457, 2547, 2496, 3563, 2481, 2473, 2647, 3649, 2490, 3349, 3359, 2457,
     2478, 2475, 2539, 2474, 2472, 2463, 3360, 2516, 2441, 3448, 2464, 2508, 2488,
    3346, 2464, 2552, 2512, 2483, 2565, 2481, 2488, 2483, 2448, 2535, 2471, 3345, 2476]
N_b=[300, 240, 300, 300, 300, 300, 300, 300, 300, 300, 300, 300, 300, 300, 300, 300,
    300, 300, 300, 300, 300, 300, 300, 300, 300, 300, 300, 300, 300, 300, 300, 300,
    300, 300, 300, 300, 300, 300, 300, 300, 300, 300, 300, 300, 300, 300, 300, 300,
    300, 300, 300, 300, 300]
N_piek=[600, 600, 600, 600, 600, 600, 600, 600, 600, 600, 600, 600, 600, 600, 600, 600,
     600, 600, 600, 600, 600, 600, 600, 600, 600, 600, 600, 600, 600, 600, 600, 600,
    600, 600, 600, 600, 600, 600, 600, 600, 600, 600, 600, 600, 600, 600, 600, 600,
    600, 600, 600, 600, 600]
N_p=[300, 300, 300, 300, 300, 300, 300, 297, 300, 300, 300, 300, 300, 300, 300, 300,
    300, 300, 300, 300, 300, 300, 300, 300, 300, 300, 300, 300, 300, 300, 300, 300,
    300, 300, 300, 300, 300, 300, 300, 300, 300, 300, 300, 300, 300, 300, 300, 300,
    300, 300, 300, 300, 300]

```

```
def reflect_data(data,sample):
    dataMeasurement = data[baseline_b[sample]:plateau_e[sample]]
    reversedData = dataMeasurement[::-1]
    reflectedData = np.concatenate((reversedData, dataMeasurement, reversedData))
    return reflectedData

def scale(voice):
    v=voice #define the value for voice
    num_octaves = np.log2(200 / 2) #calculate the amount of octaves
    num_scales = int(num_octaves * v) + 1
    scales = 2 * 2 ** (np.arange(num_scales) / v)
    return scales

def plot_wavelet_total_amplitude(data,wavelet,sample,ax):
    scales = scale(10)
    coeffs, freqs = pywt.cwt(data,scales,wavelet)
    power = np.abs(coeffs[:,baseline_b[sample]:plateau_e[sample]])
    plot = ax.imshow(power, extent=[0, plateau_e[sample]-baseline_b[sample], freqs[-1],
        freqs[0]], cmap='viridis', aspect='auto')
    ax.set_yscale("log")
    ax.set_xlabel("Time (s)")
    ax.set_ylabel("Frequency (Hz)")
    ax.set_title("Wavelet coefficients plot total for " + wavelet)
    plt.colorbar(plot, ax=ax)
    return ax

def plot_wavelet_total_amplitude_reflecting(data,wavelet,sample,ax,title):
    scales = scale(10)
    reflectedData = reflect_data(data,sample)
    coeffs, freqs = pywt.cwt(reflectedData,scales,wavelet)
    segmentLength = plateau_e[sample]-baseline_b[sample]
    power = np.abs(coeffs[ : , segmentLength : 2*segmentLength])
    plot = ax.imshow(power, extent=[0, segmentLength, freqs[-1], freqs[0]], cmap='
        viridis', aspect='auto')
    ax.set_yscale("log")
    ax.set_xlabel("Time (s)")
    ax.set_ylabel("Frequency (Hz)")
    ax.set_title(title)
    plt.colorbar(plot, ax=ax)
    return ax

def plot_wavelet_total(data,wavelet,sample,ax):
    scales = scale(10)
    coeffs, freqs = pywt.cwt(data,scales,wavelet)
    power = np.abs(coeffs[ : , baseline_b[sample] : plateau_e[sample]])**2
    plot = ax.imshow(power, extent=[0, plateau_e[sample]-baseline_b[sample], freqs[-1],
        freqs[0]], cmap='viridis', aspect='auto')
    ax.set_yscale("log")
    ax.set_xlabel("Time (s)")
    ax.set_ylabel("Frequency (Hz)")
    ax.set_title("Wavelet coefficients plot total for " + wavelet)
    plt.colorbar(plot, ax=ax)
    return ax

def power_wavelet_total_with_reflecting(data,wavelet,sample):
    scales = scale(10)
    reflectedData = reflect_data(data,sample)
    coeffs, freqs = pywt.cwt(reflectedData,scales,wavelet)
    segmentLength = plateau_e[sample]-baseline_b[sample]
    power = np.abs(coeffs[ : , segmentLength : 2*segmentLength])**2
    return power

def plot_wavelet_total_with_reflecting(data,wavelet,sample,ax,title):
    scales = scale(10)
    reflectedData = reflect_data(data,sample)
    coeffs, freqs = pywt.cwt(reflectedData,scales,wavelet)
    segmentLength = plateau_e[sample]-baseline_b[sample]
    power = np.abs(coeffs[ : , segmentLength : 2*segmentLength])**2
    plot = ax.imshow(power, extent=[0, segmentLength, freqs[-1], freqs[0]], cmap='
        viridis', aspect='auto')
    ax.set_yscale("log")
```

```
    ax.set_xlabel("Time (s)")
    ax.set_ylabel("Frequency (Hz)")
    ax.set_title(title)
    plt.colorbar(plot, ax=ax)
    return ax

def plot_data(data,wavelet,sample,ax,title):
    scales = scale(10)
    reflectedData = reflect_data(data,sample)
    coeffs, freqs = pywt.cwt(reflectedData,scales,wavelet)
    segmentLength = plateau_e[sample]-baseline_b[sample]
    plot = ax.imshow(data, extent=[0, segmentLength, freqs[-1], freqs[0]], cmap='viridis', aspect='auto')
    ax.set_yscale("log")
    ax.set_xlabel("Time (s)")
    ax.set_ylabel("Frequency (Hz)")
    ax.set_title(title)
    plt.colorbar(plot, ax=ax)
    return ax

def plot_wavelet_total_with_reflecting_scale(data,wavelet,sample,ax,title,scaleValue):
    scales = scale(scaleValue)
    reflectedData = reflect_data(data,sample)
    coeffs, freqs = pywt.cwt(reflectedData,scales,wavelet)
    segmentLength = plateau_e[sample]-baseline_b[sample]
    power = np.abs(coeffs[ : , segmentLength : 2*segmentLength])**2
    plot = ax.imshow(power, extent=[0, segmentLength, freqs[-1], freqs[0]], cmap='viridis', aspect='auto')
    ax.set_yscale("log")
    ax.set_xlabel("Time (s)")
    ax.set_ylabel("Frequency (Hz)")
    ax.set_title(title)
    plt.colorbar(plot, ax=ax)
    return ax

def COI(data, wavelet, eFoldingTimeFactor): #eFoldingTimeFactor is normally equal to sqrt(2) for morlet
    scales = scale(10)
    coeffs, freqs = pywt.cwt(data, scales, wavelet)
    power = np.abs(coeffs)**2
    reliableCoefficientsBoolean = np.ones((len(power),len(power[0])), bool)
    for i, s in enumerate(scales):
        eFoldingTime = int(np.ceil(s * eFoldingTimeFactor))
        reliableCoefficientsBoolean[i, : eFoldingTime] = False
        reliableCoefficientsBoolean[i, -eFoldingTime : ] = False
    reliableCoefficients = np.where(reliableCoefficientsBoolean, power, np.nan)
    return reliableCoefficients

def plot_wavelet_total_with_COI(data, wavelet, sample, ax, eFoldingTimeFactor,person):
    scales = scale(10)
    coeffs, freqs = pywt.cwt(data, scales, wavelet)
    power = np.abs(coeffs)**2

    reliableCoefficients = COI(data, wavelet, eFoldingTimeFactor)
    plot = ax.imshow(reliableCoefficients, extent=[0, len(data), freqs[-1], freqs[0]], cmap='viridis', aspect='auto')
    ax.set_yscale("log")
    ax.set_xlabel("Time (s)")
    ax.set_ylabel("Frequency (Hz)")
    ax.set_title("Wavelet coefficients plot total for " + wavelet + " with COI" + "person " + str(person))
    plt.colorbar(plot, ax=ax)
    return reliableCoefficients

def plot_wavelet_baseline(data,wavelet,sample,ax):
    scales = scale(10)
    coeffs, freqs = pywt.cwt(data,scales,wavelet)
    power = np.abs(coeffs[:,baseline_b[sample]:baseline_e[sample]])**2
    plot = ax.imshow(power, extent=[0, baseline_e[sample]-baseline_b[sample], freqs[-1], freqs[0]], cmap='viridis', aspect='auto')
    ax.set_yscale("log")
```

```
153     ax.set_xlabel("Time (s)")
154     ax.set_ylabel("Frequency (Hz)")
155     ax.set_title("Wavelet coefficients plot baseline for " + wavelet)
156     plt.colorbar(plot, ax=ax)
157     return ax
158 
159 def plot_wavelet_baseline_reflecting(data,wavelet,sample,ax):
160     power = power_wavelet_total_with_reflecting(data,wavelet,sample)[:,:(baseline_e[
            sample]-baseline_b[sample])]
161     scales = scale(10)
162     reflectedData = reflect_data(data,sample)
163     coeffs, freqs = pywt.cwt(reflectedData,scales,wavelet)
164     plot = ax.imshow(power, extent=[0, baseline_e[sample]-baseline_b[sample], freqs
            [-1], freqs[0]], cmap='viridis', aspect='auto')
165     ax.set_yscale("log")
166     ax.set_xlabel("Time (s)")
167     ax.set_ylabel("Frequency (Hz)")
168     ax.set_title("Wavelet coefficients plot baseline for " + wavelet + " with
            reflecting")
169     plt.colorbar(plot, ax=ax)
170     return ax
171 
172 def plot_wavelet_peak(data,wavelet,sample,ax):
173     scales = scale(10)
174     coeffs, freqs = pywt.cwt(data,scales,wavelet)
175     power = np.abs(coeffs[:,piek_b[sample]-baseline_b[sample]:piek_e[sample]-baseline_b
            [sample]])**2
176     plot = ax.imshow(power, extent=[piek_b[sample]-baseline_b[sample], piek_b[sample]-
            baseline_b[sample], freqs[-1], freqs[0]], cmap='viridis', aspect='auto')
177     ax.set_yscale("log")
178     ax.set_xlabel("Time (s)")
179     ax.set_ylabel("Frequency (Hz)")
180     ax.set_title("Wavelet coefficients plot peak for " + wavelet)
181     plt.colorbar(plot, ax=ax)
182     return ax
183 
184 def plot_wavelet_peak_reflecting(data,wavelet,sample,ax):
185     scales = scale(10)
186     power = power_wavelet_total_with_reflecting[ : , piek_b[sample]-baseline_b[sample
            ]:(piek_e[sample]-baseline_b[sample])]
187     scales = scale(10)
188     reflectedData = reflect_data(data,sample)
189     coeffs, freqs = pywt.cwt(reflectedData,scales,wavelet)
190     plot = ax.imshow(power, extent=[piek_b[sample]-baseline_b[sample], piek_e[sample]-
            baseline_b[sample], freqs[-1], freqs[0]], cmap='viridis', aspect='auto')
191     ax.set_yscale("log")
192     ax.set_xlabel("Time (s)")
193     ax.set_ylabel("Frequency (Hz)")
194     ax.set_title("Wavelet coefficients plot peak for " + wavelet + " with reflecting")
195     plt.colorbar(plot, ax=ax)
196     return ax
197 
198 def plot_wavelet_plateau(data,wavelet,sample,ax):
199     scales = scale(10)
200     coeffs, freqs = pywt.cwt(data,scales,wavelet)
201     power = np.abs(coeffs[:,plateau_b[sample]-baseline_b[sample]:plateau_e[sample]-
            baseline_b[sample]])**2
202     plot = ax.imshow(power, extent=[plateau_b[sample]-baseline_b[sample], plateau_e[
            sample]-baseline_b[sample], freqs[-1], freqs[0]], cmap='viridis', aspect='auto'
            )
203     ax.set_yscale("log")
204     ax.set_xlabel("Time (s)")
205     ax.set_ylabel("Frequency (Hz)")
206     ax.set_title("Wavelet coefficients plot plateau for " + wavelet)
207     plt.colorbar(plot, ax=ax)
208     return ax
209 
210 def plot_wavelet_plateau_reflecting(data,wavelet,sample,ax):
211     scales = scale(10)
212     power = power_wavelet_total_with_reflecting[ : , plateau_b[sample]-baseline_b[
            sample]:(plateau_e[sample]-baseline_b[sample])]
```

```
    scales = scale(10)
    reflectedData = reflect_data(data,sample)
    coeffs, freqs = pywt.cwt(reflectedData,scales,wavelet)
    plot = ax.imshow(power, extent=[plateau_b[sample]-baseline_b[sample], plateau_e[
        sample]-baseline_b[sample], freqs[-1], freqs[0]], cmap='viridis', aspect='auto'
        )
    ax.set_yscale("log")
    ax.set_xlabel("Time (s)")
    ax.set_ylabel("Frequency (Hz)")
    ax.set_title("Wavelet coefficients plot plateau for " + wavelet + " with reflecting
        ")
    plt.colorbar(plot, ax=ax)
    return ax

def plot_average_over_time(data,wavelet,sample,ax,label):
    scales = scale(10)
    coeffs, freqs = pywt.cwt(data, scales, wavelet)
    coeffs_sliced = coeffs[:, baseline_b[sample]:plateau_e[sample]]
    averageOverTime = np.abs(coeffs_sliced).mean(axis=1)
    ax.plot(freqs, averageOverTime,label=label)
    ax.set_xscale("log")
    ax.set_xlabel('Frequency (Hz)')
    ax.set_ylabel('Average Wavelet Coefficient Magnitude')
    ax.set_title("Average over time plot for " + wavelet)
    ax.grid(True)
    return ax

def plot_average_over_time_reflecting(data,wavelet,sample,ax,label):
    scales = scale(10)
    reflectedData = reflect_data(data,sample)
    coeffs, freqs = pywt.cwt(reflectedData,scales,wavelet)
    segmentLength = plateau_e[sample]-baseline_b[sample]
    coeffs_sliced = coeffs[ : , segmentLength : 2*segmentLength]
    averageOverTime = np.abs(coeffs_sliced).mean(axis=1)
    ax.plot(freqs, averageOverTime,label=label)
    ax.set_xscale("log")
    ax.set_xlabel('Frequency (Hz)')
    ax.set_ylabel('Average wavelet coefficients')
    ax.set_title("Average over time plot for " + wavelet + " with reflecting")
    ax.grid(True)
    return ax

def plot_average_over_time_reflecting_values(data,wavelet,sample):
    scales = scale(10)
    reflectedData = reflect_data(data,sample)
    coeffs, freqs = pywt.cwt(reflectedData,scales,wavelet)
    segmentLength = plateau_e[sample]-baseline_b[sample]
    coeffs_sliced = coeffs[ : , segmentLength : 2*segmentLength]
    averageOverTime = np.abs(coeffs_sliced).mean(axis=1)
    return (averageOverTime, freqs)

def plot_3D(data,wavelet,sample,ax):
    scales = scale(10)
    coeffs, freqs = pywt.cwt(data, scales, wavelet)
    time_range = np.arange(baseline_b[sample], plateau_e[sample])
    logFreqs = np.log10(1/freqs)
    T, F = np.meshgrid(time_range, logFreqs)
    ax.plot_surface(T, F, np.abs(coeffs[:, baseline_b[sample]:plateau_e[sample]]), cmap
        ='cividis')
    ax.set_xlabel('Time (s)')
    ax.set_ylabel('log10(1/Frequency) (Hz)')
    ax.set_zlabel('Wavelet coefficients')
    ax.set_title('3D-plot for ' + wavelet)
    return ax

def plot_3D_reflecting(data,wavelet,sample,ax,title):
    scales = scale(10)
    reflectedData = reflect_data(data,sample)
    coeffs, freqs = pywt.cwt(reflectedData,scales,wavelet)
    segmentLength = plateau_e[sample]-baseline_b[sample]
    coeffs_sliced = coeffs[ : , segmentLength : 2*segmentLength]
```

```
    time_range = np.arange(baseline_b[sample], plateau_e[sample])
    logFreqs = np.log10(1/freqs)
    T, F = np.meshgrid(time_range, logFreqs)
    ax.plot_surface(T, F, np.abs(coeffs_sliced), cmap='viridis')
    ax.set_xlabel('Time (s)')
    ax.set_ylabel('log10(1/Frequency) (Hz)')
    ax.set_zlabel('Wavelet coefficients')
    ax.set_title(title)
    return ax

def average_energy_density(data,wavelet,sample,f_i1,f_i2):
    scales = scale(10)
    coeffs, freqs = pywt.cwt(data, scales, wavelet)

    s_lower = 1 / f_i2
    s_upper = 1 / f_i1
    scalesUsed = (scales >= s_lower) & (scales <= s_upper)
    scalesFiltered = scales[scalesUsed]
    coeffsFiltered = coeffs[scalesUsed, baseline_b[sample]:plateau_e[sample]]

    power = np.abs(coeffsFiltered)**2

    res = 1 / scalesFiltered**2
    y = power.T * res

    scalesIntegration = np.trapz(y,scalesFiltered,axis=1)

    timeIntegration = np.trapz(scalesIntegration,np.arange(baseline_b[sample],plateau_e
        [sample])) / (plateau_e[sample]-baseline_b[sample])
    return timeIntegration

def average_energy_density_reflecting(data,wavelet,sample,f_i1,f_i2):
    scales = scale(10)
    reflectedData = reflect_data(data,sample)
    coeffs, freqs = pywt.cwt(reflectedData,scales,wavelet)
    segmentLength = plateau_e[sample]-baseline_b[sample]
    coeffs = coeffs[ : , segmentLength : 2*segmentLength]

    s_lower = 1 / f_i2
    s_upper = 1 / f_i1
    scalesUsed = (scales >= s_lower) & (scales <= s_upper)
    scalesFiltered = scales[scalesUsed]
    coeffsFiltered = coeffs[scalesUsed, :]

    power = np.abs(coeffsFiltered)**2

    res = 1 / scalesFiltered**2
    y = power.T * res

    scalesIntegration = np.trapz(y,scalesFiltered,axis=1)

    timeIntegration = np.trapz(scalesIntegration,np.arange(0,segmentLength)) /
        segmentLength
    return timeIntegration

def average_energy_density_reflecting_baseline(data,wavelet,sample,f_i1,f_i2):
    scales = scale(10)
    reflectedData = reflect_data(data,sample)
    coeffs, freqs = pywt.cwt(reflectedData,scales,wavelet)
    segmentLength = plateau_e[sample]-baseline_b[sample]
    coeffs = coeffs[ : , segmentLength : 2*segmentLength]

    s_lower = 1 / f_i2
    s_upper = 1 / f_i1
    scalesUsed = (scales >= s_lower) & (scales <= s_upper)
    scalesFiltered = scales[scalesUsed]
    coeffsFiltered = coeffs[scalesUsed, :]

    power = np.abs(coeffsFiltered)**2

    res = 1 / scalesFiltered**2
```

```
    y = power.T * res

    scalesIntegration = np.trapz(y,scalesFiltered,axis=1)
    scalesIntegrationBaseline = scalesIntegration[:baseline_e[sample]-baseline_b[sample]]
    timeIntegration = np.trapz(scalesIntegrationBaseline,np.arange(0,len(scalesIntegrationBaseline))) / len(scalesIntegrationBaseline)
    return timeIntegration

def average_energy_density_reflecting_peak(data,wavelet,sample,f_i1,f_i2):
    scales = scale(10)
    reflectedData = reflect_data(data,sample)
    coeffs, freqs = pywt.cwt(reflectedData,scales,wavelet)
    segmentLength = plateau_e[sample]-baseline_b[sample]
    coeffs = coeffs[ : , segmentLength : 2*segmentLength]

    s_lower = 1 / f_i2
    s_upper = 1 / f_i1
    scalesUsed = (scales >= s_lower) & (scales <= s_upper)
    scalesFiltered = scales[scalesUsed]
    coeffsFiltered = coeffs[scalesUsed, :]

    power = np.abs(coeffsFiltered)**2

    res = 1 / scalesFiltered**2
    y = power.T * res

    scalesIntegration = np.trapz(y,scalesFiltered,axis=1)
    scalesIntegrationBaseline = scalesIntegration[piek_b[sample]-baseline_b[sample]:piek_e[sample]-baseline_b[sample]]
    timeIntegration = np.trapz(scalesIntegrationBaseline,np.arange(0,len(scalesIntegrationBaseline))) / len(scalesIntegrationBaseline)
    return timeIntegration

def average_energy_density_reflecting_plateau(data,wavelet,sample,f_i1,f_i2):
    scales = scale(10)
    reflectedData = reflect_data(data,sample)
    coeffs, freqs = pywt.cwt(reflectedData,scales,wavelet)
    segmentLength = plateau_e[sample]-baseline_b[sample]
    coeffs = coeffs[ : , segmentLength : 2*segmentLength]

    s_lower = 1 / f_i2
    s_upper = 1 / f_i1
    scalesUsed = (scales >= s_lower) & (scales <= s_upper)
    scalesFiltered = scales[scalesUsed]
    coeffsFiltered = coeffs[scalesUsed, :]

    power = np.abs(coeffsFiltered)**2

    res = 1 / scalesFiltered**2
    y = power.T * res

    scalesIntegration = np.trapz(y,scalesFiltered,axis=1)
    scalesIntegrationBaseline = scalesIntegration[plateau_b[sample]-baseline_b[sample]:plateau_e[sample]-baseline_b[sample]]
    timeIntegration = np.trapz(scalesIntegrationBaseline,np.arange(0,len(scalesIntegrationBaseline))) / len(scalesIntegrationBaseline)
    return timeIntegration

def relative_energy_density(data,wavelet,sample,f_i1,f_i2):
    totalEnergy = average_energy_density(data,wavelet,sample,0.005,0.5)
    energy = average_energy_density(data,wavelet,sample,f_i1,f_i2)
    return energy / totalEnergy

def relative_energy_density_reflecting(data,wavelet,sample,f_i1,f_i2):
    totalEnergy = average_energy_density_reflecting(data,wavelet,sample,0.005,0.5)
    energy = average_energy_density_reflecting(data,wavelet,sample,f_i1,f_i2)
    return energy / totalEnergy

def relative_energy_density_reflecting_baseline_part(data,wavelet,sample,f_i1,f_i2):
```

```
413     totalEnergy = average_energy_density_reflecting_baseline(data,wavelet,sample
            ,0.005,0.4)
414     energy = average_energy_density_reflecting_baseline(data,wavelet,sample,f_i1,f_i2)
415     return energy / totalEnergy
416 
417 def relative_energy_density_reflecting_peak_part(data,wavelet,sample,f_i1,f_i2):
418     totalEnergy = average_energy_density_reflecting_peak(data,wavelet,sample,0.005,0.4)
419     energy = average_energy_density_reflecting_peak(data,wavelet,sample,f_i1,f_i2)
420     return energy / totalEnergy
421 
422 def relative_energy_density_reflecting_plateau_part(data,wavelet,sample,f_i1,f_i2):
423     totalEnergy = average_energy_density_reflecting_plateau(data,wavelet,sample
            ,0.005,0.4)
424     energy = average_energy_density_reflecting_plateau(data,wavelet,sample,f_i1,f_i2)
425     return energy / totalEnergy
426 
427 def relative_energy_density_reflecting_baseline(data,wavelet,sample,f_i1,f_i2):
428     totalEnergy = average_energy_density_reflecting_baseline(data,wavelet,sample
            ,0.005,0.5)
429     energy = average_energy_density_reflecting_baseline(data,wavelet,sample,f_i1,f_i2)
430     return energy / totalEnergy
431 
432 def relative_energy_density_reflecting_peak(data,wavelet,sample,f_i1,f_i2):
433     totalEnergy = average_energy_density_reflecting_peak(data,wavelet,sample,0.005,0.5)
434     energy = average_energy_density_reflecting_peak(data,wavelet,sample,f_i1,f_i2)
435     return energy / totalEnergy
436 
437 def relative_energy_density_reflecting_plateau(data,wavelet,sample,f_i1,f_i2):
438     totalEnergy = average_energy_density_reflecting_plateau(data,wavelet,sample
            ,0.005,0.5)
439     energy = average_energy_density_reflecting_plateau(data,wavelet,sample,f_i1,f_i2)
440     return energy / totalEnergy
441 
442 def average_amplitude(data,wavelet,sample,f_i1,f_i2):
443     scales = scale(10)
444     coeffs, freqs = pywt.cwt(data, scales, wavelet)
445 
446     s_lower = 1 / f_i2
447     s_upper = 1 / f_i1
448     scalesUsed = (scales >= s_lower) & (scales <= s_upper)
449     scalesFiltered = scales[scalesUsed]
450     coeffsFiltered = coeffs[scalesUsed, baseline_b[sample]:plateau_e[sample]]
451 
452     power = np.abs(coeffsFiltered)
453 
454     res = 1 / scalesFiltered**2
455     y = power.T * res
456 
457     scalesIntegration = (1 / f_i2 - f_i1) * np.trapz(y,scalesFiltered,axis=1)
458 
459     timeIntegration = np.trapz(scalesIntegration,np.arange(baseline_b[sample],plateau_e
            [sample])) / (plateau_e[sample]-baseline_b[sample])
460     return timeIntegration
461 
462 def average_amplitude_reflecting(data,wavelet,sample,f_i1,f_i2):
463     scales = scale(10)
464     reflectedData = reflect_data(data,sample)
465     coeffs, freqs = pywt.cwt(reflectedData,scales,wavelet)
466     segmentLength = plateau_e[sample]-baseline_b[sample]
467     coeffs = coeffs[ : , segmentLength : 2*segmentLength]
468 
469     s_lower = 1 / f_i2
470     s_upper = 1 / f_i1
471     scalesUsed = (scales >= s_lower) & (scales <= s_upper)
472     scalesFiltered = scales[scalesUsed]
473     coeffsFiltered = coeffs[scalesUsed, :]
474 
475     power = np.abs(coeffsFiltered)
476 
477     res = 1 / scalesFiltered**2
478     y = power.T * res
```

```
479
480     scalesIntegration = (1 / f_i2 - f_i1) * np.trapz(y,scalesFiltered,axis=1)
481
482     timeIntegration = np.trapz(scalesIntegration,np.arange(0, segmentLength)) /
            segmentLength
483     return timeIntegration
484
485 def average_amplitude_reflecting_baseline(data,wavelet,sample,f_i1,f_i2):
486     scales = scale(10)
487     reflectedData = reflect_data(data,sample)
488     coeffs, freqs = pywt.cwt(reflectedData,scales,wavelet)
489     segmentLength = plateau_e[sample]-baseline_b[sample]
490     coeffs = coeffs[ : , segmentLength : 2*segmentLength]
491
492     s_lower = 1 / f_i2
493     s_upper = 1 / f_i1
494     scalesUsed = (scales >= s_lower) & (scales <= s_upper)
495     scalesFiltered = scales[scalesUsed]
496     coeffsFiltered = coeffs[scalesUsed, :]
497
498     power = np.abs(coeffsFiltered)
499
500     res = 1 / scalesFiltered**2
501     y = power.T * res
502
503     scalesIntegration = (1 / f_i2 - f_i1) * np.trapz(y,scalesFiltered,axis=1)
504     scalesIntegrationBaseline = scalesIntegration[:baseline_e[sample]-baseline_b[sample
            ]]
505     timeIntegration = np.trapz(scalesIntegrationBaseline,np.arange(0,len(
            scalesIntegrationBaseline))) / len(scalesIntegrationBaseline)
506     return timeIntegration
507
508 def average_amplitude_reflecting_peak(data,wavelet,sample,f_i1,f_i2):
509     scales = scale(10)
510     reflectedData = reflect_data(data,sample)
511     coeffs, freqs = pywt.cwt(reflectedData,scales,wavelet)
512     segmentLength = plateau_e[sample]-baseline_b[sample]
513     coeffs = coeffs[ : , segmentLength : 2*segmentLength]
514
515     s_lower = 1 / f_i2
516     s_upper = 1 / f_i1
517     scalesUsed = (scales >= s_lower) & (scales <= s_upper)
518     scalesFiltered = scales[scalesUsed]
519     coeffsFiltered = coeffs[scalesUsed, :]
520
521     power = np.abs(coeffsFiltered)
522
523     res = 1 / scalesFiltered**2
524     y = power.T * res
525
526     scalesIntegration = (1 / f_i2 - f_i1) * np.trapz(y,scalesFiltered,axis=1)
527     scalesIntegrationBaseline = scalesIntegration[piek_b[sample]-baseline_b[sample]:
            piek_e[sample]-baseline_b[sample]]
528     timeIntegration = np.trapz(scalesIntegrationBaseline,np.arange(0,len(
            scalesIntegrationBaseline))) / len(scalesIntegrationBaseline)
529     return timeIntegration
530
531 def average_amplitude_reflecting_plateau(data,wavelet,sample,f_i1,f_i2):
532     scales = scale(10)
533     reflectedData = reflect_data(data,sample)
534     coeffs, freqs = pywt.cwt(reflectedData,scales,wavelet)
535     segmentLength = plateau_e[sample]-baseline_b[sample]
536     coeffs = coeffs[ : , segmentLength : 2*segmentLength]
537
538     s_lower = 1 / f_i2
539     s_upper = 1 / f_i1
540     scalesUsed = (scales >= s_lower) & (scales <= s_upper)
541     scalesFiltered = scales[scalesUsed]
542     coeffsFiltered = coeffs[scalesUsed, :]
543
544     power = np.abs(coeffsFiltered)
```

```
545
546     res = 1 / scalesFiltered**2
547     y = power.T * res
548
549     scalesIntegration = (1 / f_i2 - f_i1) * np.trapz(y,scalesFiltered,axis=1)
550     scalesIntegrationBaseline = scalesIntegration[plateau_b[sample]-baseline_b[sample]:
            plateau_e[sample]-baseline_b[sample]]
551     timeIntegration = np.trapz(scalesIntegrationBaseline,np.arange(0,len(
            scalesIntegrationBaseline))) / len(scalesIntegrationBaseline)
552     return timeIntegration
553
554 def relative_amplitude(data,wavelet,sample,f_i1,f_i2):
555     totalEnergy = average_amplitude(data,wavelet,sample,0.005,0.5)
556     energy = average_amplitude(data,wavelet,sample,f_i1,f_i2)
557     return energy / totalEnergy
558
559 def relative_amplitude_reflecting(data,wavelet,sample,f_i1,f_i2):
560     totalEnergy = average_amplitude_reflecting(data,wavelet,sample,0.005,0.5)
561     energy = average_amplitude_reflecting(data,wavelet,sample,f_i1,f_i2)
562     return energy / totalEnergy
563
564 def relative_amplitude_reflecting_baseline(data,wavelet,sample,f_i1,f_i2):
565     totalEnergy = average_amplitude_reflecting_baseline(data,wavelet,sample,0.005,0.5)
566     energy = average_amplitude_reflecting_baseline(data,wavelet,sample,f_i1,f_i2)
567     return energy / totalEnergy
568
569 def relative_amplitude_reflecting_peak(data,wavelet,sample,f_i1,f_i2):
570     totalEnergy = average_amplitude_reflecting_peak(data,wavelet,sample,0.005,0.5)
571     energy = average_amplitude_reflecting_peak(data,wavelet,sample,f_i1,f_i2)
572     return energy / totalEnergy
573
574 def relative_amplitude_reflecting_plateau(data,wavelet,sample,f_i1,f_i2):
575     totalEnergy = average_amplitude_reflecting_plateau(data,wavelet,sample,0.005,0.5)
576     energy = average_amplitude_reflecting_plateau(data,wavelet,sample,f_i1,f_i2)
577     return energy / totalEnergy
578
579 def plot_boxplots_intervals_RED(ROI,ax,morlet):
580     f6 = np.zeros(53)
581     f5 = np.zeros(53)
582     f4 = np.zeros(53)
583     f3 = np.zeros(53)
584     f2 = np.zeros(53)
585
586     for i in range(53):
587         f6[i] = relative_energy_density(ROI[i],morlet,i,0.005,0.0095)
588         f5[i] = relative_energy_density(ROI[i],morlet,i,0.0095,0.02)
589         f4[i] = relative_energy_density(ROI[i],morlet,i,0.02,0.06)
590         f3[i] = relative_energy_density(ROI[i],morlet,i,0.06,0.15)
591         f2[i] = relative_energy_density(ROI[i],morlet,i,0.15,0.4)
592
593     d = [f6, f5, f4, f3, f2]
594     ax.boxplot(d)
595     ax.set_title("Boxplots of the relative energy density")
596     ax.set_xlabel("Frequency intervals")
597     ax.set_ylabel("Value")
598     ax.set_xticks([1, 2, 3, 4, 5])
599     ax.set_xticklabels(["0.005-0.0095", "0.0095-0.02", "0.02-0.06", "0.06-0.15", "
            0.15-0.4"])
600     ax.grid(True)
601     return ax
602
603 def plot_boxplots_intervals_RED_reflecting(ROI,ax,morlet):
604     f6 = np.zeros(53)
605     f5 = np.zeros(53)
606     f4 = np.zeros(53)
607     f3 = np.zeros(53)
608     f2 = np.zeros(53)
609
610     for i in range(53):
611         f6[i] = relative_energy_density_reflecting(ROI[i],morlet,i,0.005,0.0095)
612         f5[i] = relative_energy_density_reflecting(ROI[i],morlet,i,0.0095,0.02)
```

```
        f4[i] = relative_energy_density_reflecting(ROI[i],morlet,i,0.02,0.06)
        f3[i] = relative_energy_density_reflecting(ROI[i],morlet,i,0.06,0.15)
        f2[i] = relative_energy_density_reflecting(ROI[i],morlet,i,0.15,0.4)

    d = [f6, f5, f4, f3, f2]
    ax.boxplot(d)
    ax.set_title("Boxplots of the relative energy density with reflecting")
    ax.set_xlabel("Frequency intervals")
    ax.set_ylabel("Value")
    ax.set_xticks([1, 2, 3, 4, 5])
    ax.set_xticklabels(["0.005-0.0095", "0.0095-0.02", "0.02-0.06", "0.06-0.15", "
        0.15-0.4"])
    ax.grid(True)
    return ax

def plot_boxplots_intervals_RA(ROI,ax,morlet):
    f6 = np.zeros(53)
    f5 = np.zeros(53)
    f4 = np.zeros(53)
    f3 = np.zeros(53)
    f2 = np.zeros(53)

    for i in range(53):
        f6[i] = relative_amplitude(ROI[i],morlet,i,0.005,0.0095)
        f5[i] = relative_amplitude(ROI[i],morlet,i,0.0095,0.02)
        f4[i] = relative_amplitude(ROI[i],morlet,i,0.02,0.06)
        f3[i] = relative_amplitude(ROI[i],morlet,i,0.06,0.15)
        f2[i] = relative_amplitude(ROI[i],morlet,i,0.15,0.4)

    d = [f6, f5, f4, f3, f2]
    ax.boxplot(d)
    ax.set_title("Boxplots of the relative amplitude")
    ax.set_xlabel("Frequency intervals")
    ax.set_ylabel("Value")
    ax.set_xticks([1, 2, 3, 4, 5])
    ax.set_xticklabels(["0.005-0.0095", "0.0095-0.02", "0.02-0.06", "0.06-0.15", "
        0.15-0.4"])
    ax.grid(True)
    return ax

def plot_boxplots_intervals_RA_reflecting(ROI,ax,morlet):
    f6 = np.zeros(53)
    f5 = np.zeros(53)
    f4 = np.zeros(53)
    f3 = np.zeros(53)
    f2 = np.zeros(53)

    for i in range(53):
        f6[i] = relative_amplitude_reflecting(ROI[i],morlet,i,0.005,0.0095)
        f5[i] = relative_amplitude(ROI[i],morlet,i,0.0095,0.02)
        f4[i] = relative_amplitude(ROI[i],morlet,i,0.02,0.06)
        f3[i] = relative_amplitude(ROI[i],morlet,i,0.06,0.15)
        f2[i] = relative_amplitude(ROI[i],morlet,i,0.15,0.4)

    d = [f6, f5, f4, f3, f2]
    ax.boxplot(d)
    ax.set_title("Boxplots of the relative amplitude with reflecting")
    ax.set_xlabel("Frequency intervals")
    ax.set_ylabel("Value")
    ax.set_xticks([1, 2, 3, 4, 5])
    ax.set_xticklabels(["0.005-0.0095", "0.0095-0.02", "0.02-0.06", "0.06-0.15", "
        0.15-0.4"])
    ax.grid(True)
    return ax

def plot_boxplots_intervals_ED(ROI,ax,morlet):
    f6 = np.zeros(53)
    f5 = np.zeros(53)
    f4 = np.zeros(53)
    f3 = np.zeros(53)
    f2 = np.zeros(53)
```

```
681
682     for i in range(53):
683         f6[i] = average_energy_density(ROI[i],morlet,i,0.005,0.0095)
684         f5[i] = average_energy_density(ROI[i],morlet,i,0.0095,0.02)
685         f4[i] = average_energy_density(ROI[i],morlet,i,0.02,0.06)
686         f3[i] = average_energy_density(ROI[i],morlet,i,0.06,0.15)
687         f2[i] = average_energy_density(ROI[i],morlet,i,0.15,0.4)
688
689     d = [f6, f5, f4, f3, f2]
690     ax.boxplot(d)
691     ax.set_title("Boxplots of the average energy density")
692     ax.set_xlabel("Frequency intervals")
693     ax.set_ylabel("Value")
694     ax.set_xticks([1, 2, 3, 4, 5])
695     ax.set_xticklabels(["0.005-0.0095", "0.0095-0.02", "0.02-0.06", "0.06-0.15", "
            0.15-0.4"])
696     ax.grid(True)
697     return ax
698
699 def plot_boxplots_intervals_ED_reflecting(ROI,ax,morlet):
700     f6 = np.zeros(53)
701     f5 = np.zeros(53)
702     f4 = np.zeros(53)
703     f3 = np.zeros(53)
704     f2 = np.zeros(53)
705
706     for i in range(53):
707         f6[i] = average_energy_density_reflecting(ROI[i],morlet,i,0.005,0.0095)
708         f5[i] = average_energy_density_reflecting(ROI[i],morlet,i,0.0095,0.02)
709         f4[i] = average_energy_density_reflecting(ROI[i],morlet,i,0.02,0.06)
710         f3[i] = average_energy_density_reflecting(ROI[i],morlet,i,0.06,0.15)
711         f2[i] = average_energy_density_reflecting(ROI[i],morlet,i,0.15,0.4)
712
713     d = [f6, f5, f4, f3, f2]
714     ax.boxplot(d)
715     ax.set_title("Boxplots of the average energy density with reflecting")
716     ax.set_xlabel("Frequency intervals")
717     ax.set_ylabel("Value")
718     ax.set_xticks([1, 2, 3, 4, 5])
719     ax.set_xticklabels(["0.005-0.0095", "0.0095-0.02", "0.02-0.06", "0.06-0.15", "
            0.15-0.4"])
720     ax.grid(True)
721     return ax
722
723 def plot_boxplots_intervals_AA(ROI,ax,morlet):
724     f6 = np.zeros(53)
725     f5 = np.zeros(53)
726     f4 = np.zeros(53)
727     f3 = np.zeros(53)
728     f2 = np.zeros(53)
729
730     for i in range(53):
731         f6[i] = average_amplitude(ROI[i],morlet,i,0.005,0.0095)
732         f5[i] = average_amplitude(ROI[i],morlet,i,0.0095,0.02)
733         f4[i] = average_amplitude(ROI[i],morlet,i,0.02,0.06)
734         f3[i] = average_amplitude(ROI[i],morlet,i,0.06,0.15)
735         f2[i] = average_amplitude(ROI[i],morlet,i,0.15,0.4)
736
737     d = [f6, f5, f4, f3, f2]
738     ax.boxplot(d)
739     ax.set_title("Boxplots of the average amplitude")
740     ax.set_xlabel("Frequency intervals")
741     ax.set_ylabel("Value")
742     ax.set_xticks([1, 2, 3, 4, 5])
743     ax.set_xticklabels(["0.005-0.0095", "0.0095-0.02", "0.02-0.06", "0.06-0.15", "
            0.15-0.4"])
744     ax.grid(True)
745     return ax
746
747 def plot_boxplots_intervals_AA_reflecting(ROI,ax,morlet):
748     f6 = np.zeros(53)
```

```
    f5 = np.zeros(53)
    f4 = np.zeros(53)
    f3 = np.zeros(53)
    f2 = np.zeros(53)

    for i in range(53):
        f6[i] = average_amplitude_reflecting(ROI[i],morlet,i,0.005,0.0095)
        f5[i] = average_amplitude_reflecting(ROI[i],morlet,i,0.0095,0.02)
        f4[i] = average_amplitude_reflecting(ROI[i],morlet,i,0.02,0.06)
        f3[i] = average_amplitude_reflecting(ROI[i],morlet,i,0.06,0.15)
        f2[i] = average_amplitude_reflecting(ROI[i],morlet,i,0.15,0.4)

    d = [f6, f5, f4, f3, f2]
    ax.boxplot(d)
    ax.set_title("Boxplots of the average amplitude with reflecting")
    ax.set_xlabel("Frequency intervals")
    ax.set_ylabel("Value")
    ax.set_xticks([1, 2, 3, 4, 5])
    ax.set_xticklabels(["0.005-0.0095", "0.0095-0.02", "0.02-0.06", "0.06-0.15", "
        0.15-0.4"])
    ax.grid(True)
    return ax

def twoBoxplots(ROI,data1,data2,ax,morlet,begin,end,function,label,title):
    mig = np.zeros(len(data1))
    noMig= np.zeros(len(data2))

    m=0
    nm=0

    for i in range(53):
        if label[i] == 1:
            mig[m] = function(ROI[i],morlet,i,begin,end)
            m+=1
        if label[i] == 0:
            noMig[nm] = function(ROI[i],morlet,i,begin,end)
            nm+=1

    d = [noMig, mig]
    ax.boxplot(d)
    ax.set_title(title)
    # ax.set_xlabel("Frequency intervals")
    ax.set_ylabel("Value")
    ax.set_xticks([1, 2])
    ax.set_xticklabels(["No migraine", "Migraine"])
    ax.grid(True)
    return ax

def twoBoxplots_values(ROI,data1,data2,morlet,begin,end,function,label):
    mig = np.zeros(len(data1))
    noMig= np.zeros(len(data2))

    m=0
    nm=0

    for i in range(53):
        if label[i] == 1:
            mig[m] = function(ROI[i],morlet,i,begin,end)
            m+=1
        if label[i] == 0:
            noMig[nm] = function(ROI[i],morlet,i,begin,end)
            nm+=1

    return (mig,noMig)

def twoBoxplotsaura(ROI,data1,data2,ax,morlet,begin,end,function,label,title):
    mig = np.zeros(len(data1))
    noMig= np.zeros(len(data2))

    m=0
    nm=0
```

```
819
820     for i in range(53):
821         if label[i] == 2:
822             mig[m] = function(ROI[i],morlet,i,begin,end)
823             m+=1
824         if label[i] == 0:
825             noMig[nm] = function(ROI[i],morlet,i,begin,end)
826             nm+=1
827
828     d = [noMig, mig]
829     ax.boxplot(d)
830     ax.set_title(title)
831     # ax.set_xlabel("Frequency intervals")
832     ax.set_ylabel("Value")
833     ax.set_xticks([1, 2])
834     ax.set_xticklabels(["No migraine", "Migraine with aura"])
835     ax.grid(True)
836     return ax
837
838 def twoBoxplots_valuesaura(ROI,data1,data2,morlet,begin,end,function,label):
839     mig = np.zeros(len(data1))
840     noMig= np.zeros(len(data2))
841
842     m=0
843     nm=0
844
845     for i in range(53):
846         if label[i] == 2:
847             mig[m] = function(ROI[i],morlet,i,begin,end)
848             m+=1
849         if label[i] == 0:
850             noMig[nm] = function(ROI[i],morlet,i,begin,end)
851             nm+=1
852
853     return (mig,noMig)
854
855 def twoBoxplots_fourier(ROI,data1,data2,ax,f_i1,f_i2,function,label,title,start,end):
856     mig = np.zeros(len(data1))
857     noMig= np.zeros(len(data2))
858
859     m=0
860     nm=0
861
862     for i in range(53):
863         if label[i] == 1:
864             mig[m] = function(ROI[i],i,f_i1,f_i2,start,end)
865             m+=1
866         if label[i] == 0:
867             noMig[nm] = function(ROI[i],i,f_i1,f_i2,start,end)
868             nm+=1
869
870     d = [noMig, mig]
871     ax.boxplot(d)
872     ax.set_title(title)
873     # ax.set_xlabel("Frequency intervals")
874     ax.set_ylabel("Value")
875     ax.set_xticks([1, 2])
876     ax.set_xticklabels(["No migraine", "Migraine"])
877     ax.grid(True)
878     return ax
879
880 def twoBoxplots_values_fourier(ROI,data1,data2,f_i1,f_i2,function,label,start,end):
881     mig = np.zeros(len(data1))
882     noMig= np.zeros(len(data2))
883
884     m=0
885     nm=0
886
887     for i in range(53):
888         if label[i] == 1:
889             mig[m] = function(ROI[i],i,f_i1,f_i2,start,end)
```

```
            m+=1
        if label[i] == 0:
            noMig[nm] = function(ROI[i],i,f_i1,f_i2,start,end)
            nm+=1

    return (mig,noMig)

def threeBoxplots(ROI,data,ax,morlet,begin,end,function1,function2,function3,
    labelNumber,label,title):
    baselineValues = np.zeros(len(data))
    peakValues = np.zeros(len(data))
    plateauValues = np.zeros(len(data))

    m=0
    nm=0

    if labelNumber == 1:
        for i in range(53):
            if label[i] == 1:
                baselineValues[m] = function1(ROI[i],morlet,i,begin,end)
                peakValues[m] = function2(ROI[i],morlet,i,begin,end)
                plateauValues[m] = function3(ROI[i],morlet,i,begin,end)
                m+=1
    if labelNumber == 0:
        for i in range(53):
            if label[i] == 0:
                baselineValues[nm] = function1(ROI[i],morlet,i,begin,end)
                peakValues[nm] = function2(ROI[i],morlet,i,begin,end)
                plateauValues[nm] = function3(ROI[i],morlet,i,begin,end)
                nm+=1

    d = [baselineValues, peakValues,plateauValues]
    ax.boxplot(d)
    ax.set_title(title)
    ax.set_xlabel("Frequency intervals")
    ax.set_ylabel("Value")
    ax.set_xticks([1, 2, 3])
    ax.set_xticklabels(["Baseline", "Peak", "Plateau"])
    ax.grid(True)
    return ax

def threeBoxplots_values(ROI,data,morlet,begin,end,function1,function2,function3,
    labelNumber,label):
    baselineValues = np.zeros(len(data))
    peakValues = np.zeros(len(data))
    plateauValues = np.zeros(len(data))

    m=0
    nm=0

    if labelNumber == 1:
        for i in range(53):
            if label[i] == 1:
                baselineValues[m] = function1(ROI[i],morlet,i,begin,end)
                peakValues[m] = function2(ROI[i],morlet,i,begin,end)
                plateauValues[m] = function3(ROI[i],morlet,i,begin,end)
                m+=1
    if labelNumber == 0:
        for i in range(53):
            if label[i] == 0:
                baselineValues[nm] = function1(ROI[i],morlet,i,begin,end)
                peakValues[nm] = function2(ROI[i],morlet,i,begin,end)
                plateauValues[nm] = function3(ROI[i],morlet,i,begin,end)
                nm+=1
    return (baselineValues,peakValues,plateauValues)

def threeBoxplotsROI(ROI1,ROI2,ROI3,data,ax,morlet,begin,end,function,labelNumber,label
    ,title):
    roi1 = np.zeros(len(data))
    roi2 = np.zeros(len(data))
    roi3 = np.zeros(len(data))
```

```
958
959     m=0
960     nm=0
961
962     if labelNumber == 1:
963         for i in range(53):
964             if label[i] == 1:
965                 roi1[m] = function(ROI1[i],morlet,i,begin,end)
966                 roi2[m] = function(ROI2[i],morlet,i,begin,end)
967                 roi3[m] = function(ROI3[i],morlet,i,begin,end)
968                 m+=1
969     if labelNumber == 0:
970         for i in range(53):
971             if label[i] == 0:
972                 roi1[nm] = function(ROI1[i],morlet,i,begin,end)
973                 roi2[nm] = function(ROI2[i],morlet,i,begin,end)
974                 roi3[nm] = function(ROI3[i],morlet,i,begin,end)
975                 nm+=1
976
977     d = [roi1, roi3,roi2]
978     ax.boxplot(d)
979     ax.set_title(title)
980     ax.set_xlabel("Frequency intervals")
981     ax.set_ylabel("Value")
982     ax.set_xticks([1, 2, 3])
983     ax.set_xticklabels(["ROI1", "ROI3", "ROI2"])
984     ax.grid(True)
985     return ax
986
987 def threeBoxplotsROI_values(ROI1,ROI2,ROI3,data,morlet,begin,end,function,labelNumber,
        label):
988     roi1 = np.zeros(len(data))
989     roi2 = np.zeros(len(data))
990     roi3 = np.zeros(len(data))
991
992     m=0
993     nm=0
994
995     if labelNumber == 1:
996         for i in range(53):
997             if label[i] == 1:
998                 roi1[m] = function(ROI1[i],morlet,i,begin,end)
999                 roi2[m] = function(ROI2[i],morlet,i,begin,end)
1000                roi3[m] = function(ROI3[i],morlet,i,begin,end)
1001                m+=1
1002    if labelNumber == 0:
1003        for i in range(53):
1004            if label[i] == 0:
1005                roi1[nm] = function(ROI1[i],morlet,i,begin,end)
1006                roi2[nm] = function(ROI2[i],morlet,i,begin,end)
1007                roi3[nm] = function(ROI3[i],morlet,i,begin,end)
1008                nm+=1
1009    return (roi1,roi2,roi3)
1010
1011 def threeBoxplotsROI_fourier(ROI1,ROI2,ROI3,data,ax,start,end,function,labelNumber,
        label,title,f_i1,f_i2):
1012    roi1 = np.zeros(len(data))
1013    roi2 = np.zeros(len(data))
1014    roi3 = np.zeros(len(data))
1015
1016    m=0
1017    nm=0
1018
1019    if labelNumber == 1:
1020        for i in range(53):
1021            if label[i] == 1:
1022                roi1[m] = function(ROI1[i],i,f_i1,f_i2,start,end)
1023                roi2[m] = function(ROI2[i],i,f_i1,f_i2,start,end)
1024                roi3[m] = function(ROI3[i],i,f_i1,f_i2,start,end)
1025                m+=1
1026    if labelNumber == 0:
```

```
        for i in range(53):
            if label[i] == 0:
                roi1[nm] = function(ROI1[i],i,f_i1,f_i2,start,end)
                roi2[nm] = function(ROI2[i],i,f_i1,f_i2,start,end)
                roi3[nm] = function(ROI3[i],i,f_i1,f_i2,start,end)
                nm+=1

    d = [roi1, roi3,roi2]
    ax.boxplot(d)
    ax.set_title(title)
    ax.set_ylabel("Value")
    ax.set_xticks([1, 2, 3])
    ax.set_xticklabels(["ROI1", "ROI3", "ROI2"])
    ax.grid(True)
    return ax

def threeBoxplotsROI_values_fourier(ROI1,ROI2,ROI3,data,start,end,function,labelNumber,
    label,f_i1,f_i2):
    roi1 = np.zeros(len(data))
    roi2 = np.zeros(len(data))
    roi3 = np.zeros(len(data))

    m=0
    nm=0

    if labelNumber == 1:
        for i in range(53):
            if label[i] == 1:
                roi1[m] = function(ROI1[i],i,f_i1,f_i2,start,end)
                roi2[m] = function(ROI2[i],i,f_i1,f_i2,start,end)
                roi3[m] = function(ROI3[i],i,f_i1,f_i2,start,end)
                m+=1
    if labelNumber == 0:
        for i in range(53):
            if label[i] == 0:
                roi1[nm] = function(ROI1[i],i,f_i1,f_i2,start,end)
                roi2[nm] = function(ROI2[i],i,f_i1,f_i2,start,end)
                roi3[nm] = function(ROI3[i],i,f_i1,f_i2,start,end)
                nm+=1
    return (roi1,roi2,roi3)

def discrete_fourier_transform(ROI,sample,start,end):
    start = start[sample]
    end = end[sample]
    data = ROI[start:end]-np.mean(ROI[start:end])
    res = fft(data)
    frequencies =fftfreq(len(data),1)
    mask = frequencies >= 0.005
    return (res[mask],frequencies[mask])

def energy_density_fourier(ROI,sample,f_i1,f_i2,start,end):
    res,frequencies = discrete_fourier_transform(ROI,sample,start,end)
    mask = (frequencies >= f_i1) & (frequencies <= f_i2)
    res = res[mask]
    frequencies = frequencies[mask]
    return np.sum(np.abs(res)**2)

def relative_energy_density_fourier(ROI,sample,f_i1,f_i2,start,end):
    total = energy_density_fourier(ROI,sample,0.005,0.5,start,end)
    part = energy_density_fourier(ROI,sample,f_i1,f_i2,start,end)
    return part/total

def amplitude_fourier(ROI,sample,f_i1,f_i2,start,end):
    res,frequencies = discrete_fourier_transform(ROI,sample,start,end)
    mask = (frequencies >= f_i1) & (frequencies <= f_i2)
    res = res[mask]
    frequencies = frequencies[mask]
    return 1/(f_i2-f_i1) * np.sum(np.abs(res))

def relative_amplitude_fourier(ROI,sample,f_i1,f_i2,start,end):
    total = amplitude_fourier(ROI,sample,0.005,0.4,start,end)
```

```
1097     part = amplitude_fourier(ROI,sample,f_i1,f_i2,start,end)
1098     return (part/total)
```

Listing B.1: Base document code containing all functions used in the main script.